Supplementary Information of

A multivariate library of Zirconia metal-organic frameworks with dissolved *p*-nitroaniline dipoles and concentration-dependent optical and dielectric response

Kyle R. Langlois,[a,b] Yangyang Wang,[c] FNU Joshua,[a,d] Wesley J. Newsome,[a] Lei Zhai,[a,d] James K. Harper,[e] Fernando Uribe-Romo*[a,b]

[a] Department of Chemistry. University of Central Florida, Orlando, FL 32814, USA.
[b] REACT: Renewable Energy and Chemical Transformations cluster. University of Central Florida, Orlando, FL 32814, USA.
[c] Center for Nanophase Materials Sciences, Oak Ridge National Laboratory, Oak Ridge, TN 37831, USA.
[d] Nanoscience and Technology Center, University of Central Florida, Orlando, FL 32814, USA.
[e] Department of Chemistry, University of Utah, Salt Lake City, UT 84112, USA.

Correspondence Address

*Prof. Fernando J. Uribe-Romo
Department of Chemistry
University of Central Florida
4111 Libra Drive
Physical Sciences Building Rm. 255
Orlando, FL 32816 (USA)
Tel: (+1) 407-823-4876
Email: *fernando@ucf.edu*

Contents

Section S1. General Materials and Methods

All starting materials and solvents, unless otherwise specified, were obtained from commercial sources (Aldrich, Fisher, Strem) and used without further purification. All reactions were performed at ambient laboratory conditions, and no precautions were taken to exclude oxygen or atmospheric moisture unless otherwise specified. Utmost safety precautions were taken in the preparation of the aforementioned project. Anhydrous *N*,*N*-dimethylformamide (DMF) and Tetrahydrofuran (THF) were purified using a custom-built alumina-column based solvent purification system (Inovative Technology). Deuterated solvents ($CDCl_3$, DMSO-d_6, D_2SO_4 96-98 wt% in D_2O) were obtained from Cambridge Isotope Lab and Sigma-Aldrich. H_2PEPEP-Me and $Zr_6O_4(OH)_4(OPiv)_{12}$ were synthesized according to published procedures.[S1, S2]

High-resolution ^1H, and ^{13}C nuclear magnetic resonance (NMR) spectra were recorded using Bruker AVANCE-III 400 MHz spectrometer. The ^1H chemical shifts are given relative to tetramethylsilane as zero ppm, calibrated using the residual solvent signal. Data processing was performed using MNova version 9.0.1.

Powder X-ray diffraction measurements were performed using a Rigaku Miniflex 600 diffractometer, with θ - 2θ Bragg-Brentano geometry, and a 600 W (40 kV, 15 mA) Cu X-ray tube source using Kα (λ = 1.5418 Å) radiation. Samples were measured from 2 to 30 θ-degrees with a step size of 0.02° and a scan rate of 1.5 s per step. Samples were prepared by dropping the powder sample on a Si zero background plate and pressing the powder with a razor blade spatula till smooth. Measurements were performed under spinning at a rate of 60 rpm. Pawley and Rietveld refinements were performed in *GSAS II*[S3]. Simulated crystals and diffraction patterns were calculated using the Reflex module in Materials Studio (v8.0, Biovia).

N_2 gas adsorption isotherm analysis was performed using a Micromertics ASAP 2020 porosimetry analyzer. The measurements was performed at 77 K. Mass spectra were recorded on an Agilent 6230 TOF LC-MS instrument with an Agilent Zorbax SB-C18 analytical column. Fourier-transform infrared spectra were recorded using a Perkin Elmer Spectrum ONE Universal FT-IR ATR. A total of 32 transients were collected for each sample with a resolution of 0.05 cm^{-1} between 4000-400 cm^{-1}. $NEt(iPr)_2$ and $N(Et)_3$ was bubbled with N_2 gas prior to use.

Raman spectra were collected using a HORIBA LabRAM Evolution (HORIBA Scientific, Japan), with a 532 nm (Nd:YAG) laser, operating at a power of < 10 mW. Each spectrum was acquired with an integration time of 4 seconds and averaged over 5 scans. The fluorescence background of the sample was normalized using polynomial background fitting. A grating with 300 grooves/mm was employed, and 100x objectives (0.9 N.A.) were utilized for all experiments.

Solid-state ^{13}C nuclear magnetic resonance was measured on an Agilent DD2 500 MHz narrow-bore spectrometer with a frequency 125.6816571 MHz with an Agilent 1.6 mm T3 probe. A spectral width of 29.7 kHz was employed, and 500 complex points were collected. All spectra employed ^{1}H decoupling at a frequency of 499.77755 MHz using SPINAL decoupling with a 3.0 μs decoupling pulse. Samples were packed in a 1.6 mm zirconia oxide rotor. The spectra were acquired at a spinning speed of 15.0 kHz.

Section S2. Synthesis procedures

General Synthetic Scheme S1. Synthesis of H_2PEPEP-PNA Link**.**

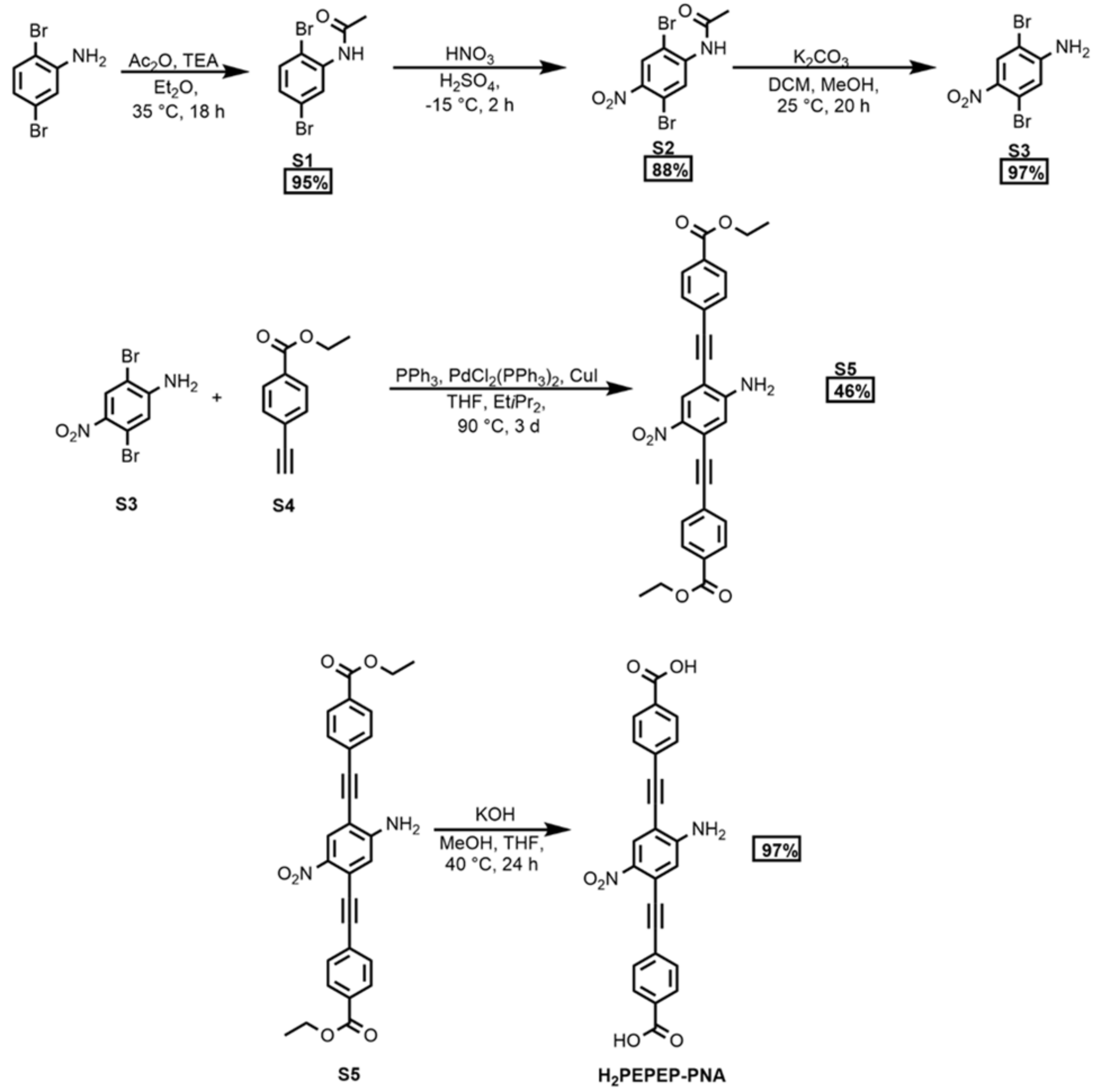

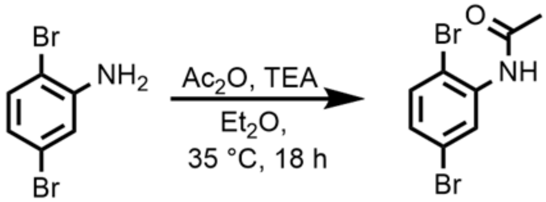

2,5-dibromoacetanilide (S1): 2,5-dibromoaniline (10.0 g, 39.85 mmol, 1 eq.) was added to a 250 mL two neck round bottom flask with a magnetic stir bar. Diethyl ether (30 mL) was added to the flask followed by acetic anhydride (22.56 mL, 239.1 mmol, 6 eq.). The solution was stirred at room temperature for 10 min. Triethylamine (6.11 mL, 43.84 mmol, 1.1 eq.) was added dropwise over 5 min. The mix was heated to 35 °C with stirring for 24 h, monitored by TLC. The reaction mixture was cooled to room temperature and then crashed out with water and filtered off to obtain a white solid. Yield 11.1 g (95%). ^{1}H NMR (400 MHz, $CDCl_3$, 25 °C) δ (ppm) 8.59 (s, 1H), 7.56 (s), 7.38 (d, *J* = 8.00 Hz, 1H), 7.10 (dd, *J* = 2.36, 6.168 Hz, 1H), 2.24 (s, 3H). ^{13}C NMR (100 MHz, $CDCl_3$, 25°C) δ (ppm) 168.36, 136.85, 133.19, 128.16, 124.59, 122.16, 111.60, 25.00. MS (ESI-TOF) *m/z* calculated for $C_8H_8Br_2NO$ $[M+H]^+$ 293.8947, found 293.8961.

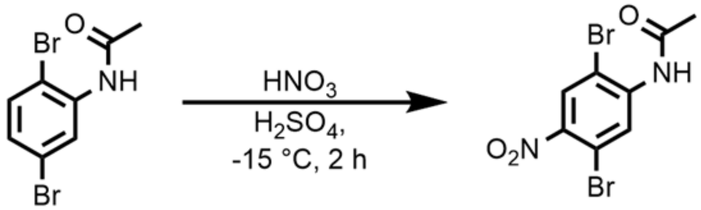

2,5-dibromo-4-nitroacetanilide (S2): Compound **S1** (11.1 g, 37.8 mmol, 1 eq.) was added to a 500 mL round bottom flask equipped with a magnetic stir bar. The flask was cooled in a salt/ice bath to -20 °C. Concentrated H_2SO_4 (50 mL, 945 mmol, 25 eq.) was added to the flask. Concentrated HNO_3 (15 mL, 363.0 mmol, 10 eq.) was added dropwise over 15 min followed by TLC. The solution was stirred keeping the temperature below -10 °C for 1 h. The reaction mixture was then poured over ice and the yellow precipitate was collected via vacuum filtration.. Yield 10.7 g (83%). ^{1}H NMR (400 MHz, $CDCl_3$, 25 °C) δ (ppm) 8.96 (s, 1H), 8.19 (s, 1H), 2.31 (s, 3H). ^{13}C NMR (101 MHz, $CDCl_3$, 25°C) δ (ppm) 168.45, 140.04, 135.39, 129.65, 125.89, 115.74, 110.49, 25.23. MS (ESI-TOF) *m/z* calculated for $C_8H_7Br_2N_2O_3$ $[M+H]^+$: 338.8803, found 338.8795.

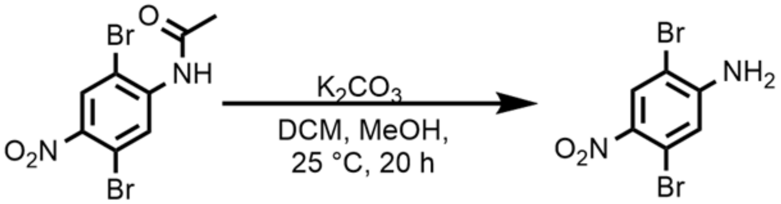

2,5-dibromo-4-nitroaniline (S3): In a 500 mL round bottom flask **S2** (10.65 g, 31.5 mmol, 1 eq.) was mixed with 150 mL of dichloromethane and 150 mL of methanol. Dry potassium carbonate (13.0 g, 94.5 mmol, 3 eq.) was added to the flask and the solution was stirred at room temperature for 20h followed by TLC. The product was then crashed out with water and filtered to obtain a bright yellow solid. Yield 9 g (97%). ^{1}H NMR (400 MHz, $CDCl_3$, 25 °C) δ (ppm) 8.25 (s, 1H), 7.03 (s, 1H), 4.74 (br s). ^{13}C NMR (101 MHz, $CDCl_3$, 25°C) δ (ppm) 138.73, 137.01, 124.29, 118.38, 116.59, 114.42. MS (ESI-TOF) *m/z* calculated for $C_6H_5Br_2N_2O_2$ $[M+H]^+$: 296.8692, found 296.8706.

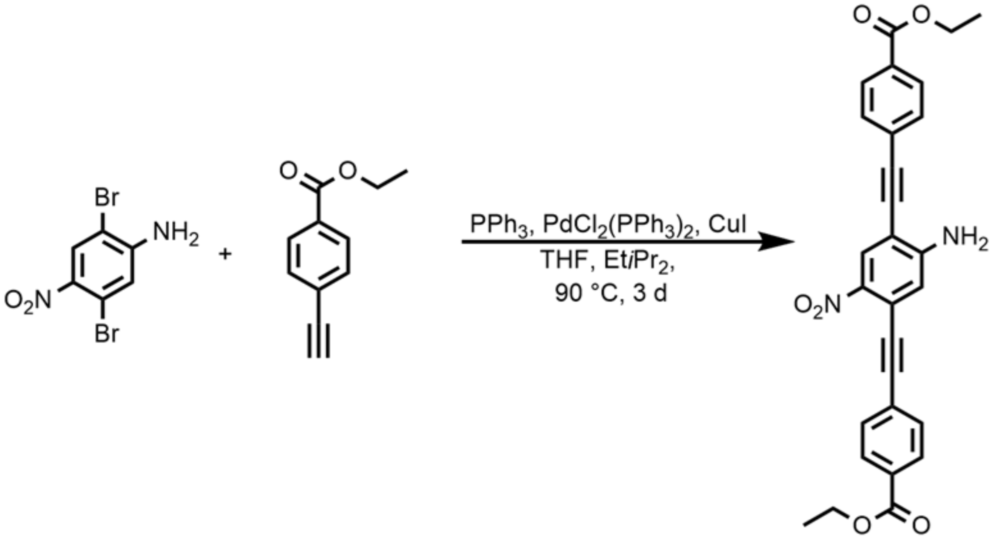

Diethyl 4,4'-((2-amino-5-nitro-1,4-phenylene)bis(ethyne-2,1-diyl))dibenzoate (S5): To a 50 mL Schlenk flask was added **S3** (0.74 g, 2.5 mmol, 1.0 eq), ethyl 4-ethynylbenzoate (1.52 g, 8.75 mmol, 3.5 eq), CuI (0.048 g, .025 mmol, 0.1 eq), PPh_3 (0.131g, 0.5 mmol, 0.2 eq), and $Pd(PPh_3)Cl_2$ (0.12 g, 0.7 mmol, 0.07 eq). The flask was evacuated to 100 mtorr and backfilled with N_2 (3x). Anhydrous air free THF (25 mL) and $NEt(iPr_2)$ (2.1 mL) were then added, and the reaction was heated to reflux for 72 h. The reaction was cooled to room temperature and quenched with water, followed by extraction with EtOAc (3, 20 mL). The organic layers were combined and washed with brine, dried over Na_2SO_4, filtered through a silica plug, and the solvent was removed under reduced pressure in a rotary evaporator. The crude product was loaded onto silica and purified by flash column chromatography (SiO2, 20% ramped to 60% v/v EtOAc/hexanes) resulting in a brownish-yellow crystals (compound contains some mono product impurity but its removed by purification in the hydrolysis step). Synthesis does not scale well above these masses. Yield 550 mg (45.8 %). ^{1}H NMR (400 MHz, $CDCl_3$) δ 8.32 (s, 1H), 8.06 (dd, *J* = 8.6, 5.6 Hz, 4H), 7.64 (d, *J* = 22.3 Hz, 4H), 6.97 (s, 1H), 4.94 (s, 2H), 4.37 (s, 5H), 1.42 (s, 8H). ^{13}C NMR (101 MHz, DMSO) δ 132.80, 132.69, 121.44, 103.93, 99.54, 98.50, 97.83, 97.30, 97.14, 96.81, 94.39, 94.07, 87.07, 85.79, 72.55, 63.09, 62.30, 56.64, 54.65, 28.72, 28.64, 12.74, -18.23. MS (ESI-TOF) *m/z* calculated for $C_{28}H_{23}N_2O_6$ [M+H]$^+$: 483.1551, found 483.1315.

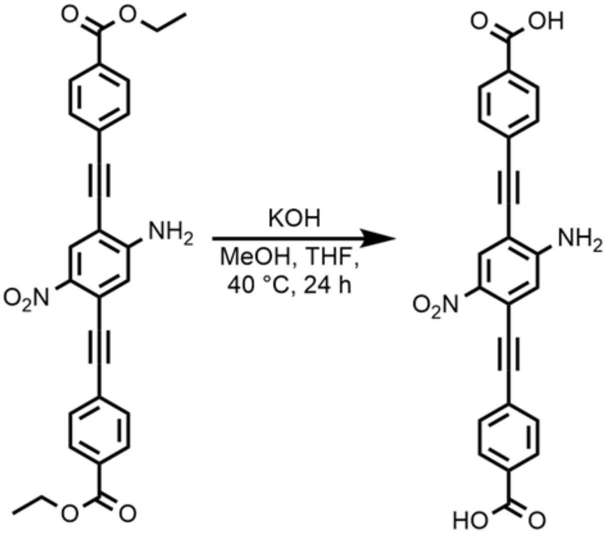

4,4'-((2-amino-5-nitro-1,4-phenylene)bis(ethyne-2,1-diyl))dibenzoic acid (H_2PEPEP-PNA): 5.0 M aqueous KOH (7 mL, 35 mmol, 35 eq.) was placed in a 25 mL round bottom flask with a magnetic stir bar. **S4** (.55 g, 1.14 mmol, 1 eq.) was dissolved in 20 mL of THF and was added to the potassium hydroxide solution. The mixture stirred at room temperature for 24 h. The reaction was quenched with 1 M hydrochloric acid (35 mL). The resulting precipitate was collected with vacuum filtration and was washed with water and cold MeOH to yield a dark brown/black solid. The compound was then dissolved in DMF and filtered over nylon, subsequently crashed out with water and refiltered over nylon to collect a black solid. Yield 0.471 g (97%). ^{1}H NMR (400 MHz, DMSO) δ 13.19 (s, 2H), 8.25 (s, 1H), 8.01 (s, 4H), 7.85 (s, 2H), 7.72 (s, 2H), 7.13 (s, 2H), 7.06 (s, 1H). ^{13}C NMR (101 MHz, DMSO) δ 167.20, 167.10, 154.27, 136.78, 132.34, 132.25, 131.66, 131.27, 131.13, 130.20, 130.15, 129.82, 126.84, 126.56, 119.94, 118.56, 105.44, 96.05, 95.29, 89.23, 87.18, 49.07. MS (ESI-TOF) *m/z* calculated for $C_{24}H_{15}N_2O_6$ [M+H]$^+$: 425.0779, found 425.2656 .

Synthesis of MTV MOFs $Zr_6O_4(OH)_4[(PNA(PEPEP)_x(Xylene\ PEPEP)_{1-x}]_6$

Stock solutions of the **PEPEP-PNA** and **PEPEP-Me** links (0.05 M in DMF) were prepared and dispensed at varying mole ratios (0.05 mmol total, 1.0 eq total) into a 20 mL vial to a total volume of 1.0 mL (Table 1). Proline (0.029 g, 0.25 mmol, 5 eq), and $ZrCl_4$ (1.04 mL, 0.049 M, 0.012 mg, 0.05 mmol, 1 eq) were then added and the solution was mixed in an ultrasound bath for 10 min. Hydrochloric acid in DMF (0.237 M, 0.23 mL, 0.055 mmol,1.1 eq) was added and the mix was sonicated for an additional ten minutes. The solution was then transferred to an 8 mL conical glass vial and sealed with a glass stopper. The vial was placed in an isothermal 120 °C oven for 24 h, after which, the vial was cooled to room temperature and the solids were isolated by filtration. The solids were rinsed with DMF (20 mL) followed by CH_2Cl_2 or THF(20 mL) . The collected crystals were then immersed in DMF for one day, where the DMF was decanted twice and replaced with fresh DMF, repeating the process for three days. The crystals were then immersed in anhydrous THF for two more days decanting three times per day. Yield 25 mg (89% based on).

Table S1: Stoichiometric ratios for MTV library synthesis

x **(mol%)**	$V_{\text{PEPEP-PNA}}$ **(µL)**	$V_{\text{PEPEP-Me}}$ **(µL)**	**mmol PEPEP-PNA**	**mmol PEPEP-Me**	**Yield (mg)**
4	40	960	0.002	0.048	22.69
6	60	940	0.003	0.047	22.72
8	80	920	0.004	0.046	23.80
10	100	900	0.005	0.045	22.78
12	120	880	0.006	0.044	22.92
20	200	800	0.010	0.040	23.06
30	300	700	0.015	0.035	23.20
40	400	600	0.033	0.022	23.35
50	500	500	0.028	0.028	22.78

Synthesis of x = 100 mol% $Zr_6O_4(OH)_4[(PNA(PEPEP)_x(Xylene\ PEPEP)_{1-x}]_6$.

PEPEP-PNA (33.78 mg, 0.079 mmol, 1.0 eq) and zirconium chloride (20.3 mg, .079 mmol, 1.1 eq) was added to a 20 mL vial, followed by DMF (4.32 mL), and acetic acid (0.44 mL, 95 eq). The solution was then sonicated for 5 min and added to an 8 mL conical vial. The vial was sealed with a glass stopper and placed in the oven at 100 °C for 2 days. The solution was then cooled and filtered by washing with DMF followed by DCM. The solids were solvent exchange for 3 d with DMF, followed by THF for 3 d. The solids were then filtered and dried under high vacuum at 50 mTorr. The samples were activated under high vacuum at 120 C° for 12 h in the sample tube for gas adsorption or in the BDS cellfor dielectric spectroscopy.

Section S3. Powder X-ray diffraction crystallography

Figure S1. PXRD of **PEPEP-PNA** and **PEPEP-Me** bulk powders input *x* = 0-12 mol%.

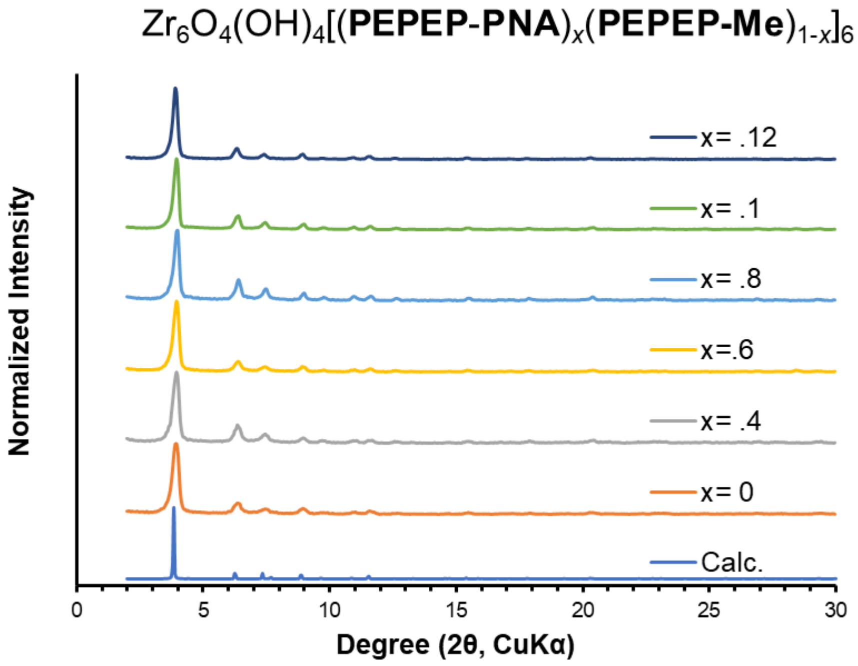

Figure S2. PXRD of **PEPEP-PNA** and **PEPEP-Me** bulk powders input x= 0-100%. Note that the non-catenated MOF, which crystallize in *Fm*-3*m* space group (No. 225), observes an allowed 200 peak at *ca*. 4.5 degrees (2-theta). This is because the reflection condition for h00 in *Fm*-3*m* is *h* = 2*n*. In the catenated phase, with Fd-3m space group (No. 227), the reflection condition changes to *h*00: *h* = 4*n*, resulting in the loss of 200 peak as a systematic absence.

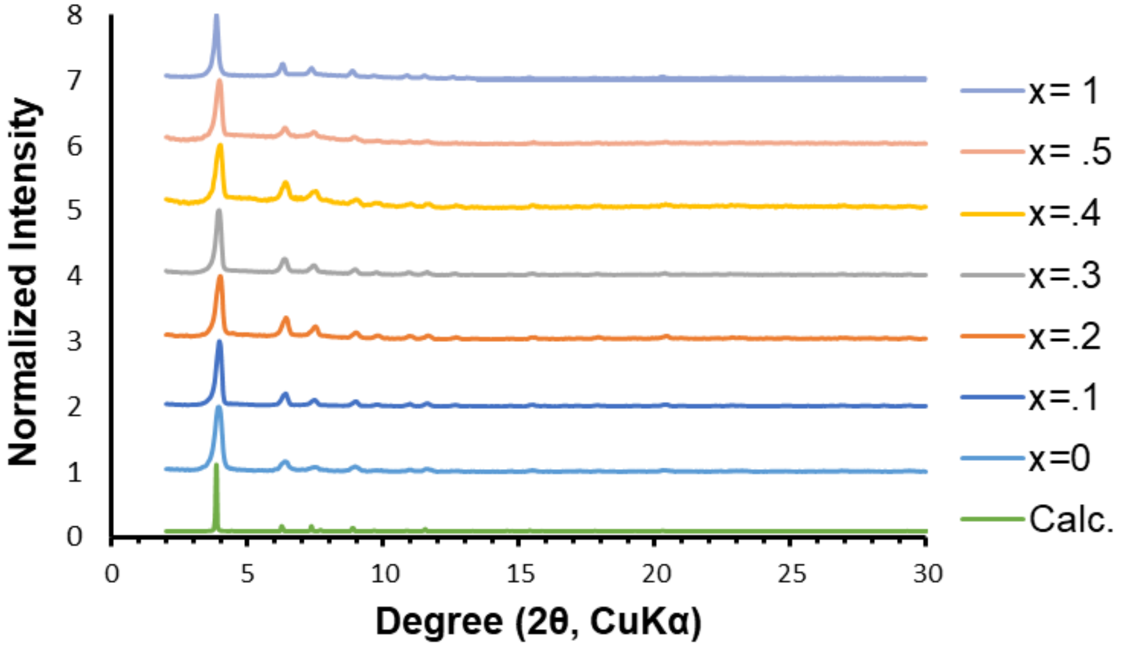

Table S2: Pawley refinements results. Pawley plots can be found in page S81.

x **(mol% input)**	***a*** **(Å)**	***Rp*** **(%)**	***wRp*** **(%)**
10	39.674(24)	13.26	16.81
20	39.7321(7)	17.75	22.59
30	39.687(40)	9.30	12.35
40	39.964(9)	10.14	12.33
50	39.843(16)	14.36	18.37
100	39.872(13)	7.22	8.70

Section S4. Molar output/input composition

General procedure for MOF digestion and composition analysis via NMR of PEPEP system. 4.0 mg of MOF were dissolved in a 4 mL vial containing 20 µL of D_2SO_4, followed by 0.6 mL of DMSO-d_6. The vial was immersed in an ultrasonic bath for 2 min and placed in the oven for 3 min until all solid was completely dissolved. The solutions were then transferred to an NMR tube. NMR data was processed using MNova version 9.0.1.

Figure S3. NMR compositional analysis output/Input Ratios of **PEPEP-PNA** and **PEPEP-Me** MOFs.

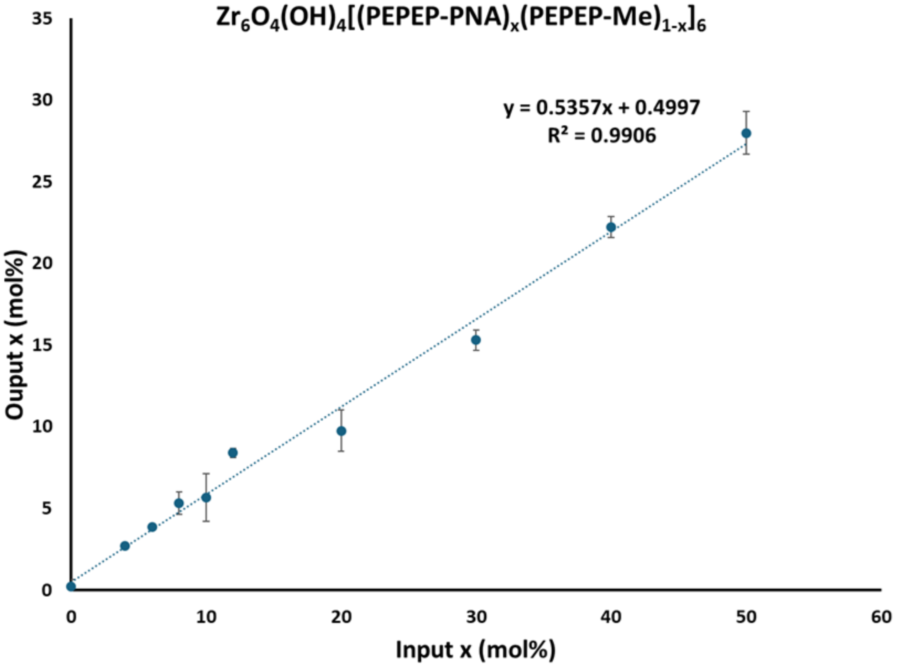

Table S3: Input/output compositions of MTV library.

Input (mol%)	Output (mol%)
0	0.22 ± 0.41
4	2.72 ± 0.12
6	3.85 ± 0.14
8	5.33 ± 0.68
10	5.67 ± 1.45
12	8.39 ± 0.29
20	9.75 ± 1.27
30	15.30 ± 0.64
40	22.22 ± 0.64
50	27.98 ± 1.32

Figure S4. Stacked ^{1}H NMR from MOF decomposition in DMSO-d_6. Integration values from the chemical shifts at 7.9 ppm and 7.58 ppm were used to calculate the output ratios of **PEPEP-PNA** to **PEPEP-Me**.

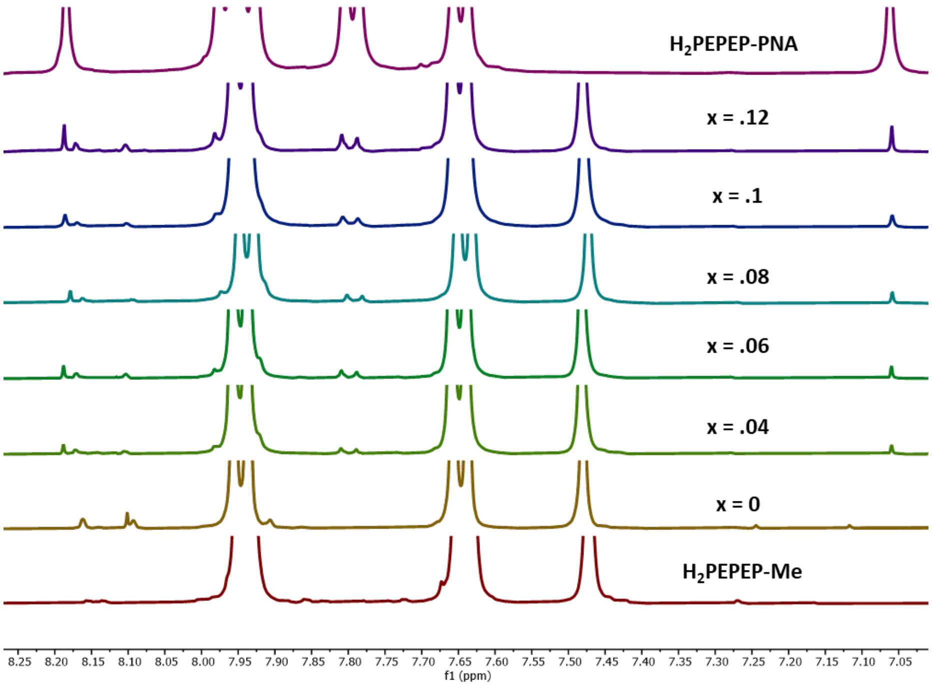

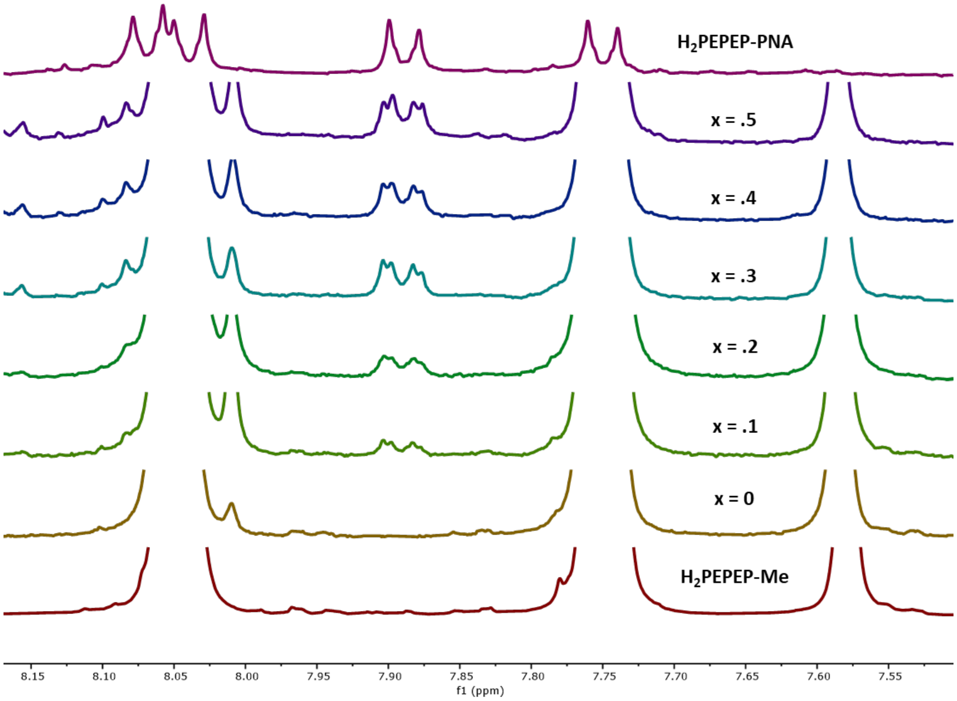

Determination of molar concentration and average intermolecular distance. The molar concentration of links in the MOF in units of mmol dm–3 was obtained from the average unit cell (*Fd*-3*m*). In this unit cell, there are 48 links/u.c. (center of the links is located in the 48*f* Wyckoff position). The experimental cell volume was obtained from Reference 3 (63420 Å^3):

$$[links] = \frac{48\ links}{63420\ \text{Å}^3} = 1250\ mmol_{links}\ dm^{-3}_{crystal}$$

and

$$[\textbf{PEPEP-PNA}] = x \cdot [links] = x \cdot \left(1250\ mmol_{links}\ dm^{-3}_{crystal}\right)$$

The average distance between solutes is calculated according to:

$$\langle r_i \rangle = (N_A c_i)^{-\frac{1}{3}}$$

where:
N_A= Avogadro number
c_i = i $^{\text{th}}$ concentration

Table S4. Molar concentration of PEPEP-PNA in the MTV library.

x output (mol%)	[**PEPEP-PNA**] (mmol dm^{-3})	$\langle r \rangle$ (Å)
0	0	0
1	13	51
1.6	20	44
3.2	40	35
5.9	74	28
11.9	149	22
16.6	208	20
21.9	274	18
27.3	341	17
100	1250	11

Section S5. Solution and Solid State UV-Visible spectroscopy

General procedure for adsorption and emission measurements. A 10 mM solution of each link was prepared by dissolving 20 mmol of compound **S5** and in 2 mL of 1,2-dichloroethane or DMF.

Figure S5. Solution UV-Vis absorbance spectra of **PEPEP-PNA** ester linker (**S5**) in 1,2-dichloroethane at 2.5, 5, 7.5, and 10 mM.

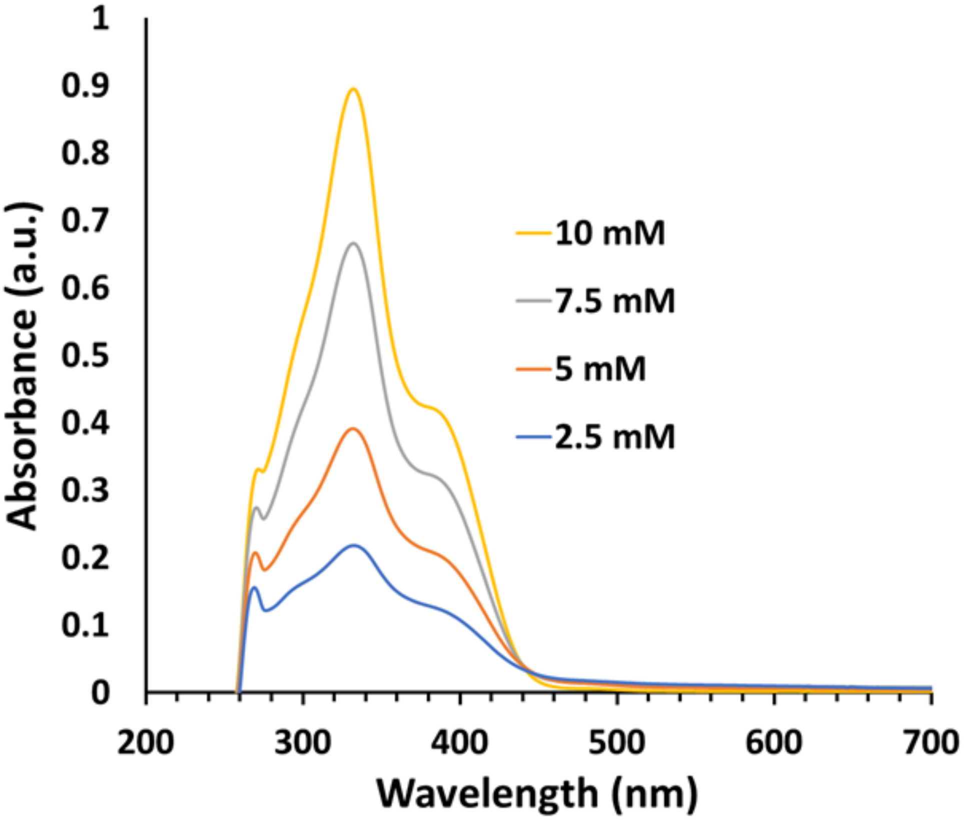

Figure S6. Solution UV-Vis absorption spectra of **PEPEP-Me** ester link in 1,2-dichloroethane at 2.5, 5, 7.5, and 10 mM.

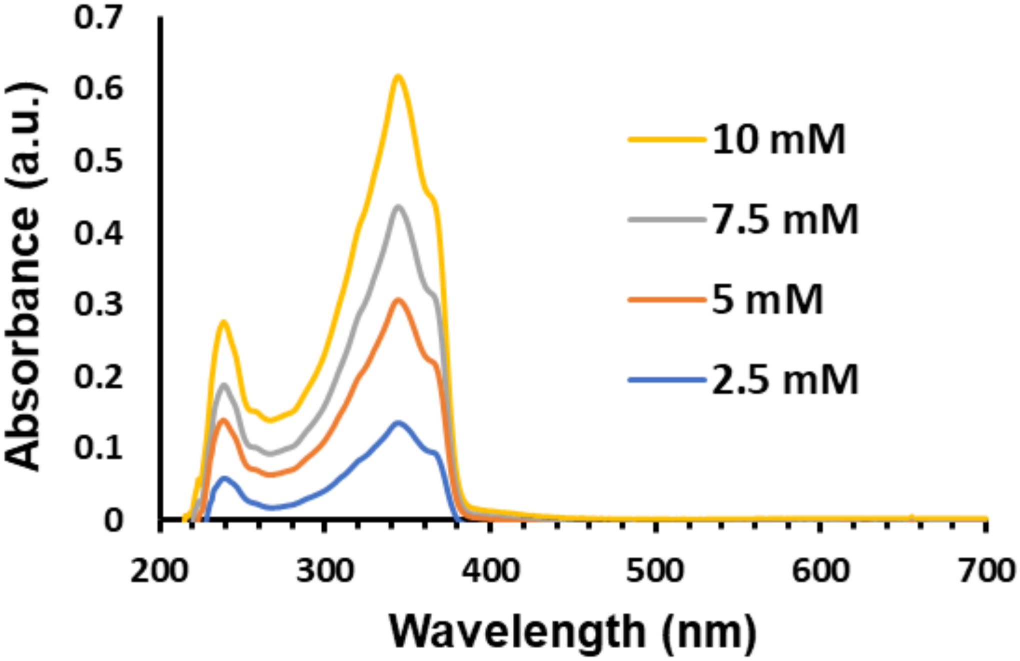

Figure S7. Solution UV-Vis fluorescence spectrum of **PEPEP-PNA** ester (**S5**) in dichloroethane (λ_{ex} = 332 nm).

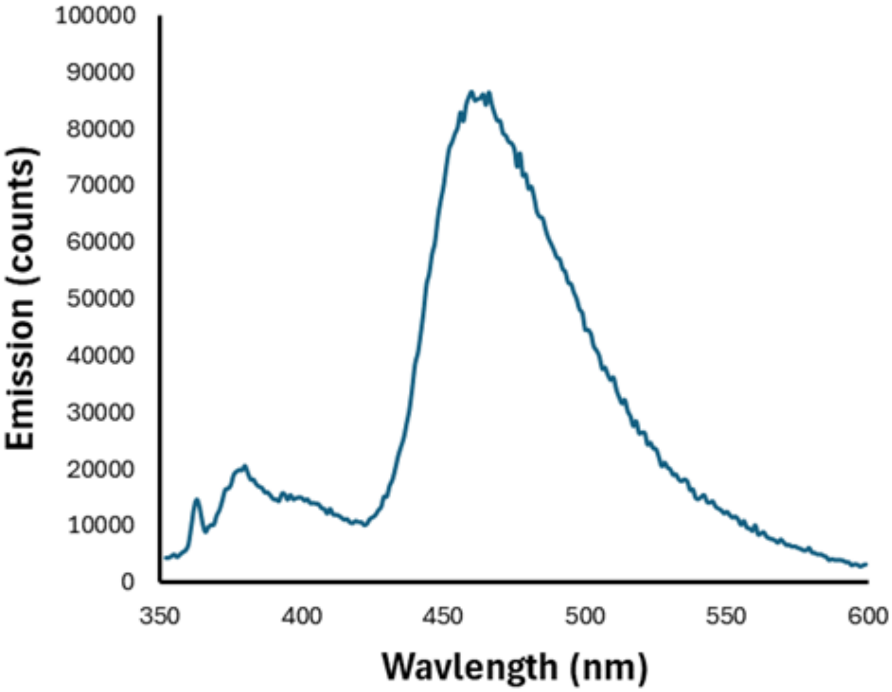

Figure S8. Solution UV-Vis fluorescence spectrum of **PEPEP-PNA** ester (**S5**) in DMF (λ_{ex} = 332 nm).

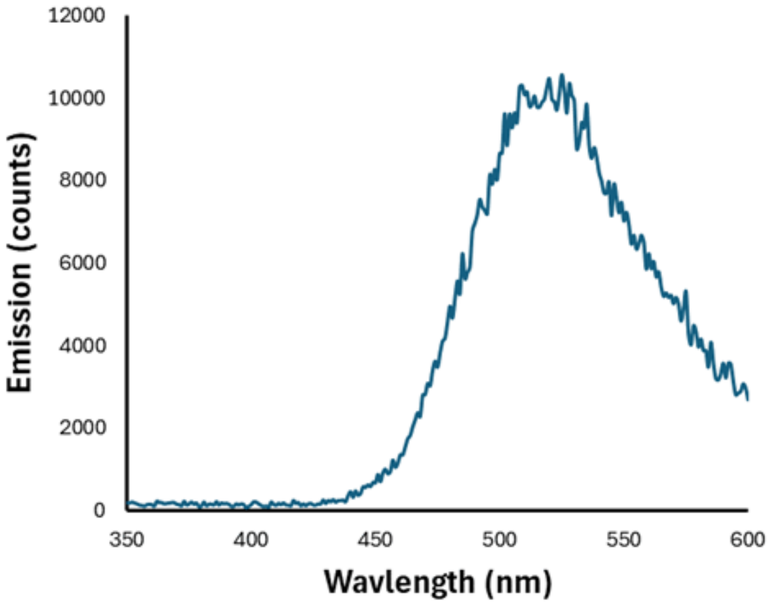

Figure S9. Solid State Diffuse Reflectance spectrum of **PEPEP-PNA/PEPEP-Me** MOFs. Output concentration is indicated.

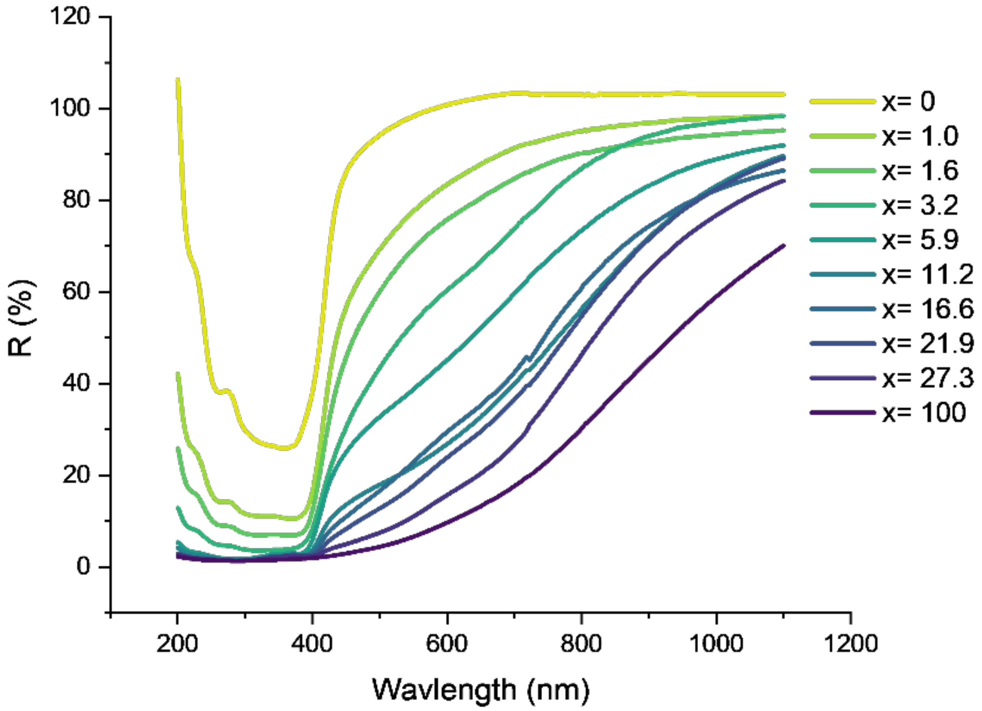

Figure S10. Absorption spectrum of **PEPEP-PNA/PEPEP-Me** MOFs. Output concentration is indicated.

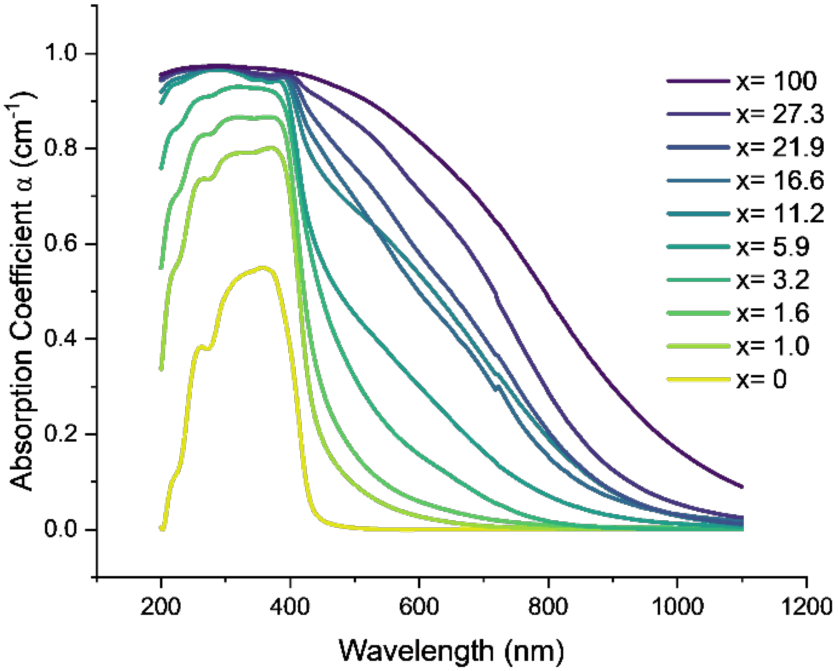

Figure S11. Scattering spectra of **PEPEP-PNA/PEPEP-Me** MOFs. Output PNA concentration is indicated.

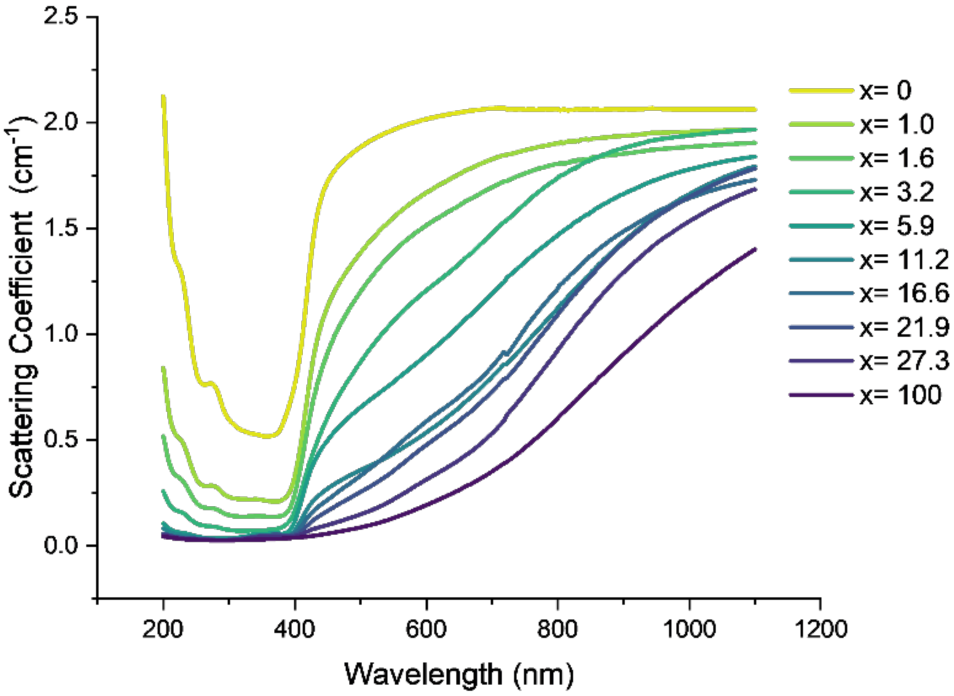

Figure S12. Kubelka Munk vs wavelength of **PEPEP-PNA** and **PEPEP-Me** MOFs.

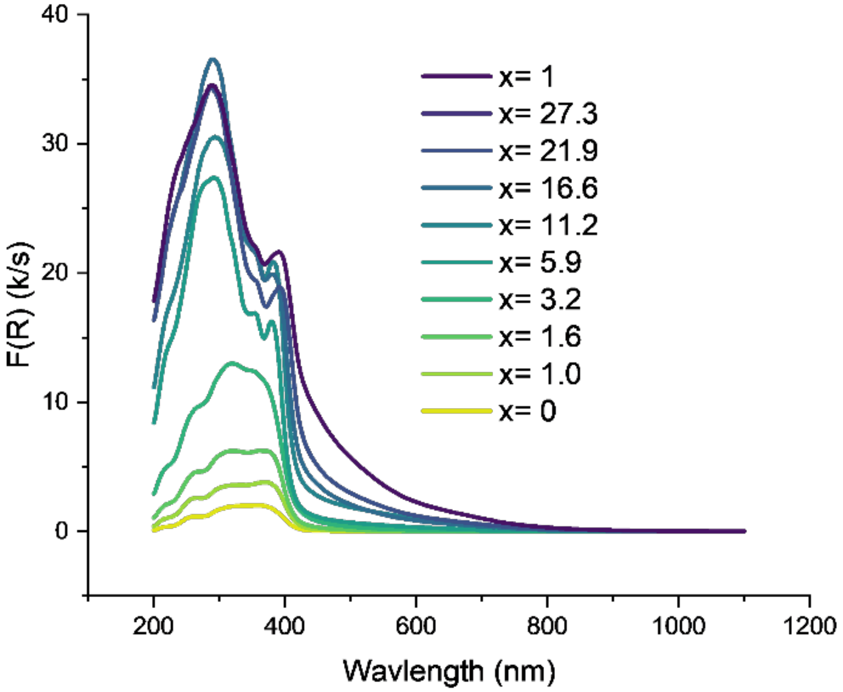

Figure S13. Absorbance coefficient versus wavelength of low concentration **PEPEP-PNA** and **PEPEP-Me** MOFs (x= mol%).

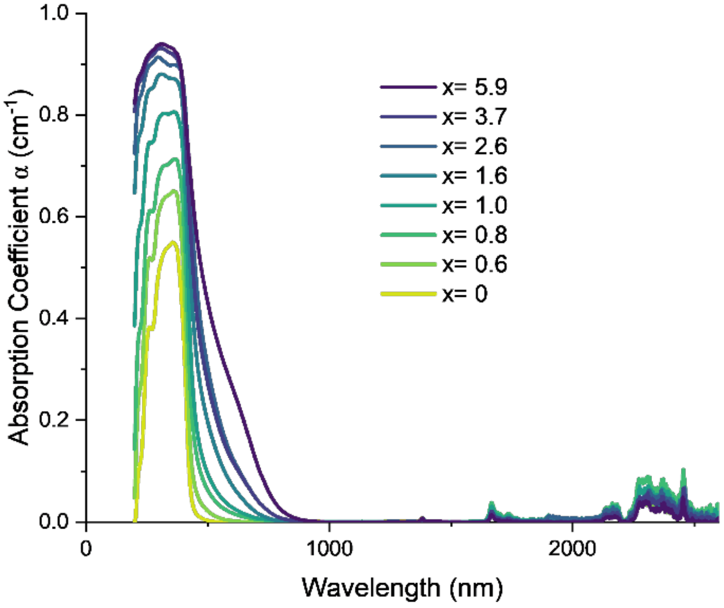

Table S5. Optical gaps determined by Tauc analysis using direct bandgap equation.

x (output mol %)	Optical gaps (eV)	
0	3.03	
1.0	3.02	
1.6	3.04	
3.2	3.06	
5.9	3.07	3.48
11.2	3.02	3.33
16.6	3.09	3.33
21.9	2.93	3.49
27.3	2.88	3.38
100	2.85	3.38

Figure S14. Tauc plot of *x* = 0 mol% **PNA-PEPEP** MOFs.

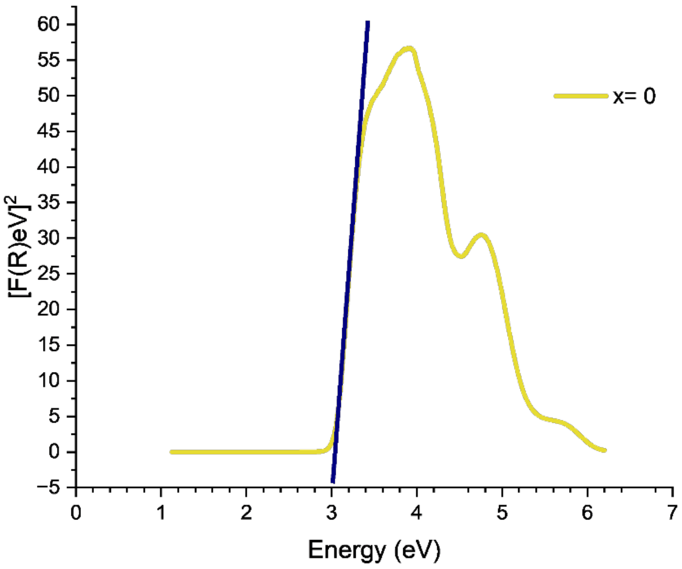

Figure S15. Tauc plot of *x* = 1 mol% **PNA-PEPEP** MOFs.

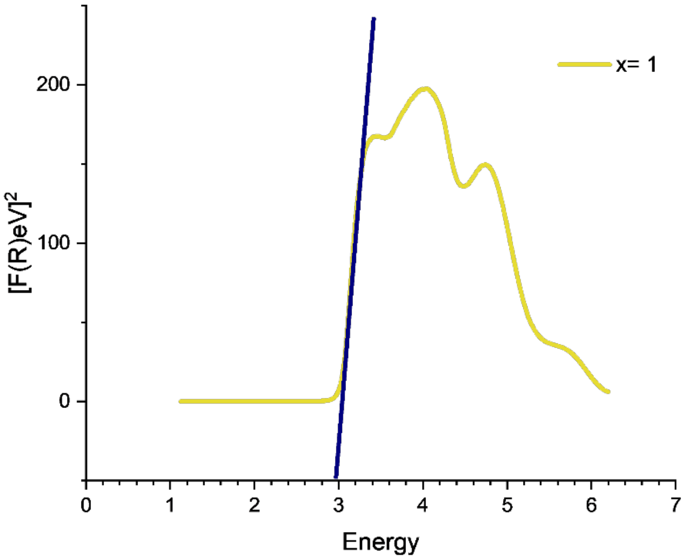

Figure S16. Tauc plot of *x* = 1.6 mol% **PNA-PEPEP** MOFs.

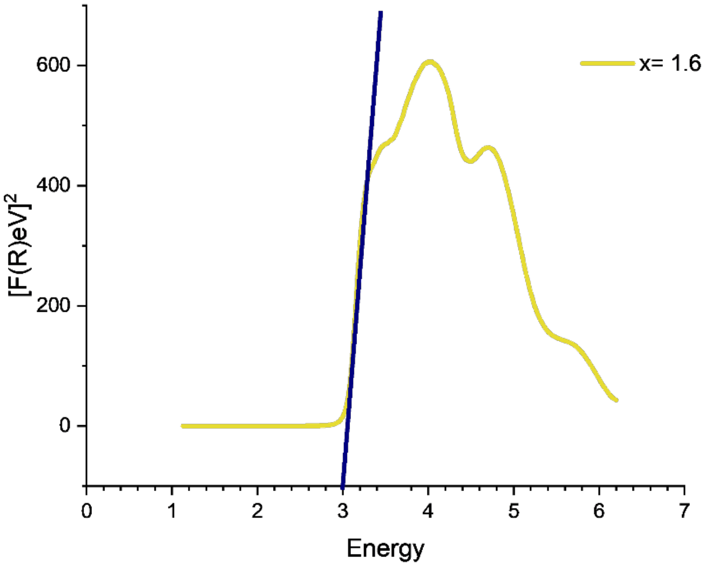

Figure S17. Tauc plot of *x* = 3.2 mol% **PNA-PEPEP** MOFs.

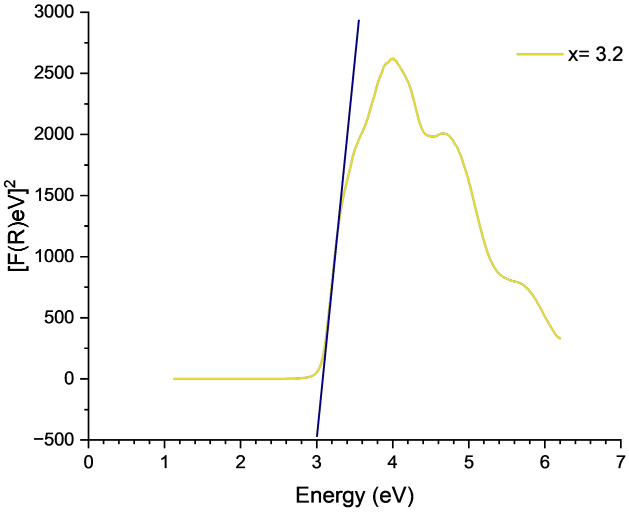

Figure S18. Tauc plot of *x* = 5.9 mol% **PNA-PEPEP** MOFs.

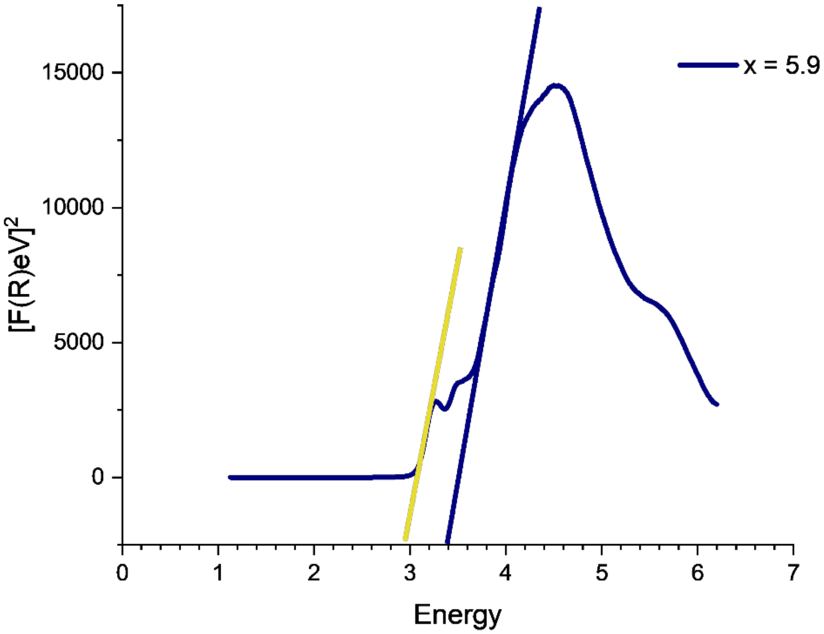

Figure S19. Tauc plot of *x* = 11.2 mol% **PNA-PEPEP** MOFs

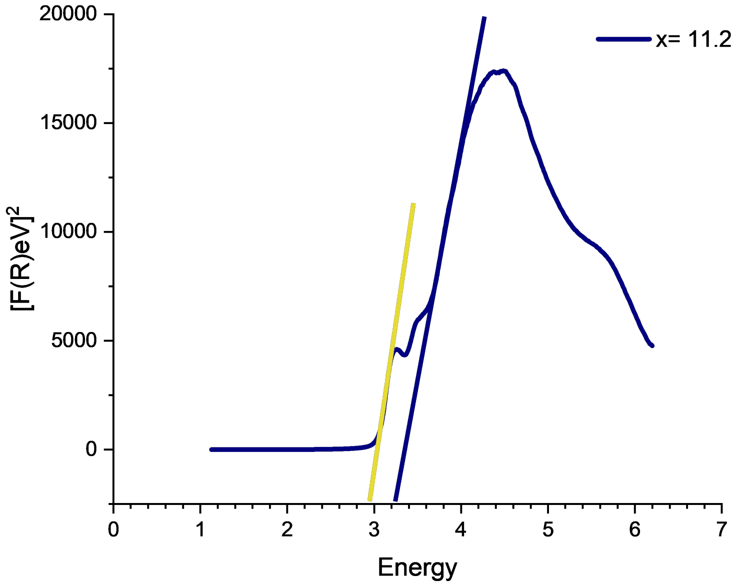

Figure S20. Tauc plot of *x* = 16.6 mol% **PNA-PEPEP** MOFs.

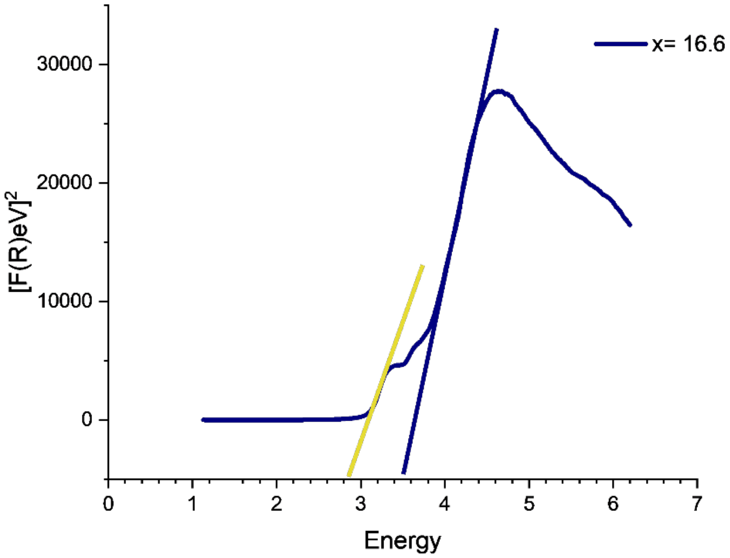

Figure S21. Tauc plot of *x* = 21.9 mol% **PNA-PEPEP** MOFs.

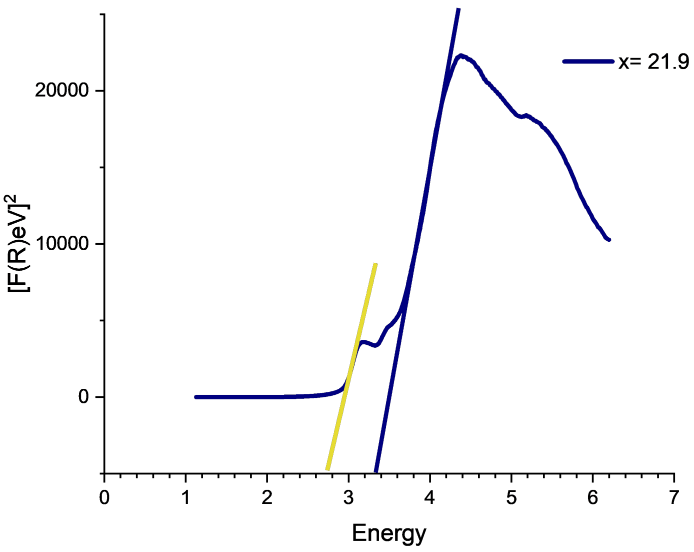

Figure S22. Tauc plot of *x* = 21.9 mol% **PNA-PEPEP** MOFs.

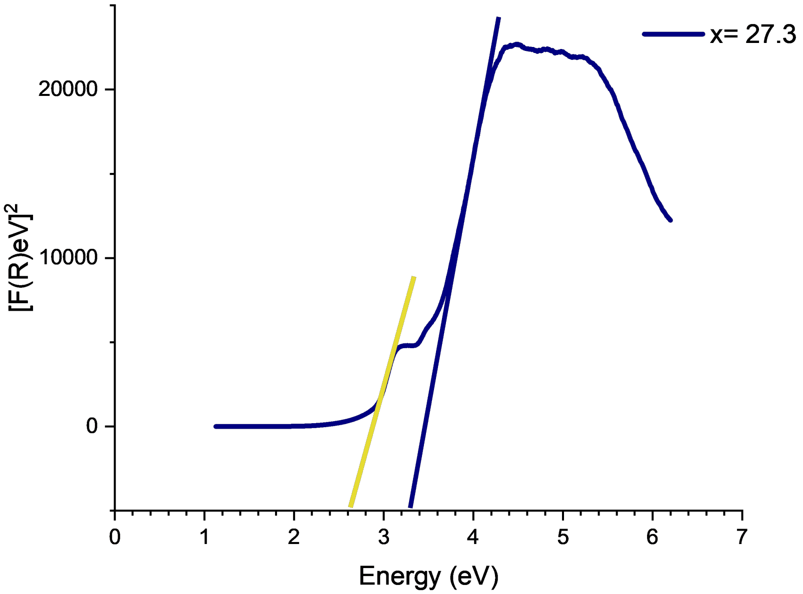

Figure S23. Tauc Plots of **PNA-PEPEP** and **PEPEP-Me** MOFs (x = 100 mol%).

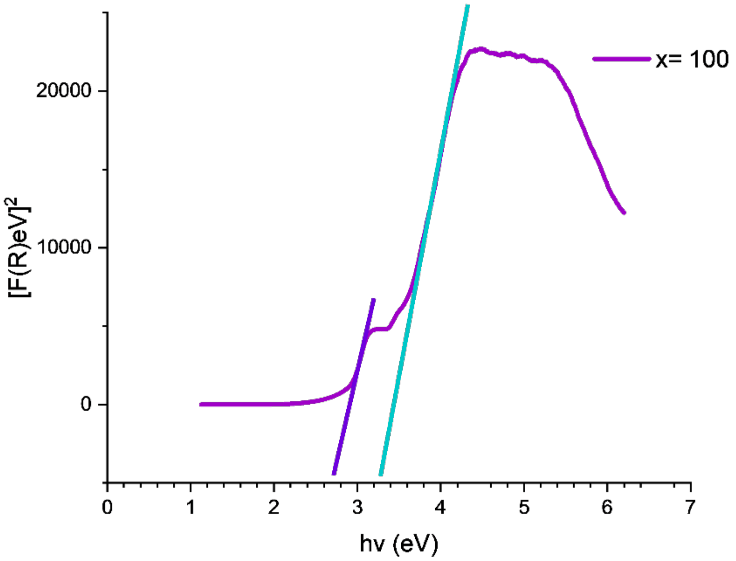

Figure S24. Solid State UV-Vis excitation (yellow) and emission (blue) of *x* = 0 mol%.

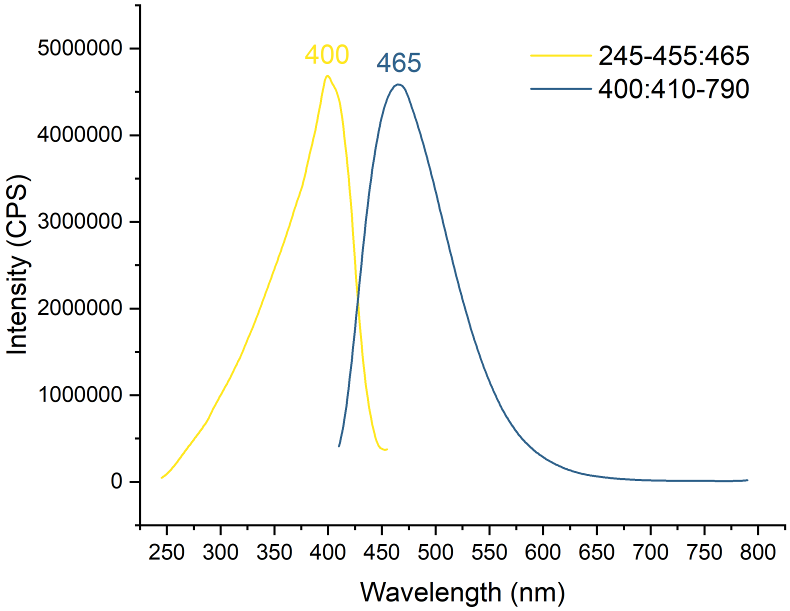

Figure S25. Solid State UV-Vis excitation (cyan) and emission (teal) of *x* = 100 mol%

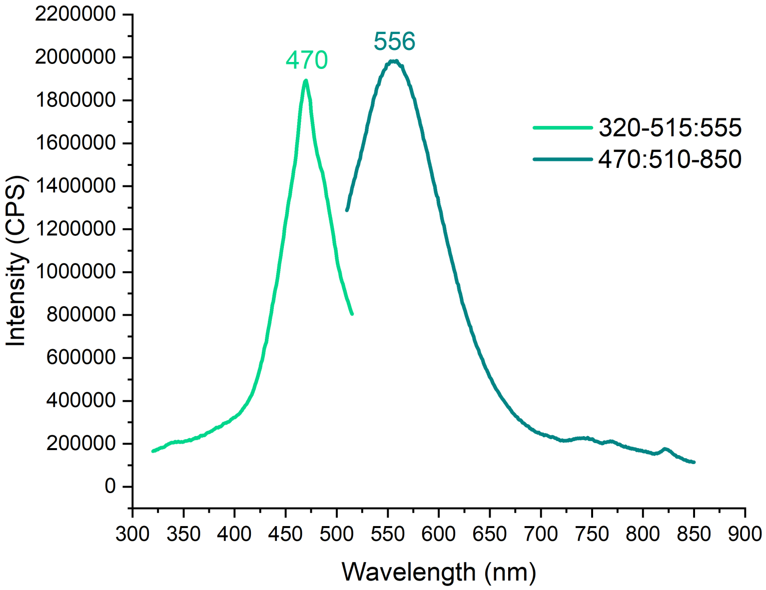

Figure S26. Solid State UV-Vis Emission (λ_{ex} = 400 nm), λ_{max} is indicated.

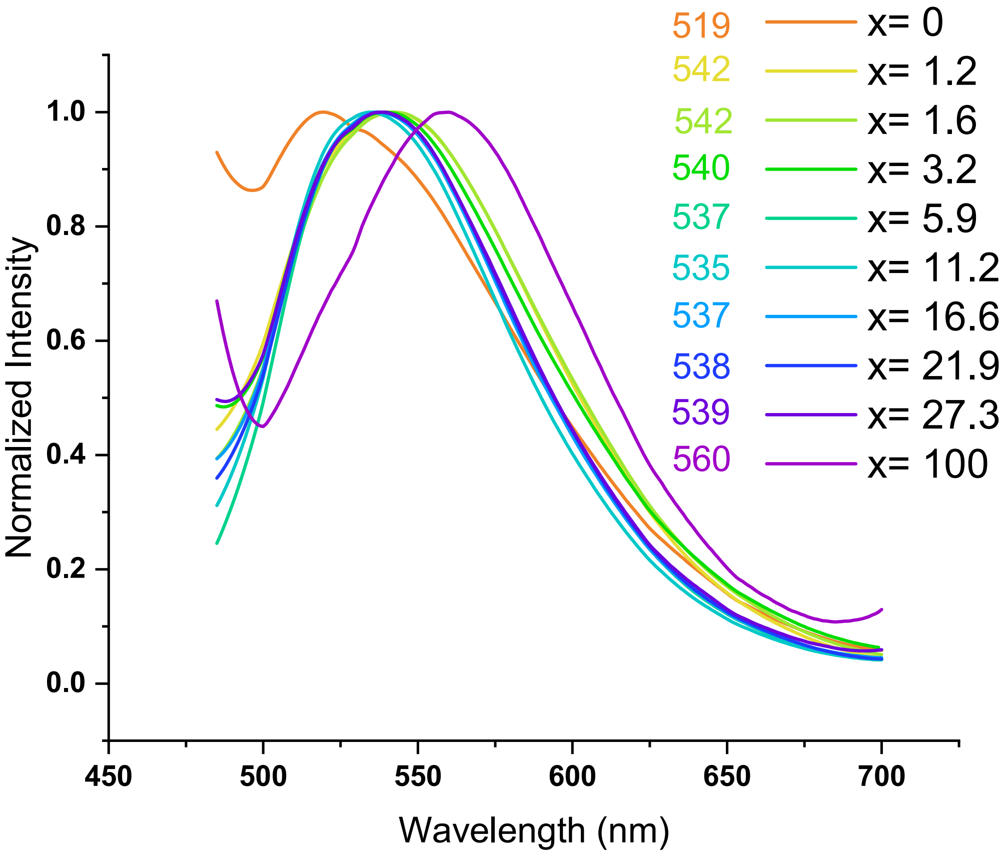
519
542
542
540
537
535
537
538
539
560
x= 0
x= 1.2
x= 1.6
x= 3.2
x= 5.9
x= 11.2
x= 16.6
x= 21.9
x= 27.3
x= 100
Normalized Intensity
1.0
0.8
0.6
0.4
0.2
0.0
450
500
550
600
650
700
Wavelength (nm)

Section S6: Scanning electron microscopy and particle size analysis

Electron microscope images were taken on a TM3000 tabletop microscope by placing a small amount of sample on carbon fiber tap and streaking the MOFs across the surface using a spatula to make a uniform surface across the carbon tape. Images were loaded into ImageJ[S4] and the scale was set according to the magnification of the image and some images were sharpened to aid in distinguishing between small particle boundaries. A total of three images for each composition (samples used for the broadband dielectric spectroscopy as well as diffuse reflectance data presented in the manuscript) was evaluated by finding the length of the particles using a total of 50 data points for each image and the data was pooled to find the confidence interval of the particles using Seaborn.[S5] Histogram plots were made to show particle size distribution by placing the particle size into 4 bins.

Table S6. 95% confidence intervals of each composition determined by pooling data.

x (mol%)	**confidence interval (μm)** ***z*** **= 1.96 (95%)**
0	14.880 ± 0.611
3.2	18.796 ± 0.586
5.9	9.510 ± 0.396
11.2	7.421 ± 0.241
16.6	18.478 ± 1.435
21.9	12.884 ± 0.781
27.3	12.730 ± 0.895
100	14.303 ± 1.301

Figure S27. SEM Image x = 0 mol % **PEPEP-PNA/PEPEP-Me** MOF**.**

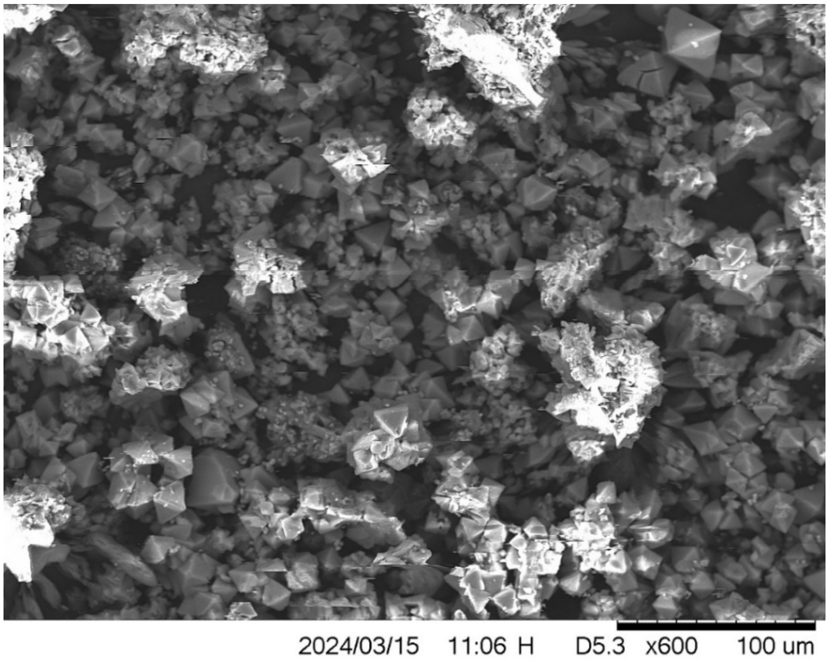

Figure S28. Particle size distribution of *x* = 0 mol% **PEPEP-PNA/PEPEP-Me** MOF.

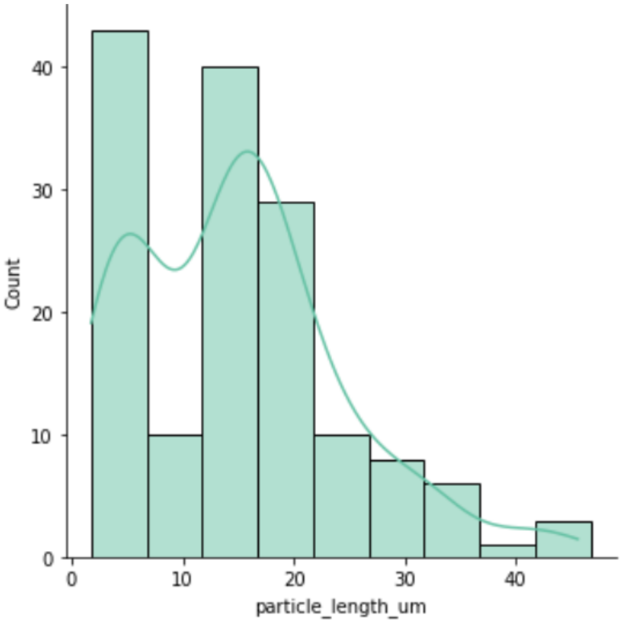

Figure S29. SEM Image x = 3.2 mol % **PEPEP-PNA/PEPEP-Me** MOF**.**

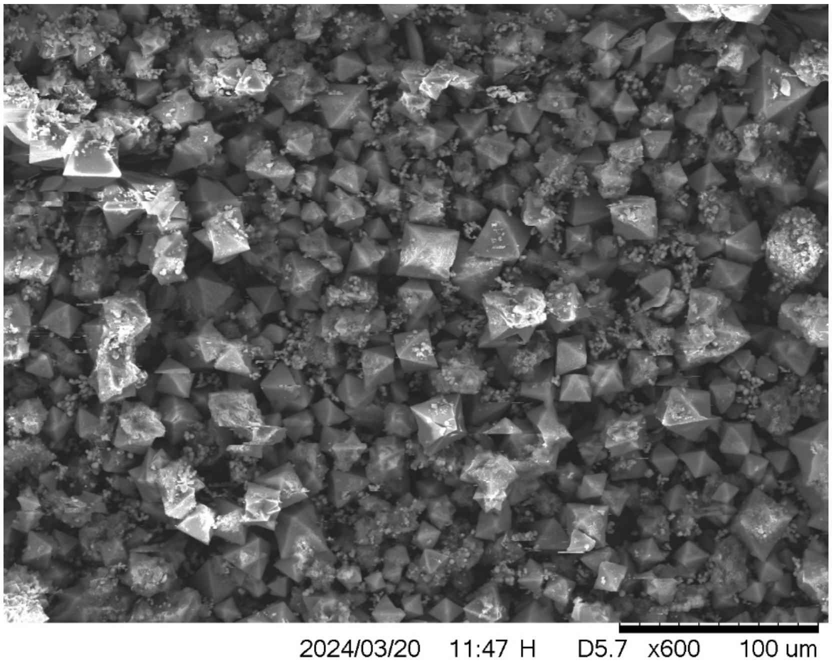

Figure S30. Particle size distribution of x = 3.2 mol% **PEPEP-PNA/PEPEP-Me** MOF.

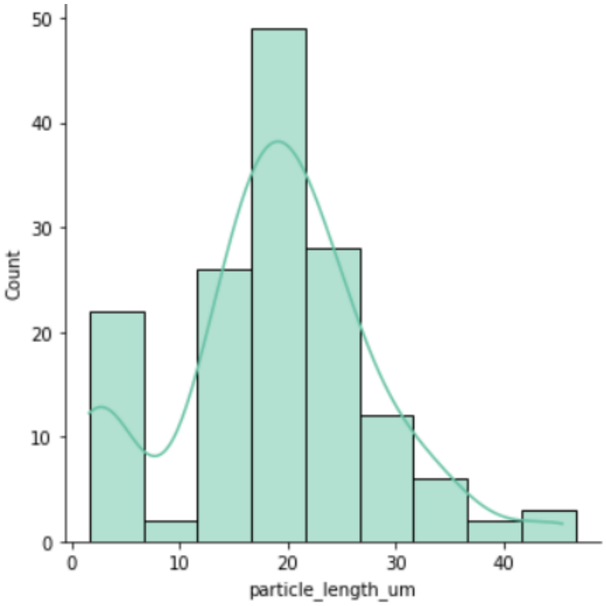

Figure S31. SEM Image *x* = 5.9 mol% **PEPEP-PNA/PEPEP-Me** MOF**.**

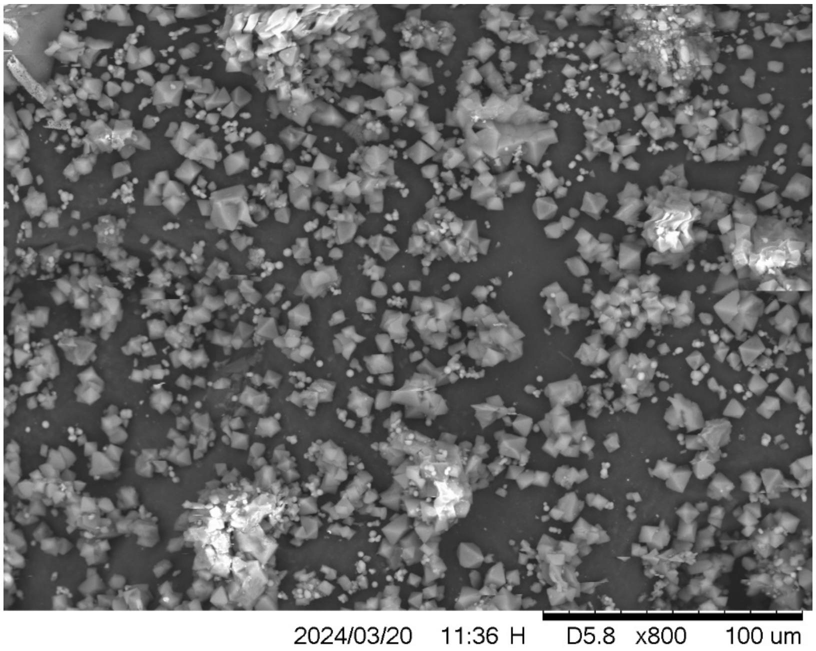

Figure S32. Particle size distribution of *x* = 5.9 mol% **PEPEP-PNA/PEPEP-Me** MOF.

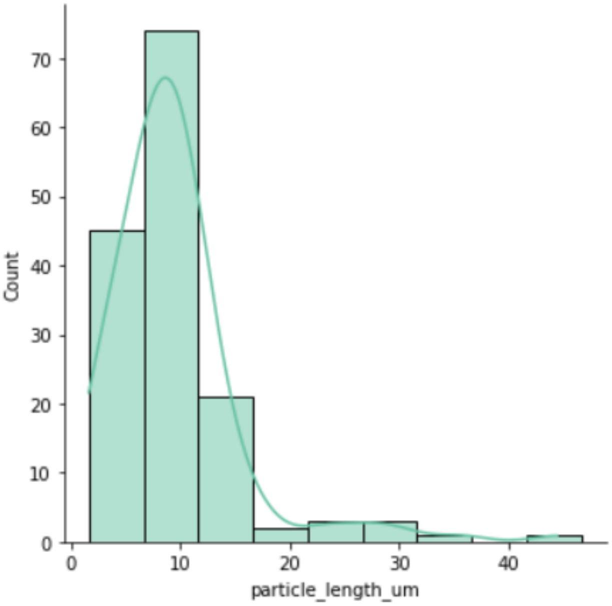

Figure S33. SEM Image *x* = 11.2 mol% **PEPEP-PNA/PEPEP-Me** MOF**.**

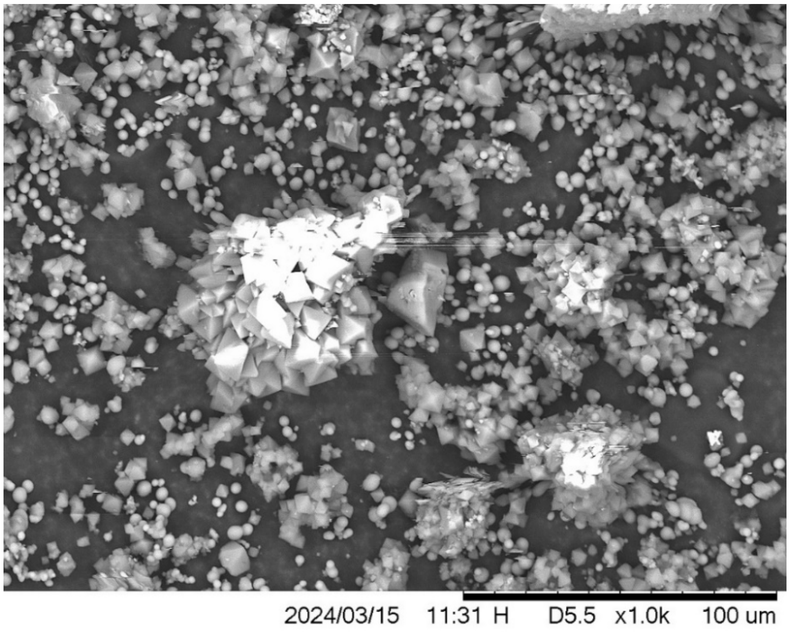

Figure S34. Particle size distribution of *x* = 11.2 mol% **PEPEP-PNA/PEPEP-Me** MOF.

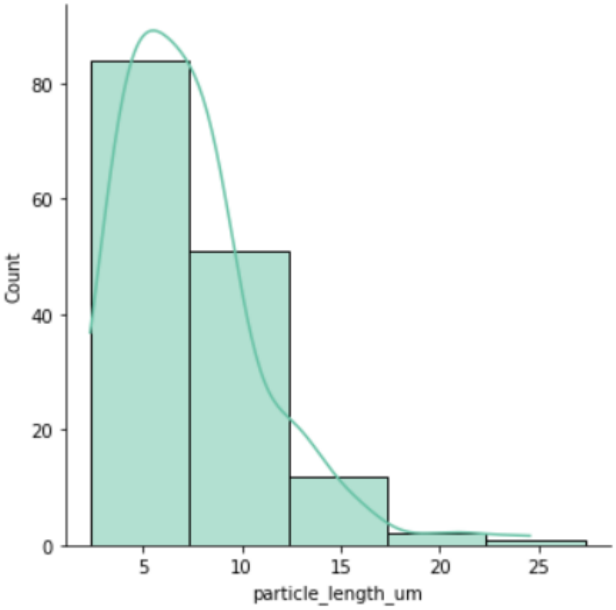

Figure S35. SEM Image *x* = 16.6 mol% **PEPEP-PNA/PEPEP-Me** MOF**.**

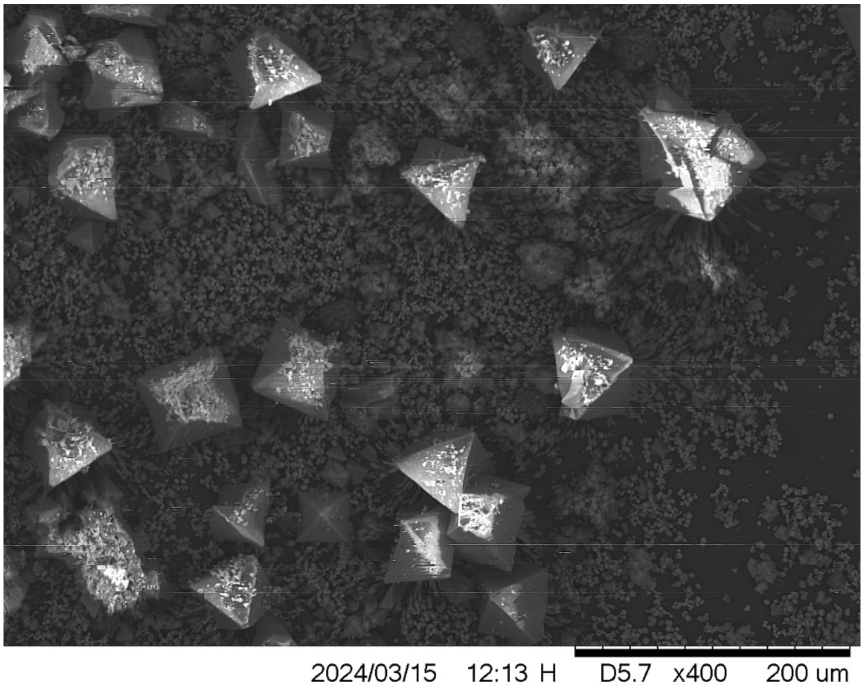

Figure S36. Particle size distribution of *x* = 16.6 mol% **PEPEP-PNA/PEPEP-Me** MOF.

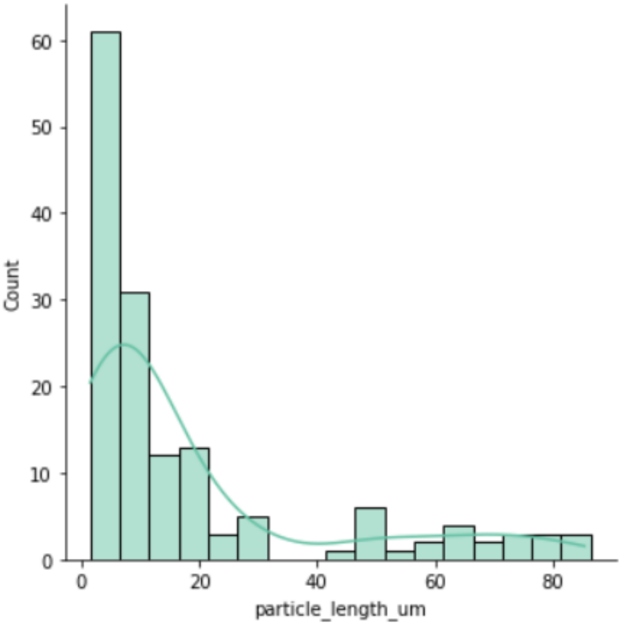

Figure S37. SEM Image x = 21.9 mol% **PEPEP-PNA/PEPEP-Me** MOF**.**

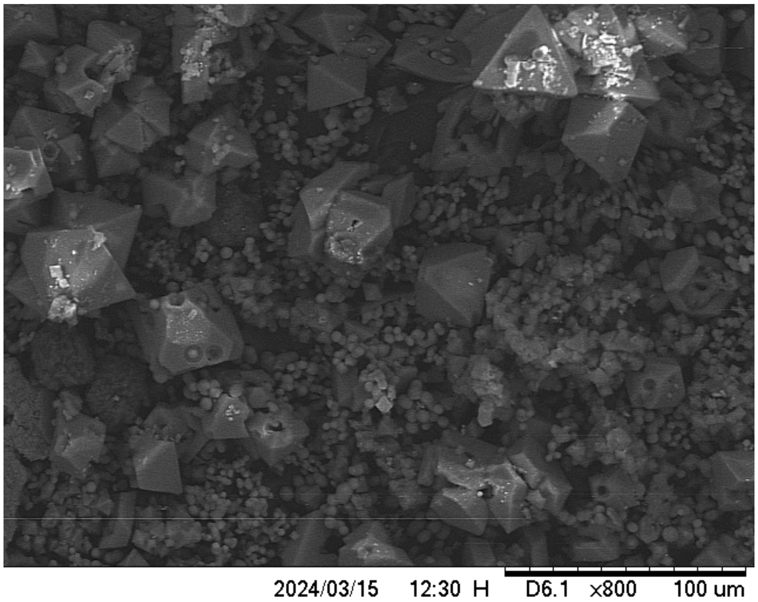

Figure S38. Particle size distribution of x = 21.9 mol% **PEPEP-PNA/PEPEP-Me** MOF.

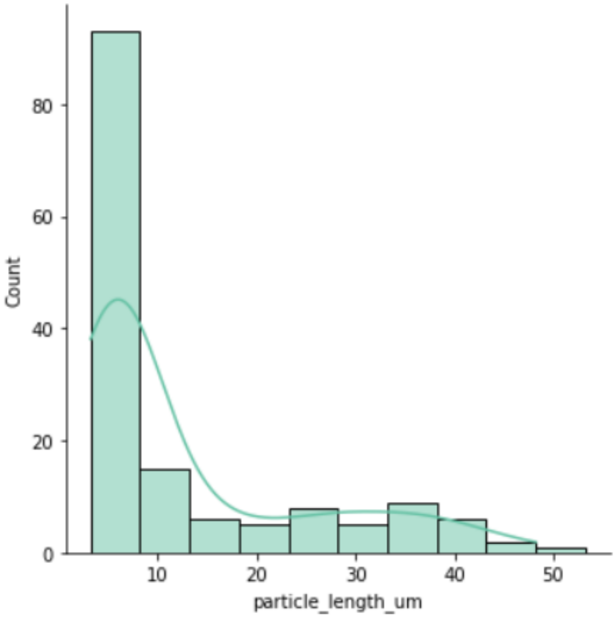

Figure S39. SEM Image x = 27.3 mol% **PEPEP-PNA/PEPEP-Me** MOF**.**

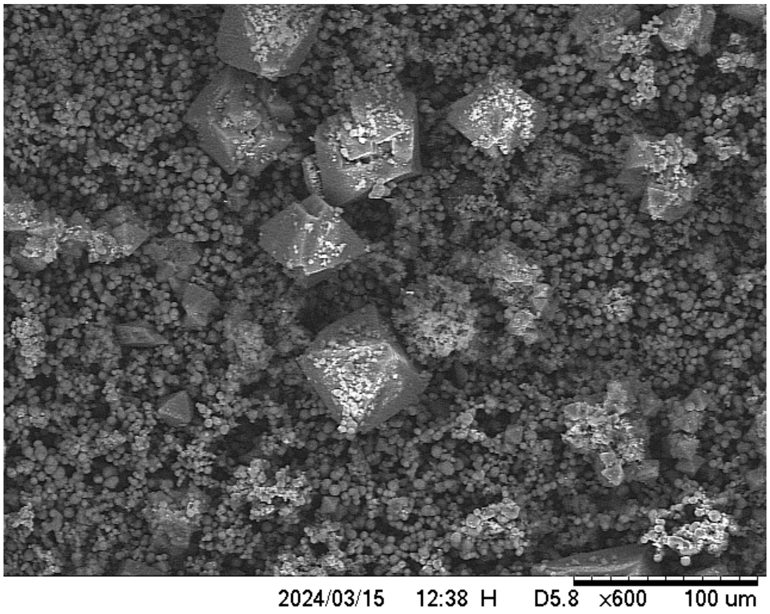

Figure S40. Particle size distribution of x = 27.3 mol% **PEPEP-PNA/PEPEP-Me** MOF.

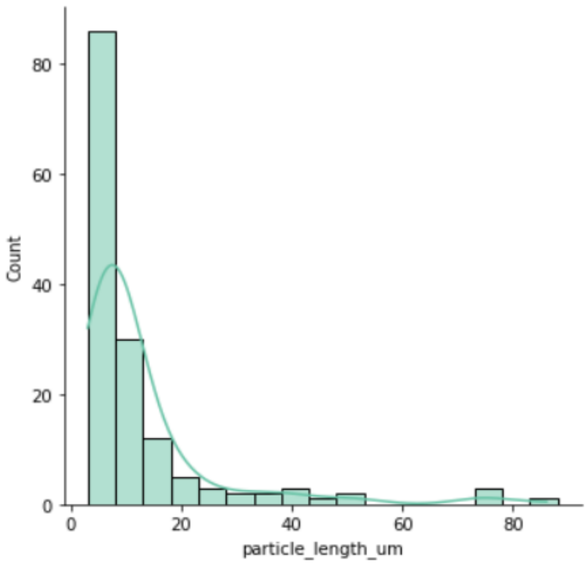

Figure S41. SEM Image *x* = 100 mol% **PEPEP-PNA/PEPEP-Me** MOF**.**

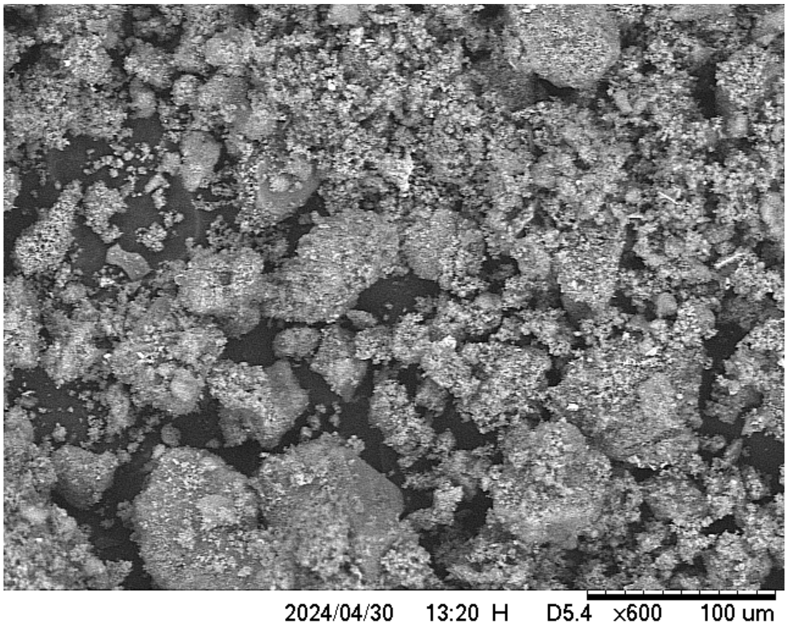

Figure S42. Particle size distribution of *x* = 100 mol% **PEPEP-PNA/PEPEP-Me** MOF.

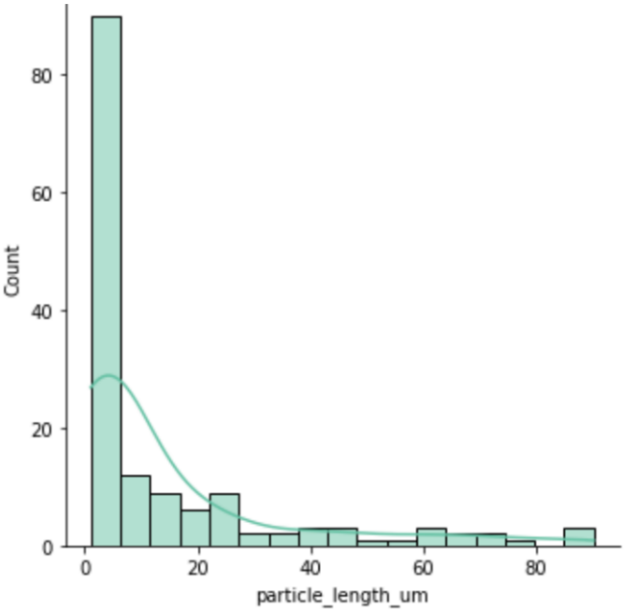

Section S7: Vibrational and solid-state NMR spectroscopy

Figure S43. ^{13}C CP MAS NMR spectra of PNA MTV. Stars indicate spinning side bands. Spin rate = 8 kHz. PNA input concentration is indicated.

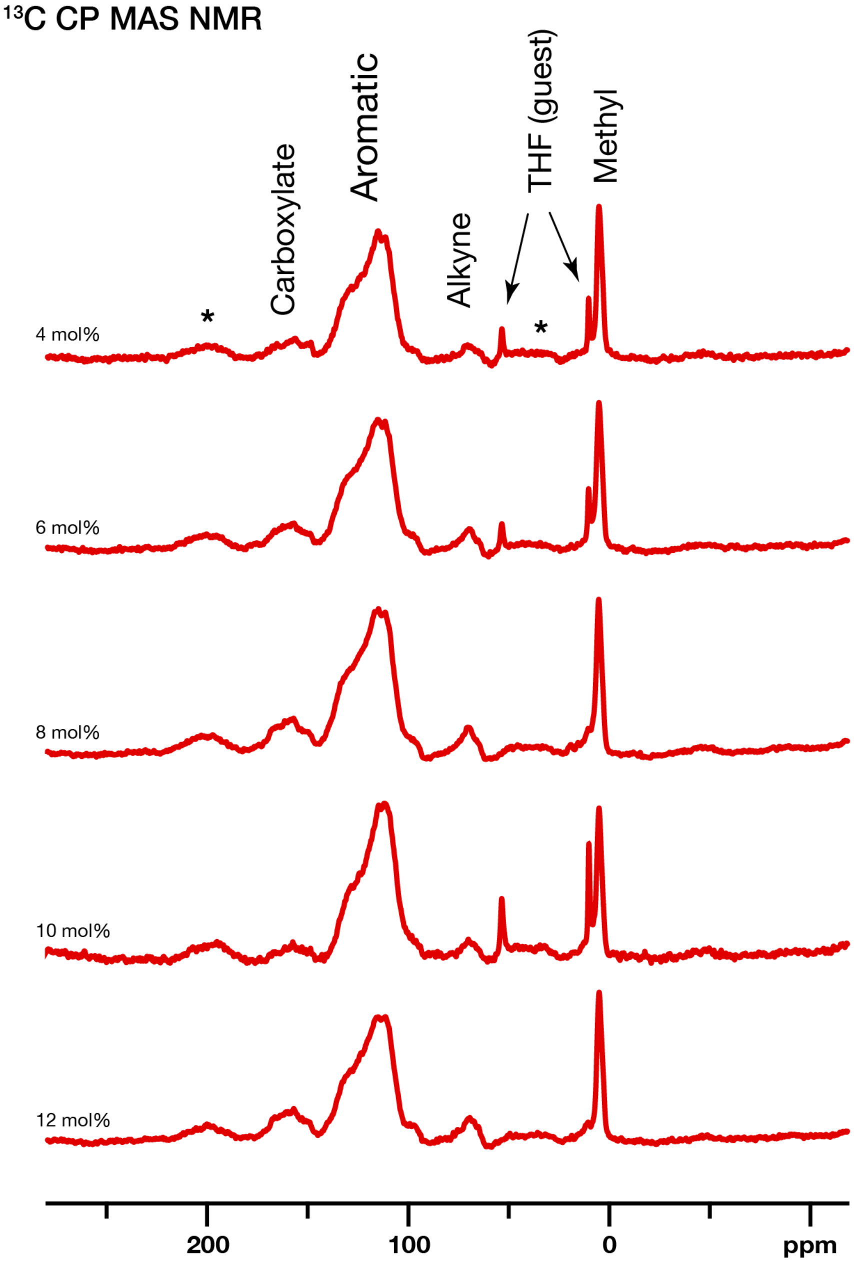

Figure S44. Infrared spectra of **PEPEP-PNA/PEPEP-Me** (0-100)% MOFs.

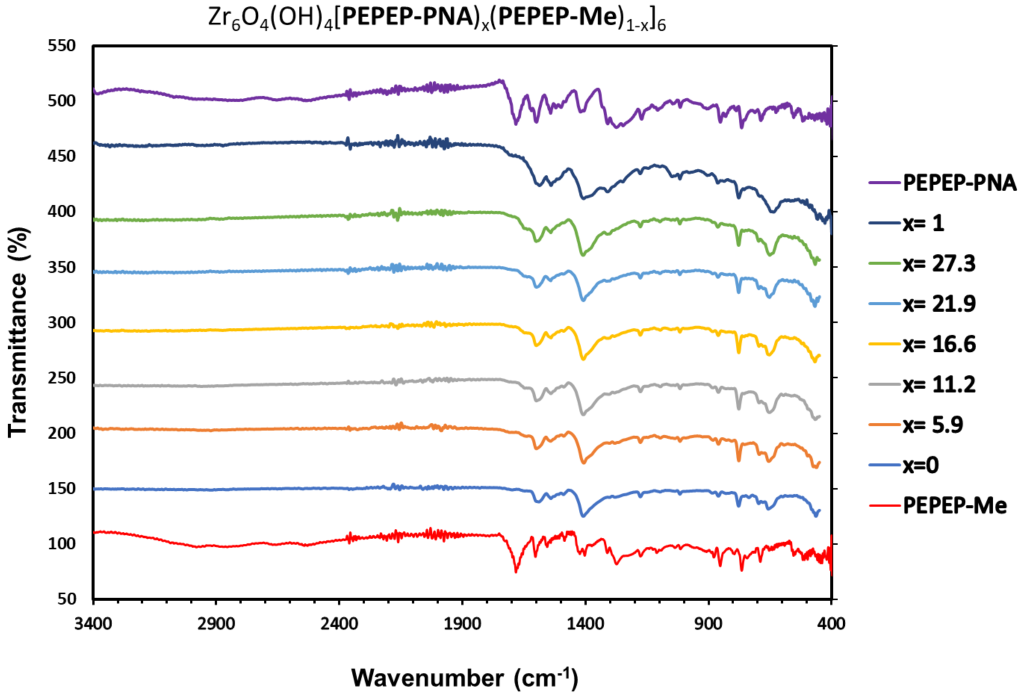

Figure S45. Raman spectra of **PEPEP-PNA/PEPEP-Me** (0-100)% MOFs.

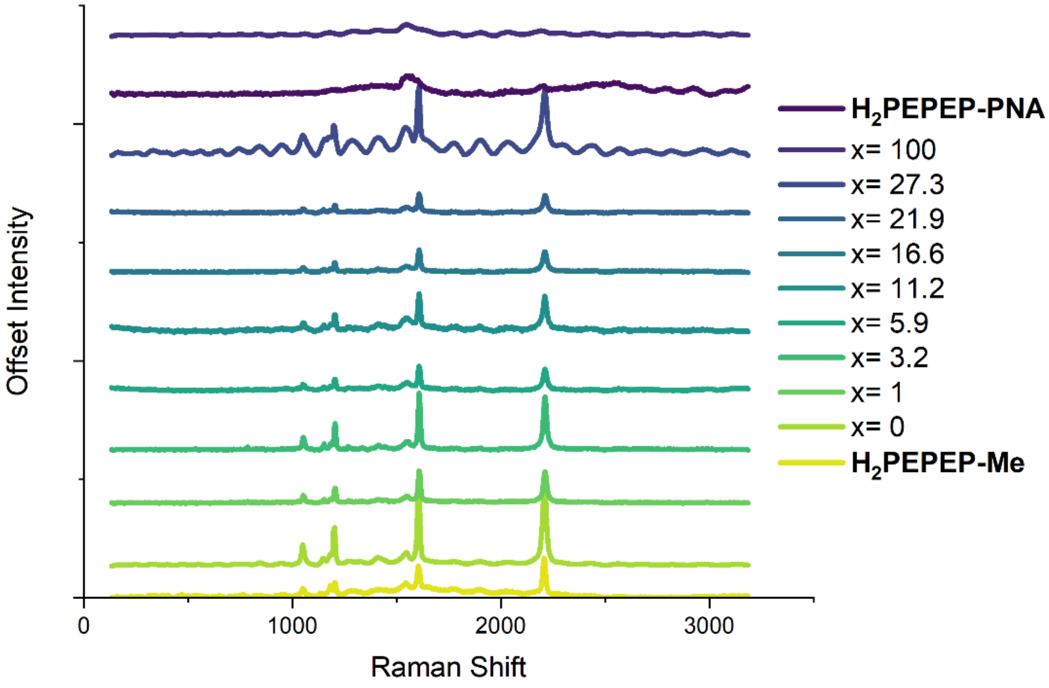

Section S8: Nitrogen adsorption

Table S7. BET surface areas for each composition determined from N_2 (77 K) isotherms.

x output (mol%)	**0**	**2.6**	**3.7**	**11.2**	**16.6**	**21.9**	**27.3**	**100**
m	3.72×10^{-3}	4.12×10^{-3}	4.34×10^{-3}	3.64×10^{-3}	3.38×10^{-3}	2.96×10^{-3}	5.23×10^{-3}	3.50×10^{-3}
σ_m	6.34×10^{-5}	9.10×10^{-5}	9.81×10^{-5}	8.49×10^{-5}	6.84×10^{-5}	5.92×10^{-5}	1.02×10^{-4}	2.05×10^{-5}
b	2.52×10^{-5}	2.09×10^{-5}	2.24×10^{-5}	2.25×10^{-5}	1.43×10^{-5}	2.05×10^{-5}	1.95×10^{-5}	3.68×10^{-6}
σ_b	1.28×10^{-6}	1.64×10^{-6}	1.75×10^{-6}	1.72×10^{-6}	1.10×10^{-6}	1.01×10^{-6}	1.24×10^{-6}	1.55×10^{-7}
V_m (cm^3 g^{-1})	266.73	241.14	229.11	272.96	294.05	334.71	190.30	285.07
σ_V_m (cm^3 g^{-1})	4.6	5.4	5.2	6.5	6.0	6.7	3.7	1.7
C_{BET}	148.8	198.9	194.8	163.1	237.6	146.0	269.8	953.4
σ_C_{BET}	8.0	16.2	15.8	13.0	18.9	7.8	18.0	40.6
S_{BET} (m^2 g^{-1})	**1160**	**1050**	**997**	**1187**	**1280**	**1456**	**828**	**1240**
σ_S_{BET} (m^2 g^{-1})	**20**	**23**	**23**	**28**	**26**	**29**	**16**	**7**

Figure S46. N_2 adsorption isotherm (77 K) of *x* = 0% **PEPEP-PNA/PEPEP-Me**.

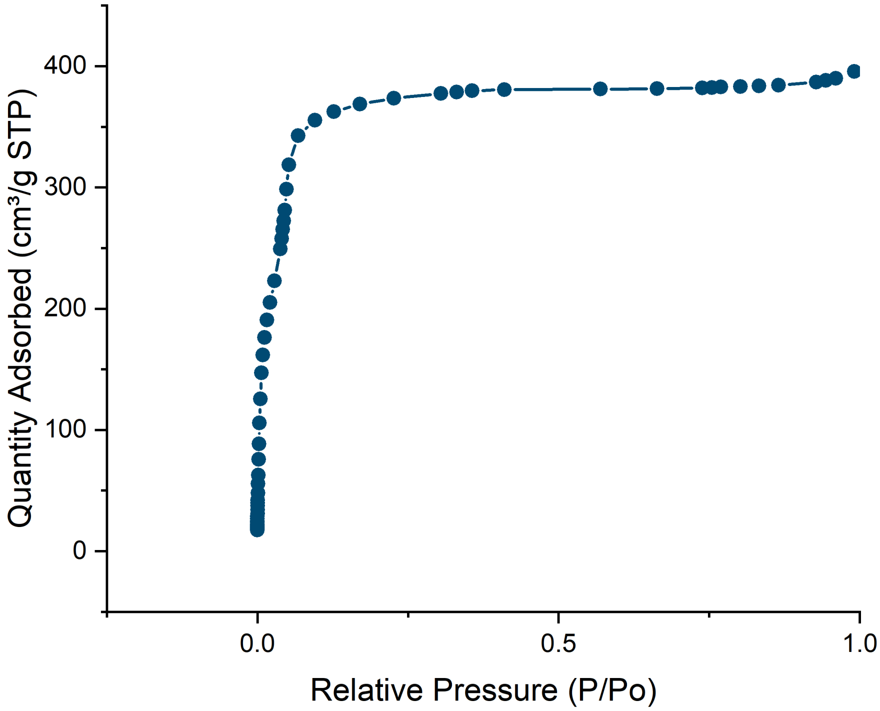

Figure S47. Pore size distribution plot of *x* = 0% **PEPEP-PNA** from NLDFT.

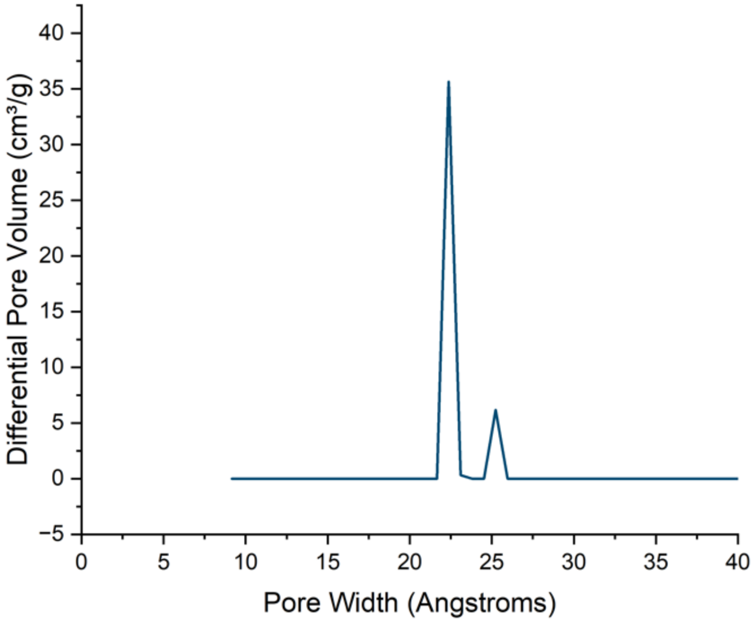

Figure S48. Rouquerol plot of *x* = 0 mol% **PEPEP-PNA**.

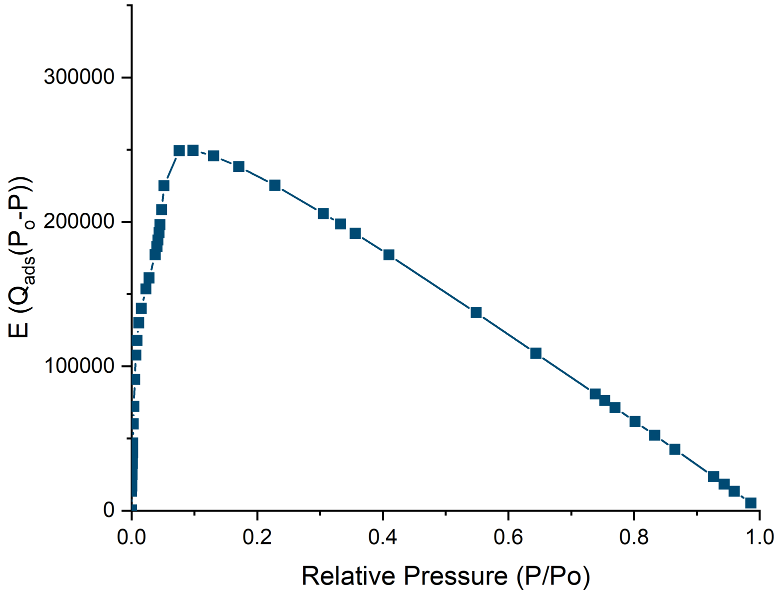

Figure S49. BET plot of *x* = 0 mol % **PEPEP-PNA/PEPEP-Me**.

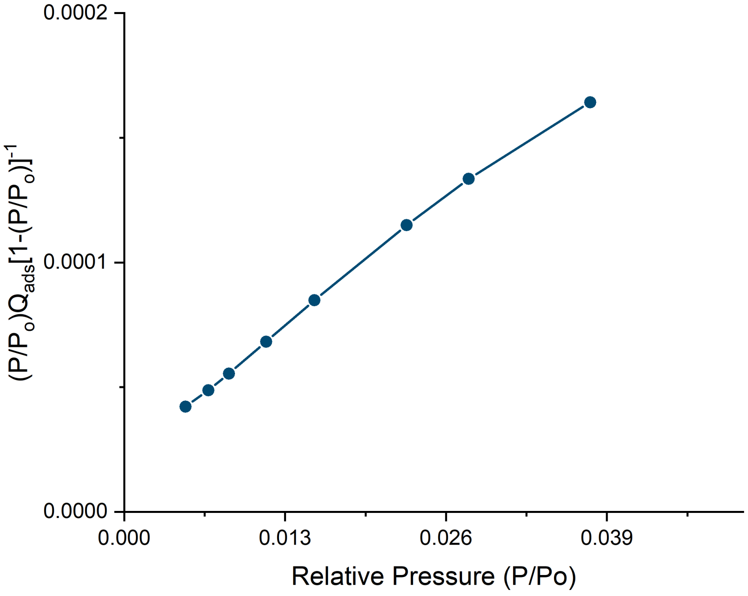

Figure S50. N_2 adsorption isotherm (77 K) of *x* = 2.6 mol% **PEPEP-PNA/PEPEP-Me**.

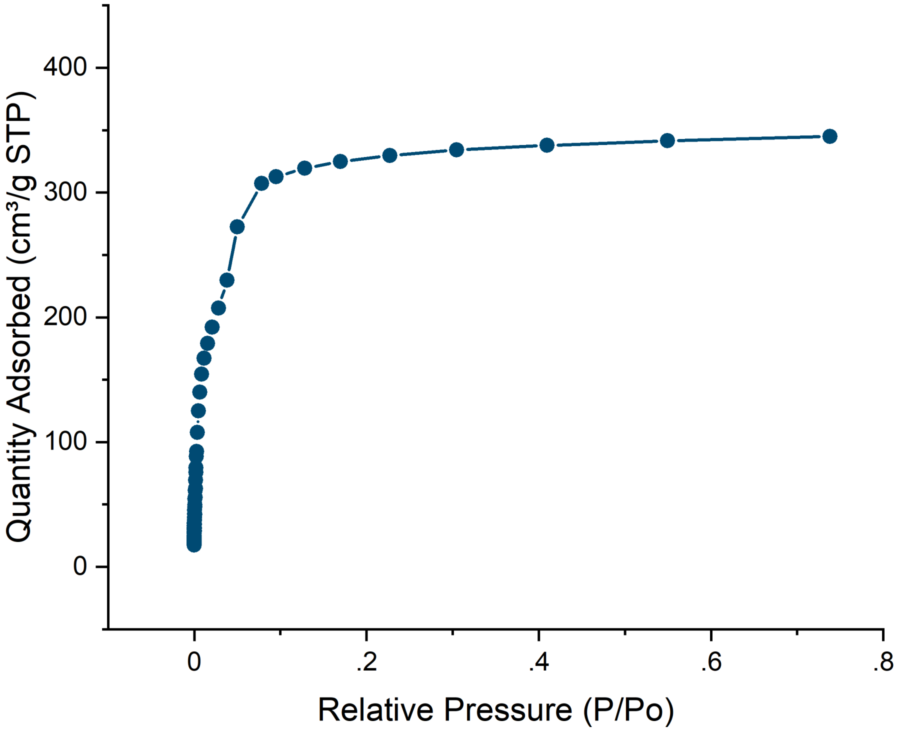

Figure S51. Pore size distribution plot of *x* = 2.6 mol% **PEPEP-PNA/PEPEP-Me**.

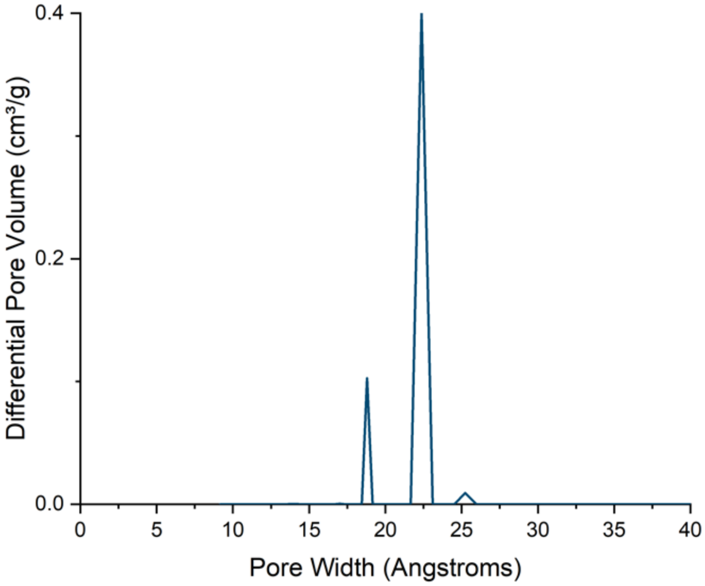

Figure S52. Rouquerol plot of *x* = 2.6 mol%.

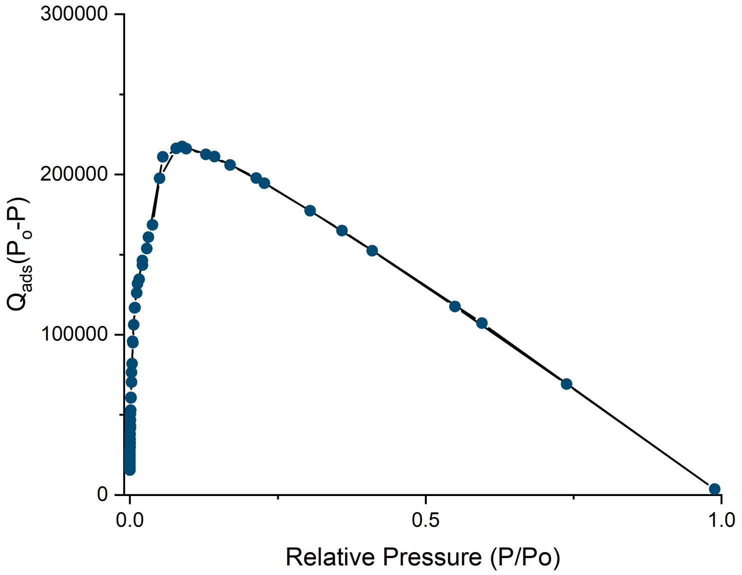

Figure S53. BET plot of x = 2.6 mol%.

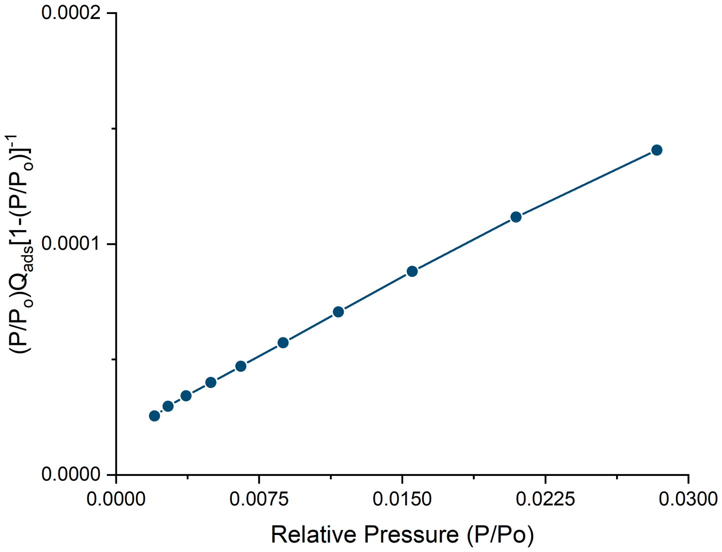

Figure S54. N_2 adsorption isotherm (77 K) of x = 3.7 mol% **PEPEP-PNA** and **PEPEP-Me**.

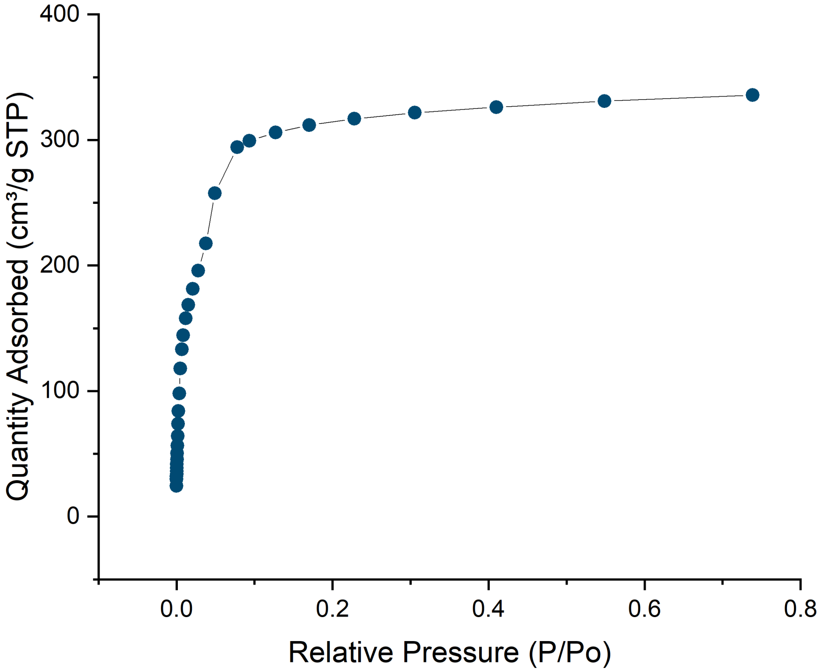

Figure S55. Pore size distribution of x = 3.7 mol% **PEPEP-PNA** and **PEPEP-Me**.

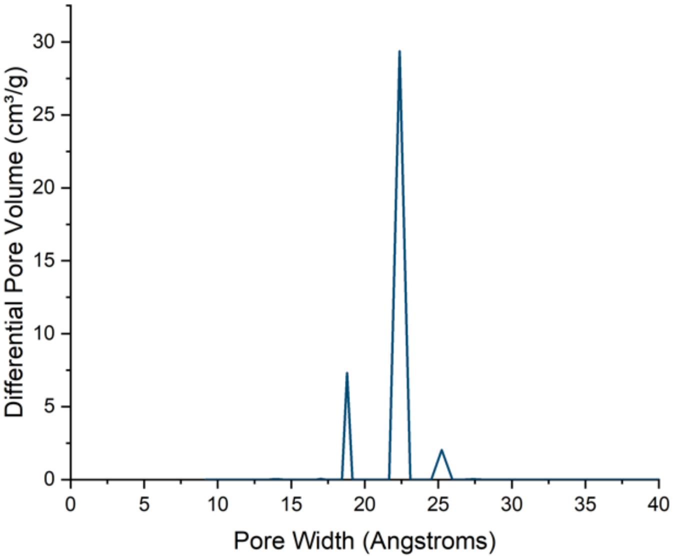

Figure S56. Rouquerol plot of *x* = 3.7 mol%.

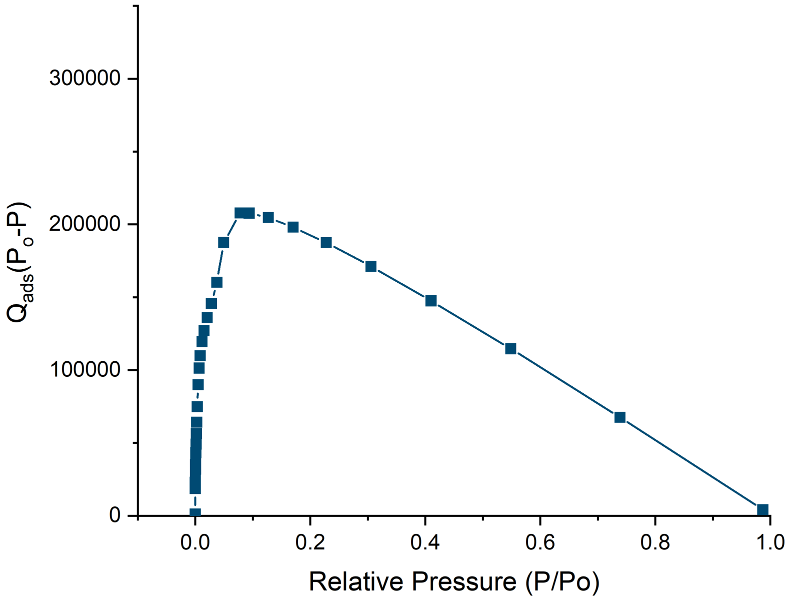

Figure S57. *x* = 3.7 mol% BET plot.

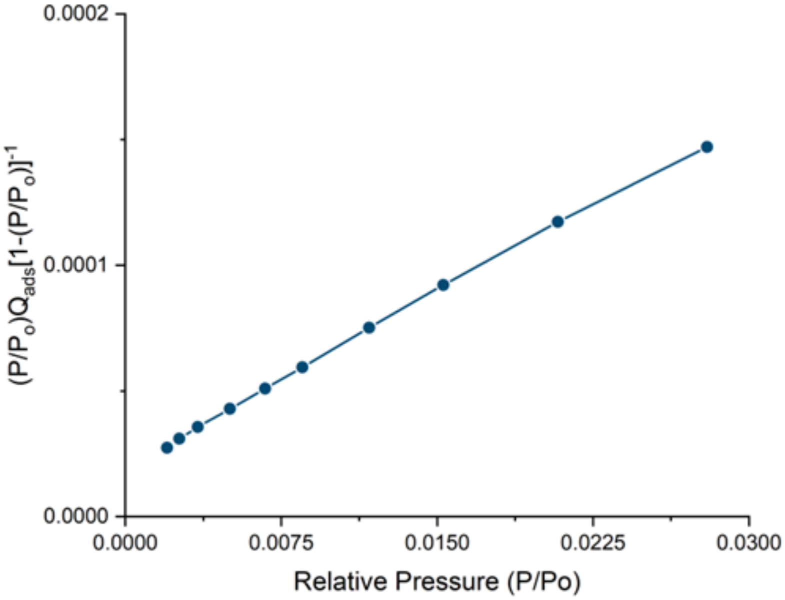

Figure S58. *x* = 11.2 mol% **PEPEP-PNA/PEPEP-Me** isotherm at 77 K.

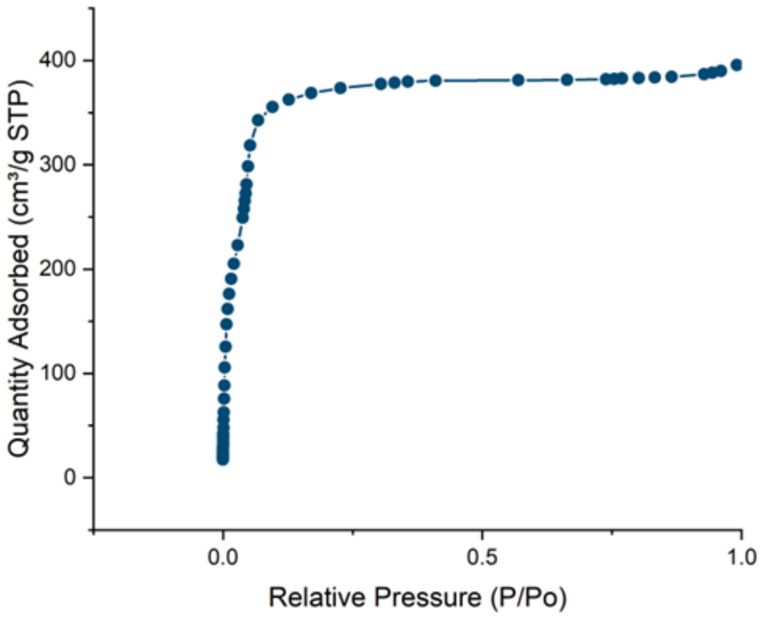

Figure S59. *x* = 11.2 mol% **PEPEP-PNA/PEPEP-Me** pore size distribution.

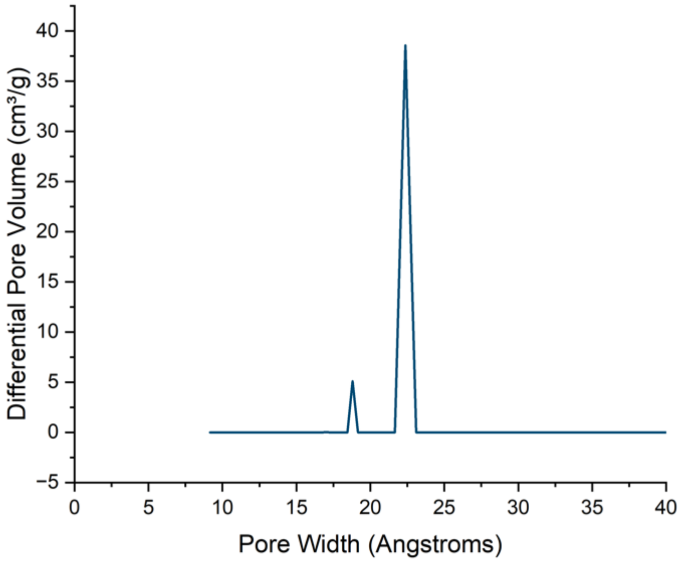

Figure S60. x = 11.2 mol % **PEPEP-PNA/PEPEP-Me** Rouquerol plot.

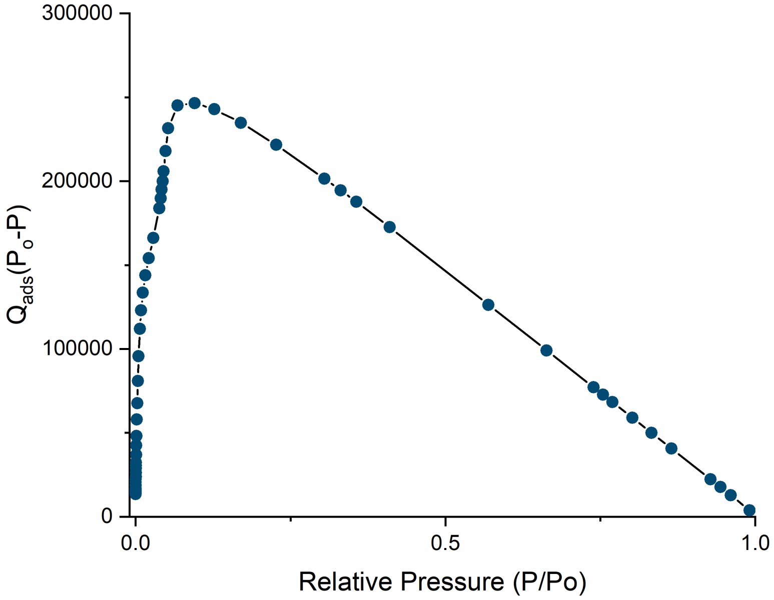

Figure S61. x = 11.2 mol % **PEPEP-PNA/PEPEP-Me** BET plot.

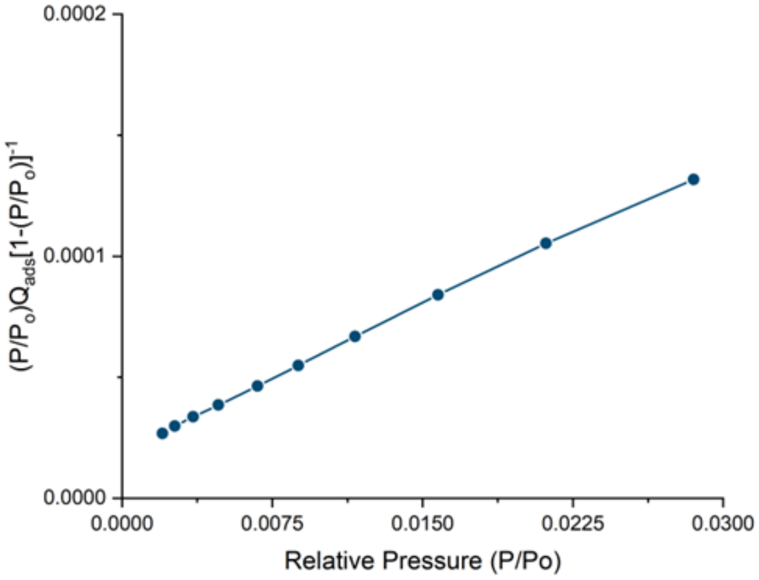

Figure S62. x = 16.6 mol% **PEPEP-PNA/PEPEP-Me** isotherm at 77 K.

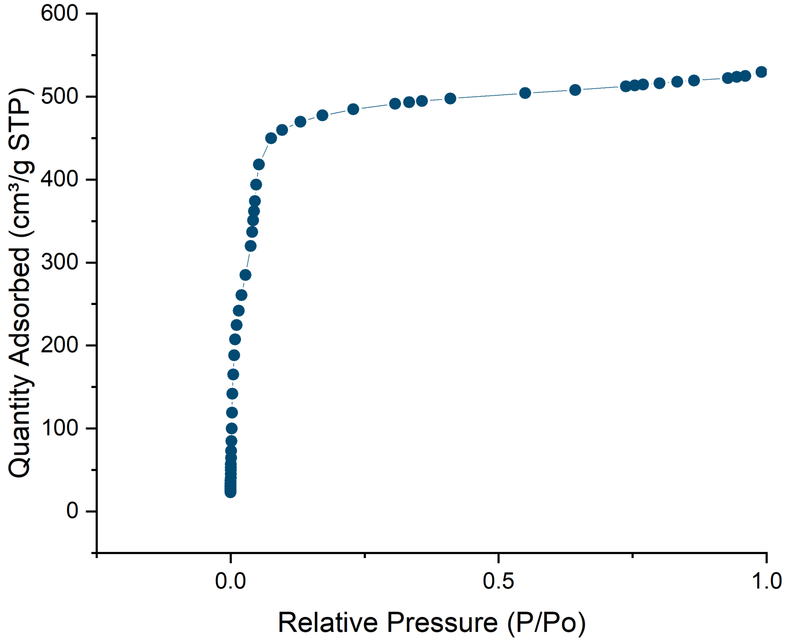

Figure S63. x = 16.6 mol% **PEPEP-PNA/PEPEP-Me** pore size distribution.

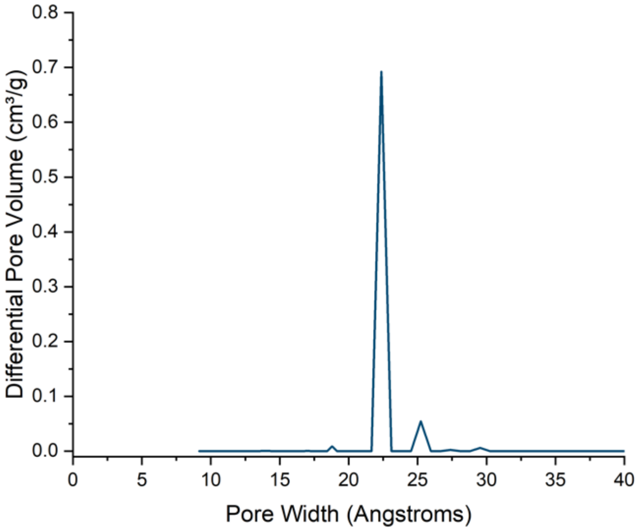

Figure S64. *x* = 16.6 mol% **PEPEP-PNA/PEPEP-Me** Rouquerol plot.

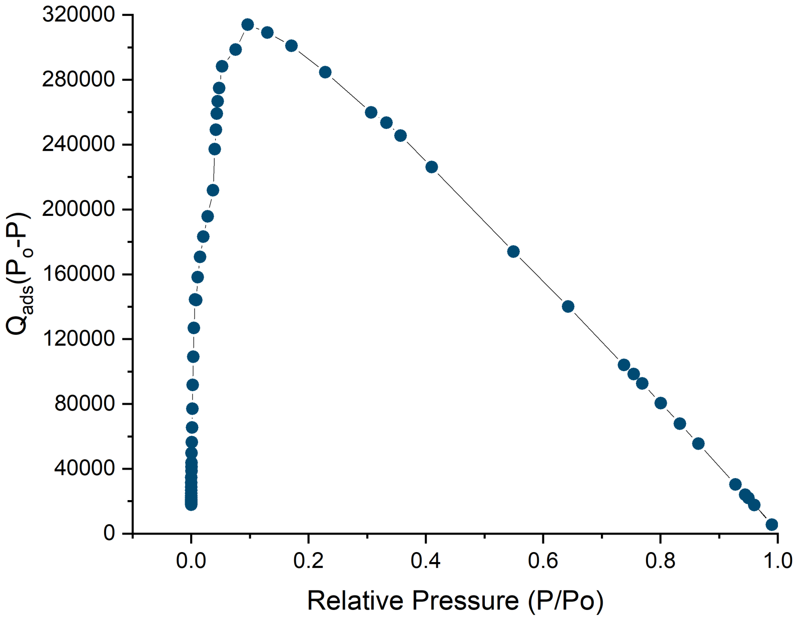

Figure S65. *x* = 16.6 mol% **PEPEP-PNA/PEPEP-Me** BET plot.

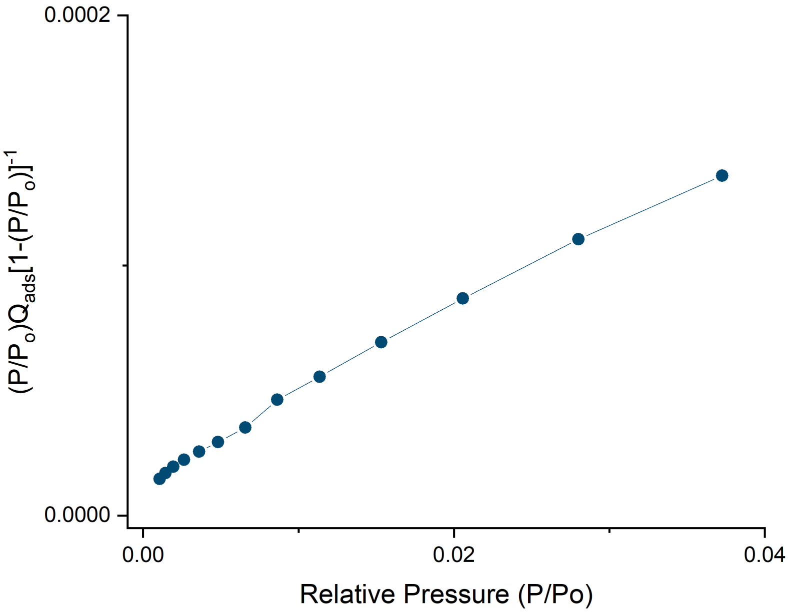

Figure S66. x = 21.9% **PEPEP-PNA/PEPEP-Me** isotherm at 77 K.

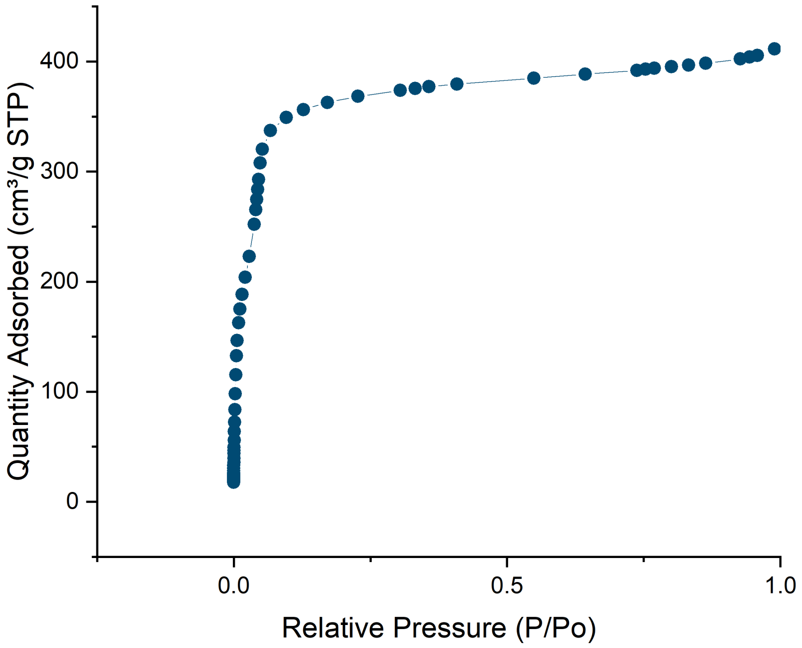

Figure S67. x = 21.9% **PEPEP-PNA/PEPEP-Me** pore size distribution.

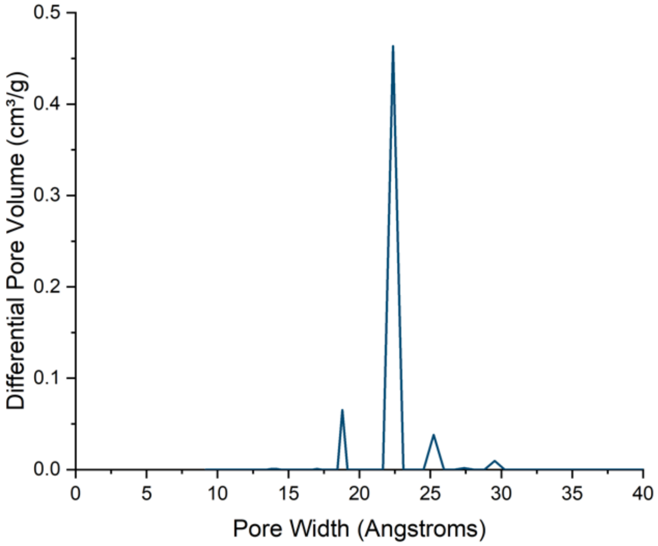

Figure S68. *x* = 21.9% **PEPEP-PNA/PEPEP-Me** Rouquerol plot.

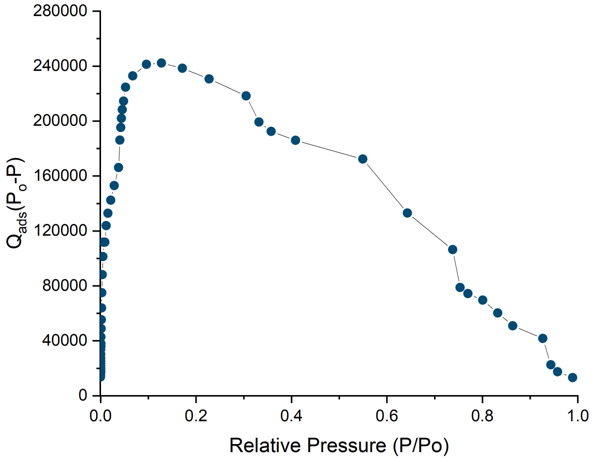

Figure S69. *x* = 21.9% **PEPEP-PNA/PEPEP-Me** BET plot.

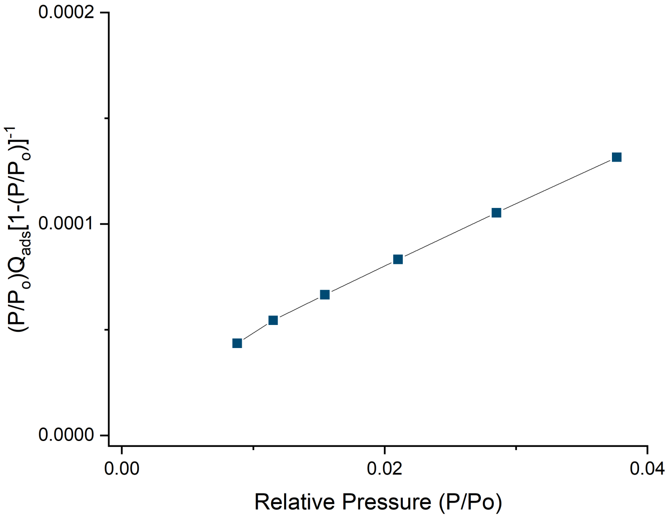

Figure S70. *x* = 27.2% **PEPEP-PNA/PEPEP-Me** isotherm at 77 K.

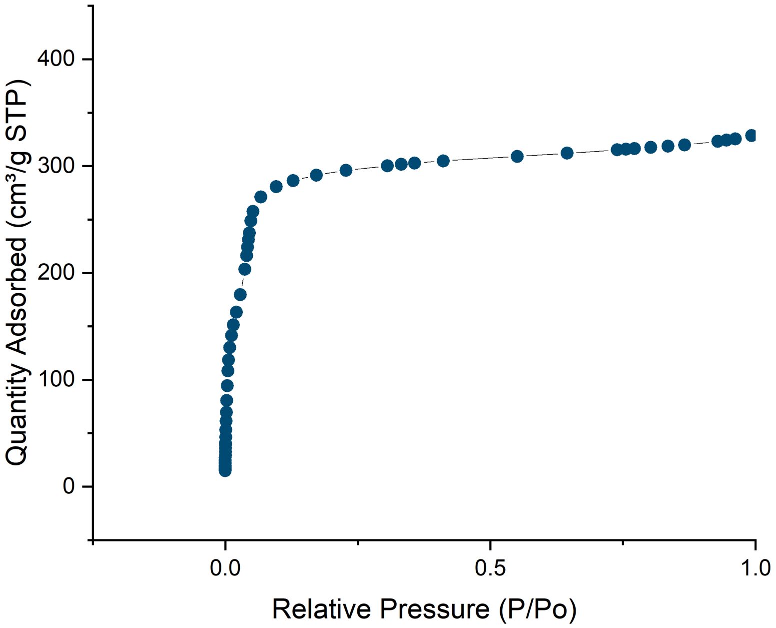

Figure S71. x= 27.2% **PEPEP-PNA/PEPEP-Me** pore size distribution.

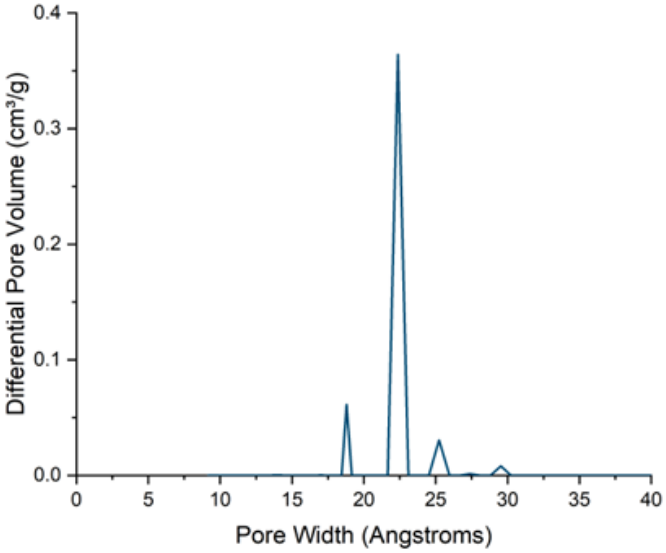

Figure S72. x= 27.2% **PEPEP-PNA/PEPEP-Me** Rouquerol plot.

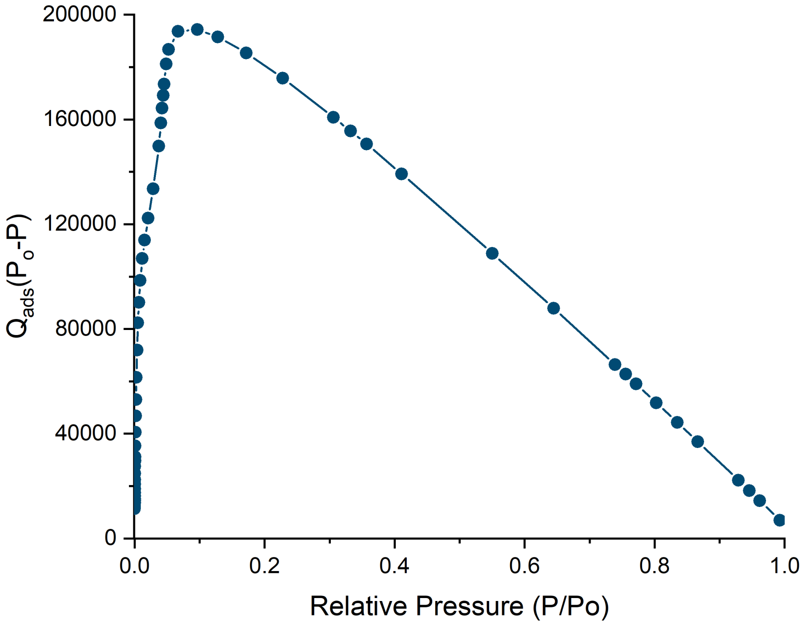

Figure S73. x= 27.2% **PEPEP-PNA/PEPEP-Me** BET plot.

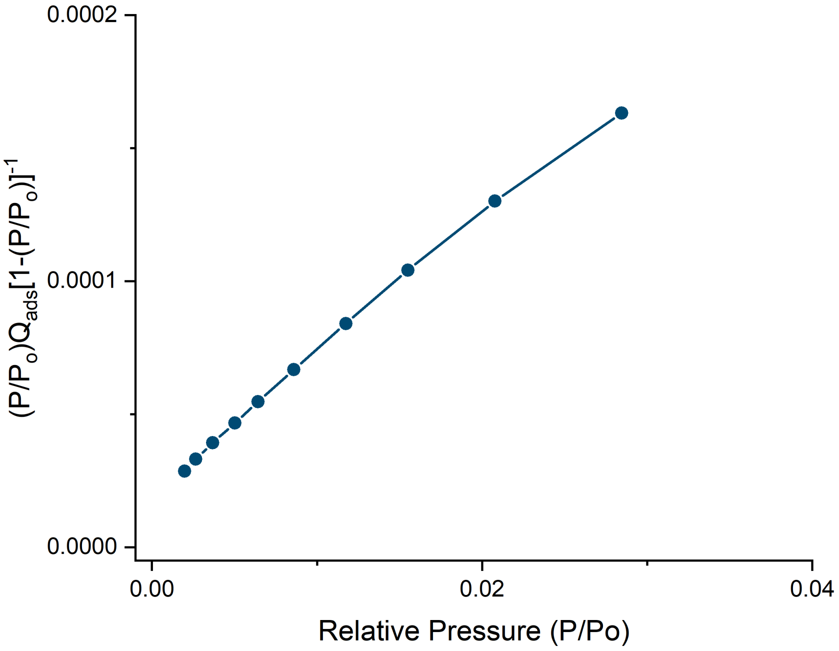

Figure S74. *x* = 100% **PEPEP-PNA/PEPEP-Me** isotherm at 77 K.

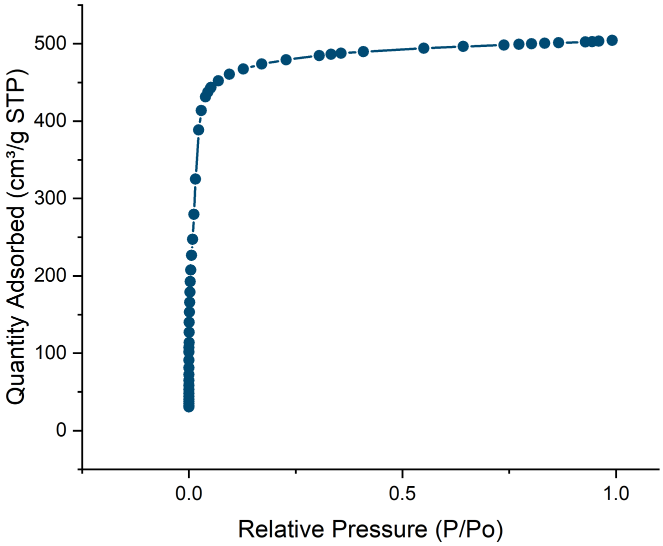

Figure S75. *x* = 100% **PEPEP-PNA/PEPEP-Me** pore size distribution.

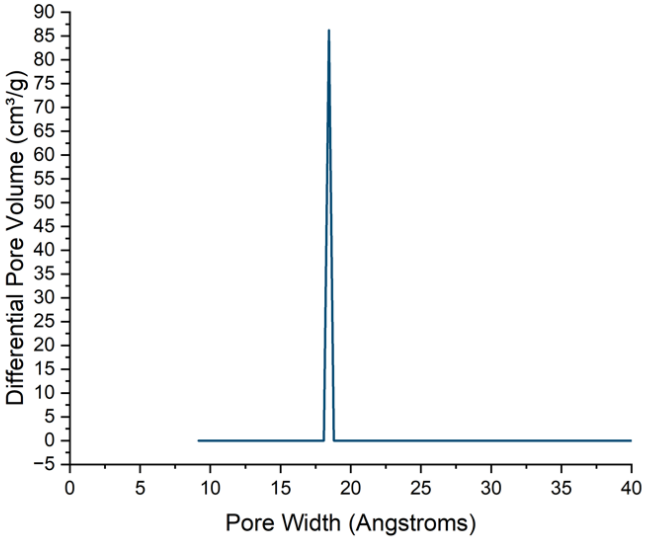

Figure S76. *x* = 100% **PEPEP-PNA/PEPEP-Me** Rouquerol plot.

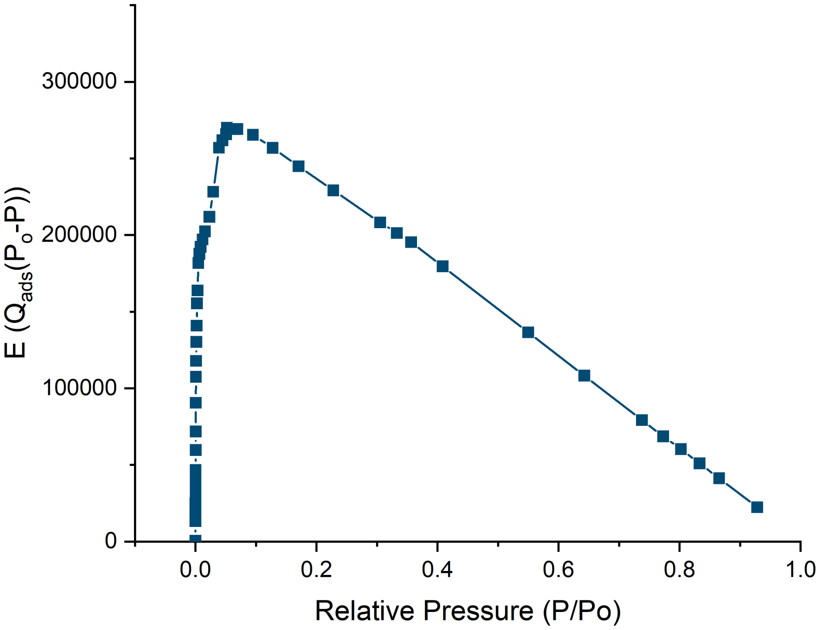

Figure S77. x= 100% **PEPEP-PNA/PEPEP-Me** BET plot.

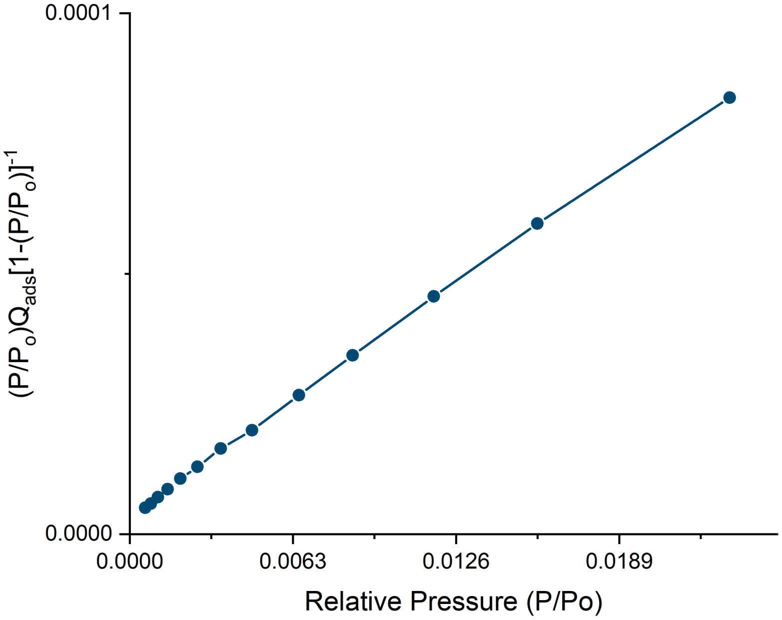

Section S9: Thermogravimetric Analysis

Thermogravimetric analysis (TGA) experiments were performed inside an ultra-high purity N_2 atmosphere glovebox, on an ISI TGA-1000 instrument with a 5 cm^3 min^{-1} flow of N_2. A platinum pan (surface area 3.44 × 10–5 m^2) was used as a sample holder, and powder samples were spread evenly across the surface of the pan before beginning each experiment. For each experiment, nominally 3 mg of material was loaded into the sample pan. The instrument was heated from 25 - 900 °C at a rate of 10 °C min^{-1}. All experiments were performed non-isothermally except for the 20 mol% sample which was held at 120 °C for 60 min to activate the sample prior to further heating.

Figure S78. TGA of **PNA PEPEP/Xylene** x= 5.9-100 mol% MOFs.

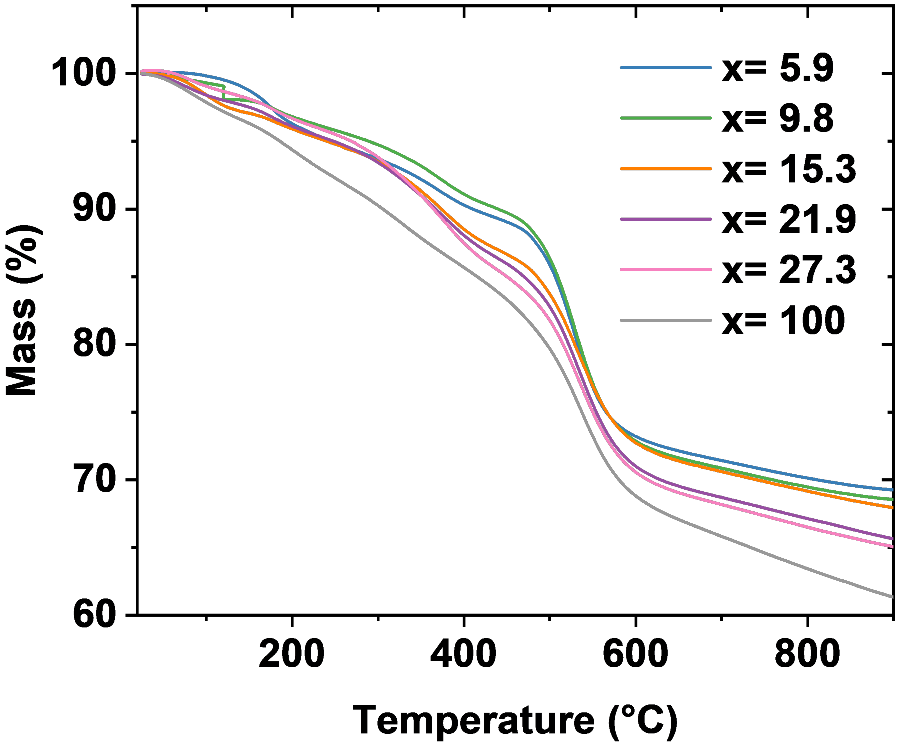

Figure S79. TGA of **PNA PEPEP/Xylene** first derivative of TGA's for x= 5.9 mol% MOF.

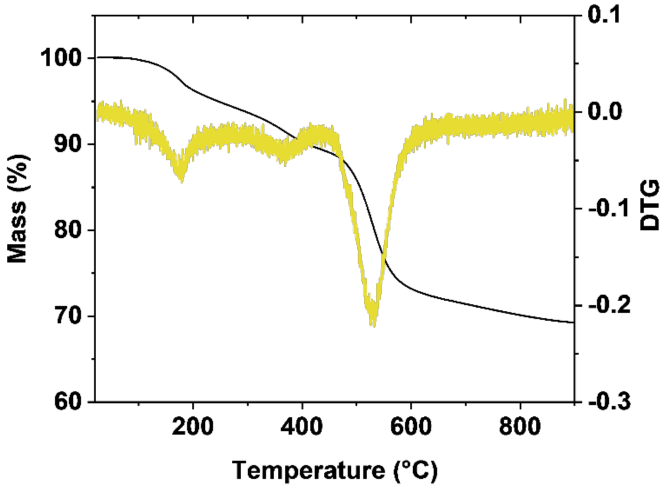

Figure S80. TGA of **PNA PEPEP/Xylene** first derivative of TGA's for x= 9.8 mol% MOF.

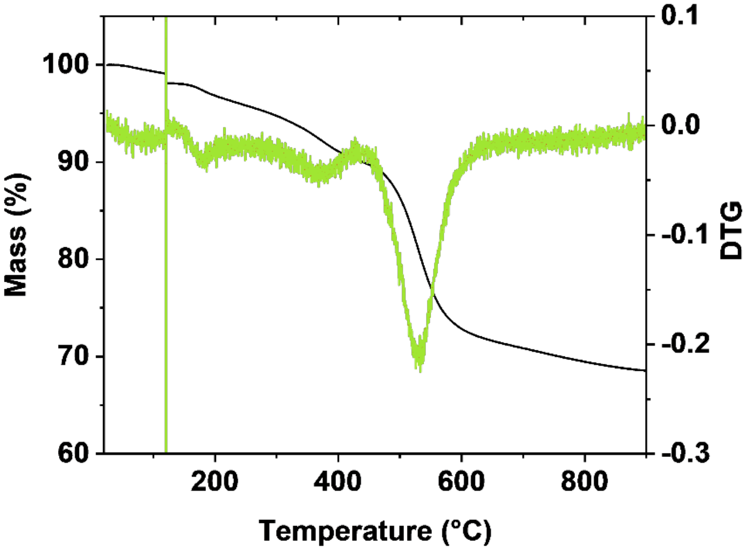

Figure S81. TGA of **PNA PEPEP/Xylene** first derivative of TGA’s for x= 15.3 mol% MOF.

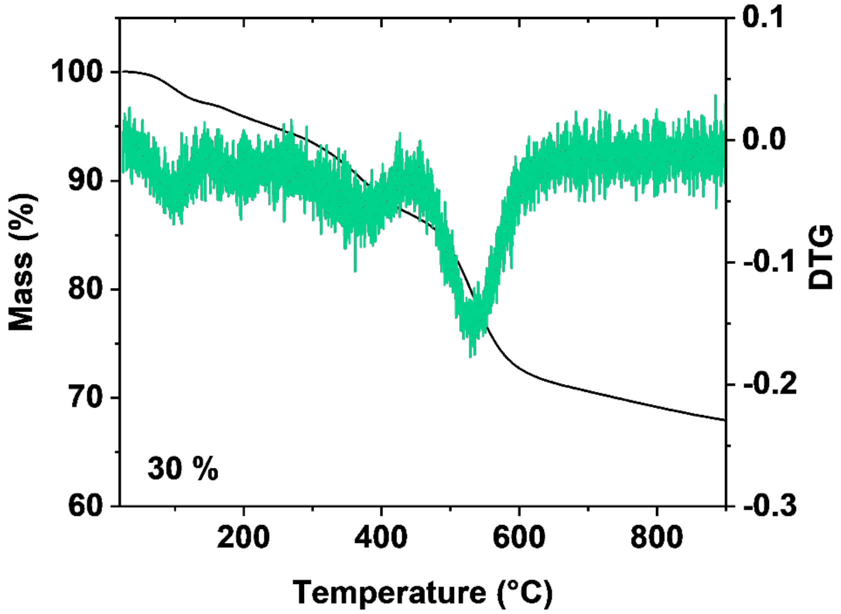

Figure S82. TGA of **PNA PEPEP/Xylene** first derivative of TGA’s for x= 21.9 mol% MOF.

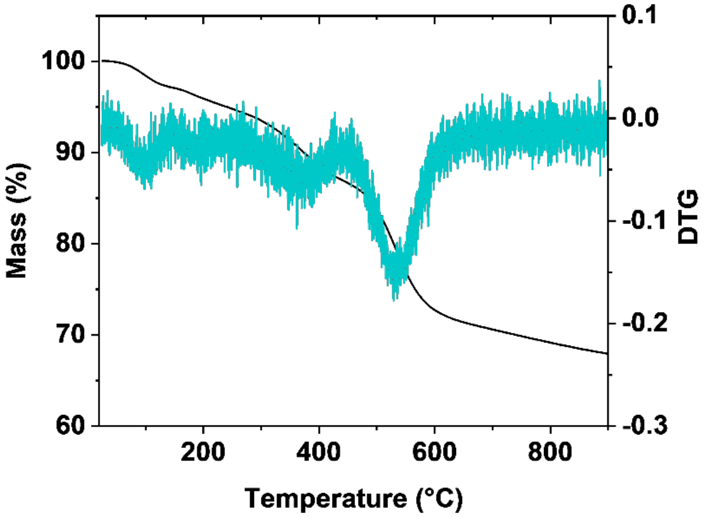

Figure S83. TGA of **PNA PEPEP/Xylene** first derivative of TGA's for x= 27.3 mol% MOF.

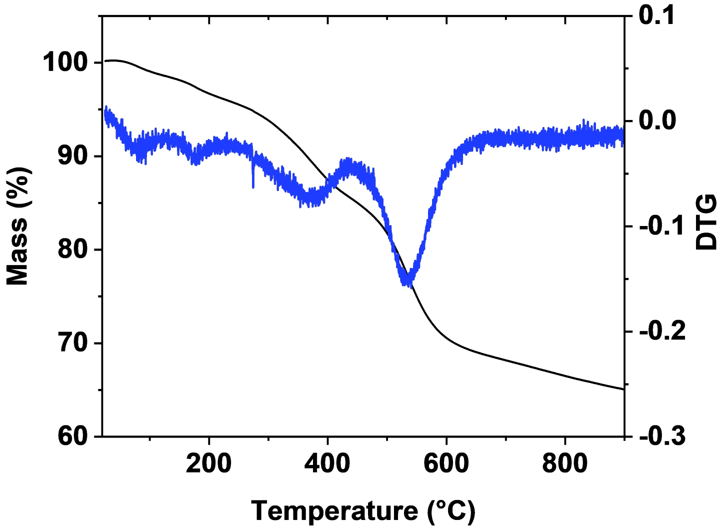

Figure S84. TGA of **PNA PEPEP/Xylene** first derivative of TGA's for x= 100 mol% MOF.

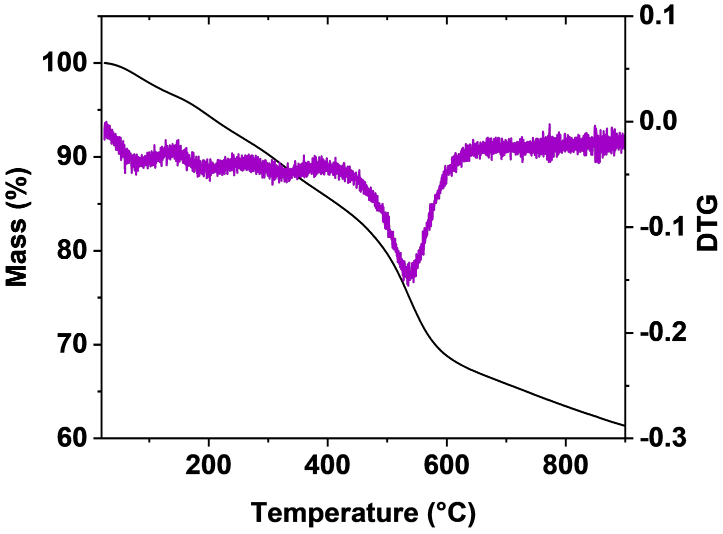

Section S10: Broadband Dielectric Spectroscopy

Variable temperature broadband dielectric spectroscopy measurements were performed on a Novocontrol Alpha-A analyzer at the Center for Nanophase Materials Sciences at the Oak Ridge National Laboratory. 5-10 mg of each sample composition were weighed out and placed between to electrodes using a Teflon containing ring (See figure below). The cell thickness was then measured using a caliper and the difference between the filled and empty cell was used to calculate the sample thickness. A data file was then created to run samples from –110 to 60 °C with 5 degree intervals while scanning each temperature from 1 Hz to 10 MHz.

The samples were activated under high vacuum at 120 C° for 12 h after being loaded in the instrument. Two relaxation regions were observed. Region I is termed the low frequency high temperature process that occurs from 0.1 to 1000 Hz from –40 to 20 °C. Region II is termed the high frequency low temperature process that spans the frequency range of 0.1 Hz to 1 MHz and the entire temperature range.

Figure S85. Variable Temperature Broadband Dielectric Spectroscopy setup.

BDS data processing.

Complex dielectric data, including complex permittivity and impedance *ε'*(*f*), *ε"*(*f*), *Z'*(*f*), and *Z"*(*f*). were loaded in Origin 2021b (9.8.5.201).

Phase angle *ϕ*(*f*) was obtained from:

$$\varphi(f) = \frac{Z''(f)}{Z'(f)}$$

The dielectric loss *D*(*f*) was obtained from:

$$D(f) = \frac{\varepsilon''(f)}{\varepsilon'(f)}$$

The characteristic relaxation time (*τ*) was obtained from non-linear function fitting of the imaginary part of the Havrilliak-Negami relation:

$$\varepsilon'' = \Delta\varepsilon(1 + 2(f\tau)^{\alpha} cos(\pi\alpha/2) + (f\tau)^{2\alpha})^{-\beta/2} sin\left(\beta tan^{-1}\left(\frac{(f\tau)^{\alpha} sin(\pi\alpha/2)}{1 + (f\tau)^{\alpha} cos(\pi\alpha/2)}\right)\right)$$

Where:
ε'' = imaginary permittivity
f = frequency (Hz)
τ = relaxation time (s)
$\Delta\varepsilon$ = dielectric strength
α, β = asymmetry parameters $\alpha, \beta \in [0,1]$

From the non-linear fittings, the relaxation times (and standard error) were extracted and plotted vs temperature in the linear form of the Eyring equation:

$$\ln[1/\tau T] = -\frac{\Delta H^{\ddagger}}{R} \cdot \frac{1}{T} + \frac{\Delta S^{\ddagger}}{R} + \ln\left[\frac{\kappa k_B}{h}\right]$$

with:

$$\Delta H^{\ddagger} = -mR$$

$$\Delta S^{\ddagger} = R\left[b - \ln\left(\frac{\kappa k_B}{h}\right)\right]$$

Where:
$\Delta H^{\ddagger}$ = Enthalpy of activation (kJ mol^{-1})
$\Delta S^{\ddagger}$ = Entropy of activation (J mol^{-1} K^{-1})
m = Slope from linear Eyring plot
b = Intercept from linear Eyring plot
R = Gas constant (8.314 J mol^{-1} K^{-1})
k_B = Boltzmann constant (1.3806×10^{-23} J K^{-1})
h = Plank constant (6.626×10^{-34} J s)
κ = Transmission coefficient (1)

Figure S86. Broadband Dielectric Spectroscopy plots of x = 0 mol% **PEPEP-PNA/PEPEP-Me** MOFs.

Bode Plot

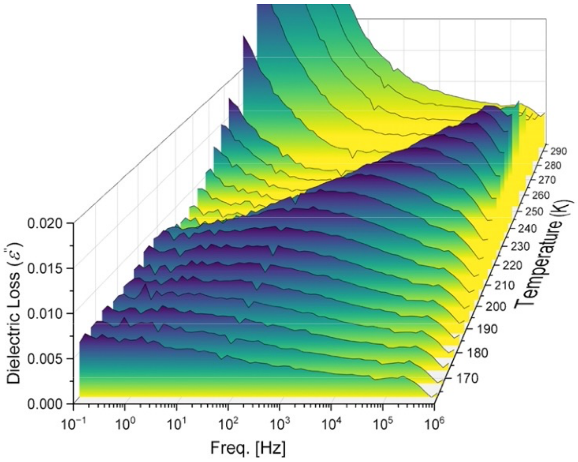

Bode plot with HN fitting

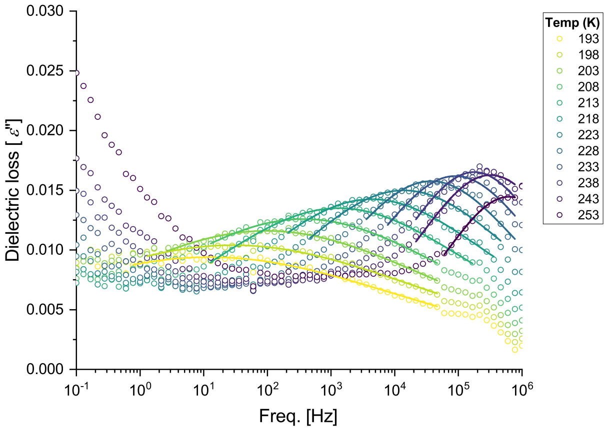

Cole-Cole plot

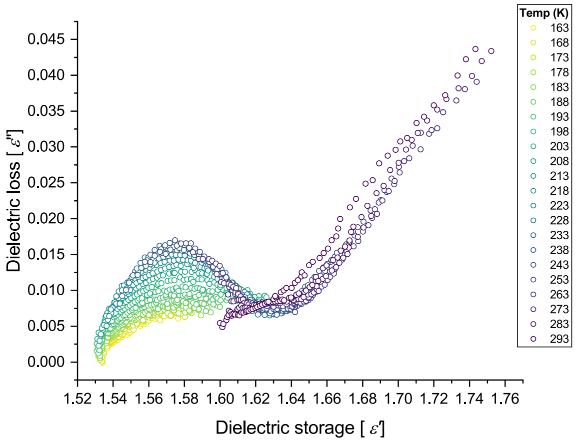

Phase Angle plot

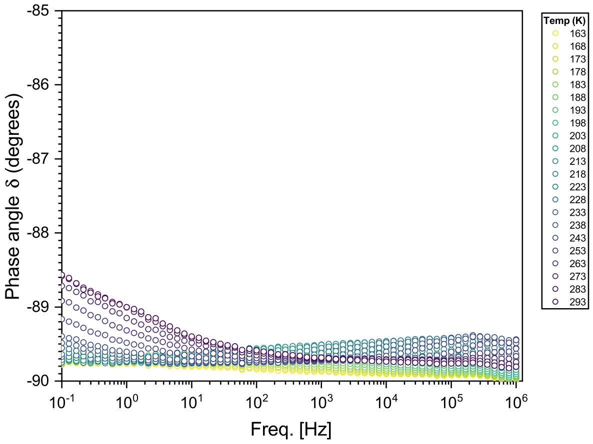

Dissipation factor plot

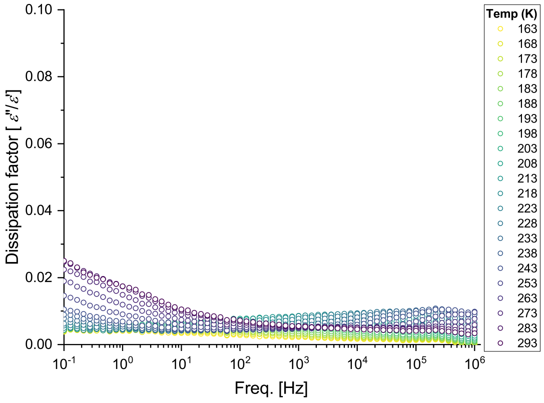

Figure S87. Broadband Dielectric Spectroscopy plots of *x* = 5.9 mol% **PEPEP-PNA/PEPEP-Me** MOFs.

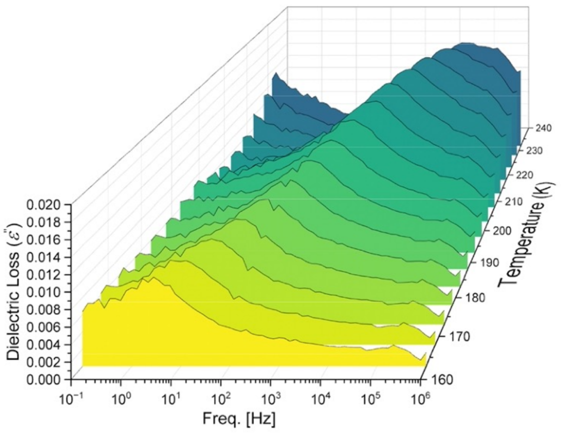
Bode Plot

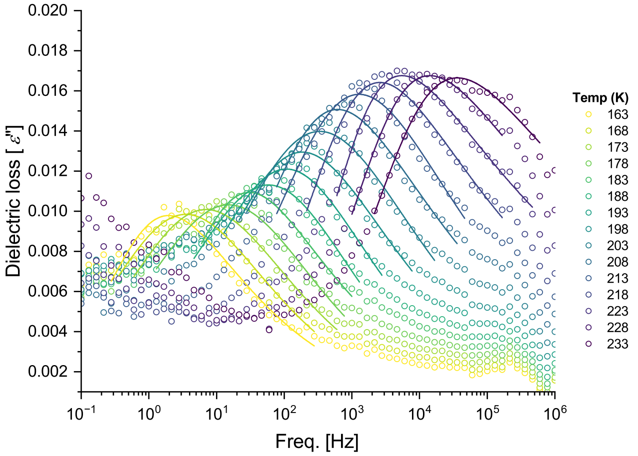
Bode plot with HN fitting

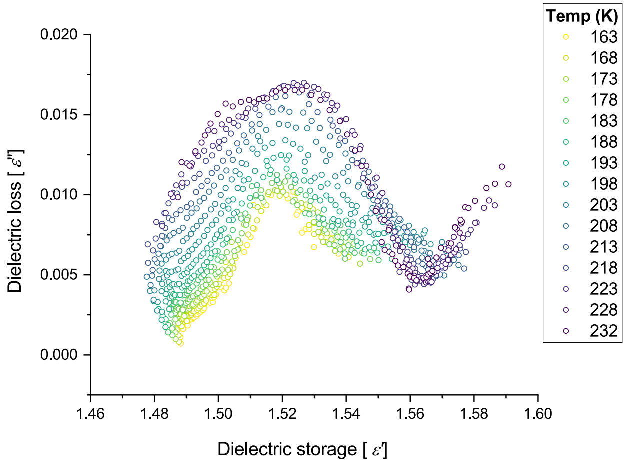
Cole-Cole plot

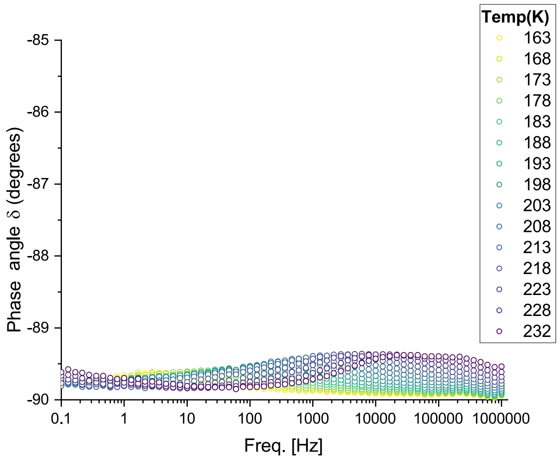
Phase Angle plot

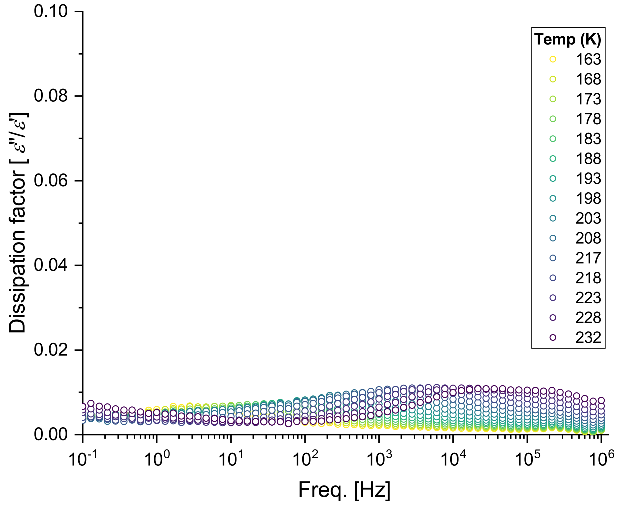
Dissipation factor plot

Figure S88. Broadband Dielectric Spectroscopy plots of x = 11.2 mol% **PEPEP-PNA/PEPEP-Me**.

Bode Plot

Bode plot with HN fitting

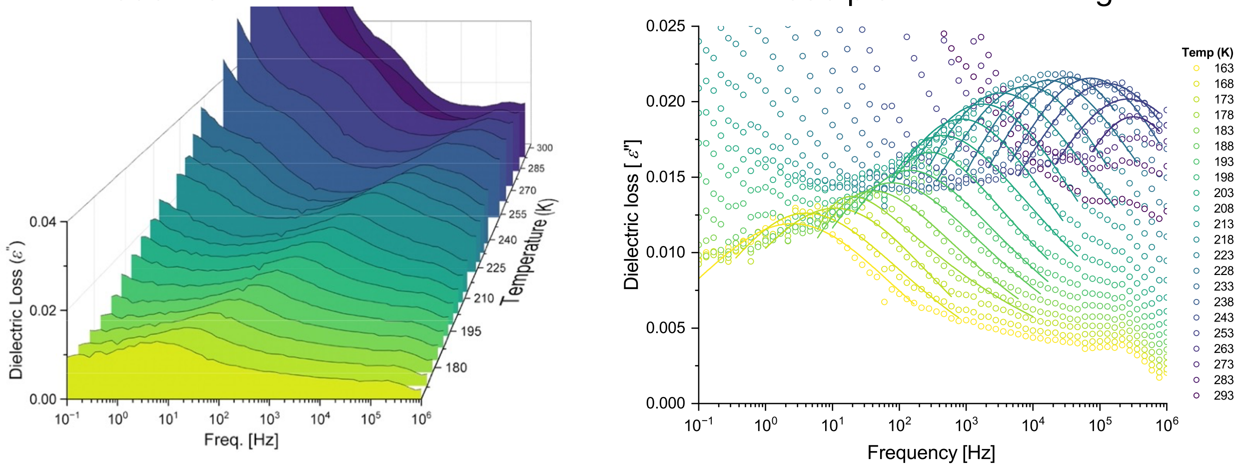

Cole-Cole plot

Phase Angle plot

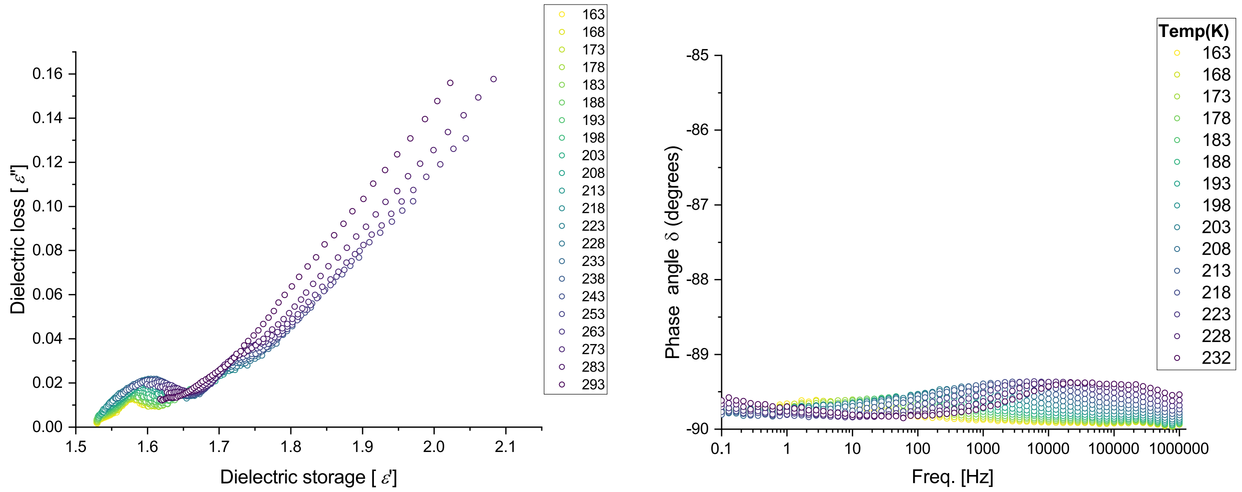

Dissipation factor plot

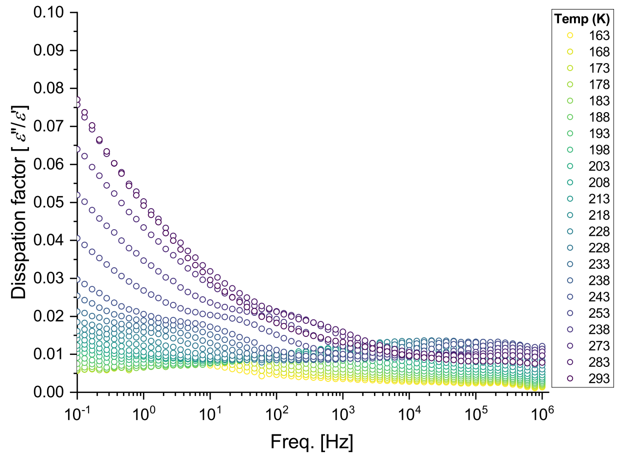

Figure S89. Broadband Dielectric Spectroscopy plots of x = 16.6 mol% **PEPEP-PNA/PEPEP-Me** MOFs.

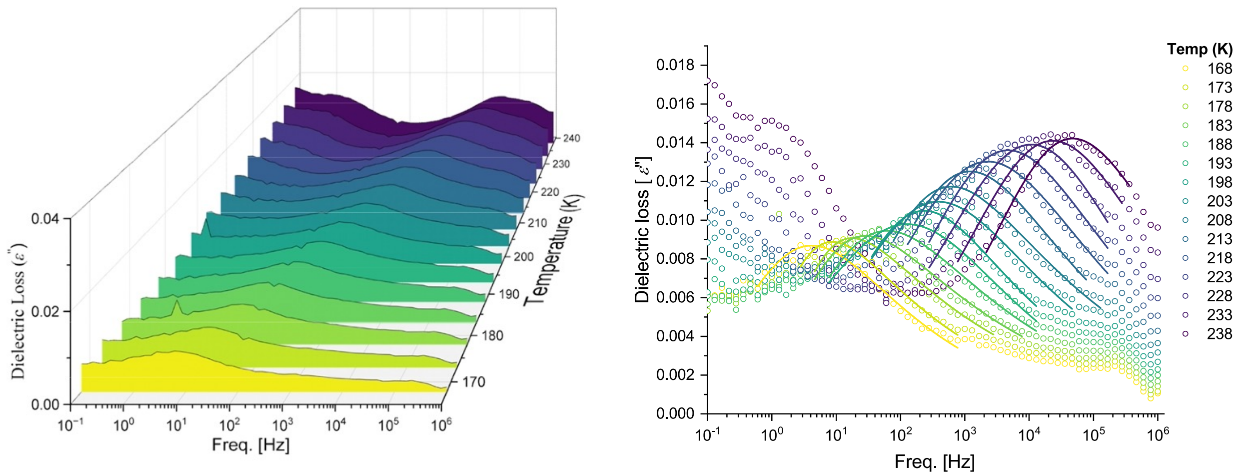
Bode Plot

Bode plot with HN fitting

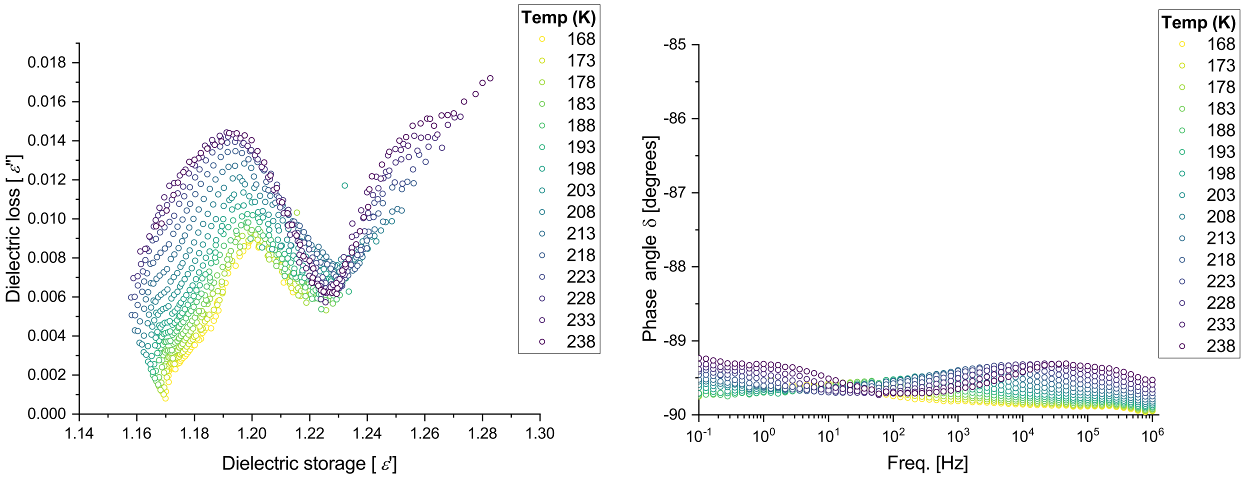
Cole-Cole plot

Phase Angle plot

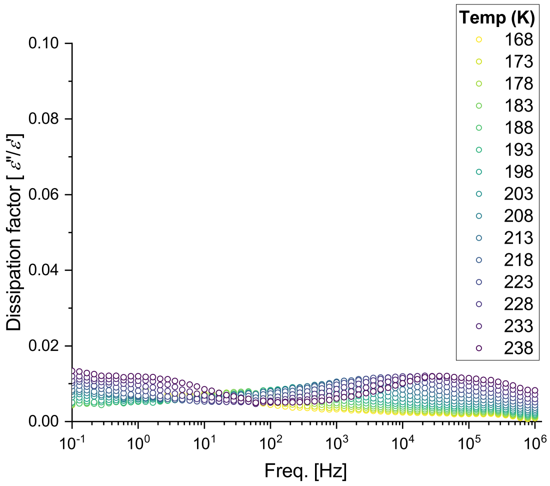
Dissipation factor plot

Figure S90. Broadband Dielectric Spectroscopy plots of x = 21.9 mol% **PEPEP-PNA/PEPEP-Me** MOFs.

Bode Plot

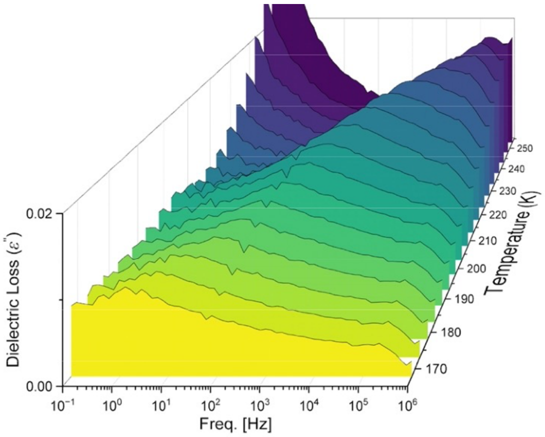

Bode plot with HN fitting

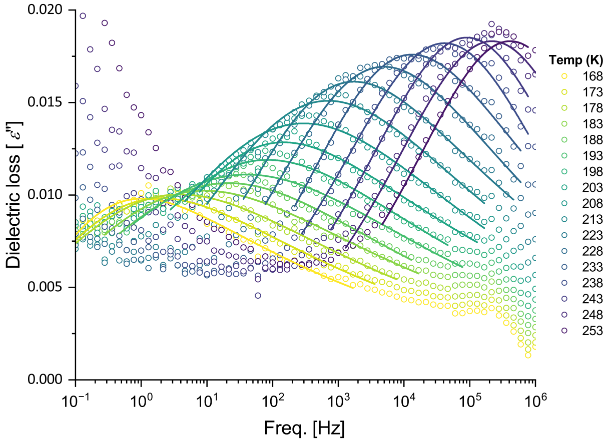

Cole-Cole plot

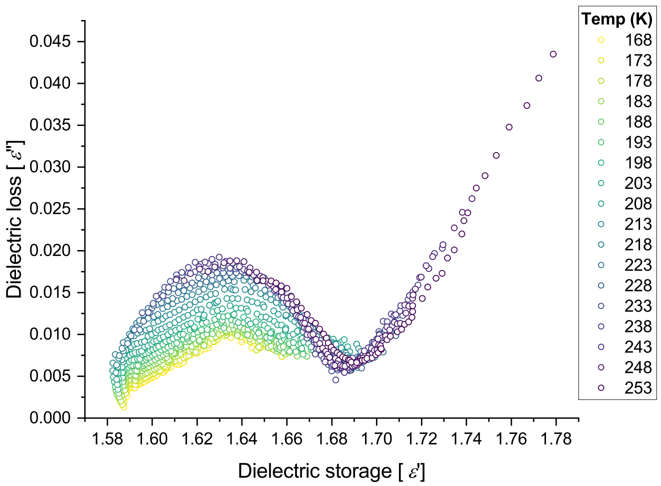

Phase Angle plot

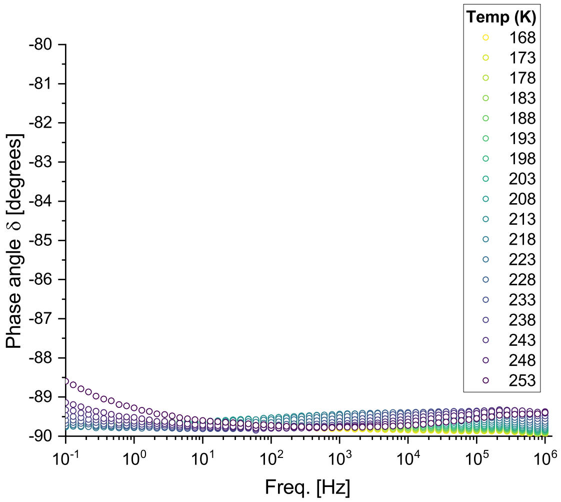

Dissipation factor plot

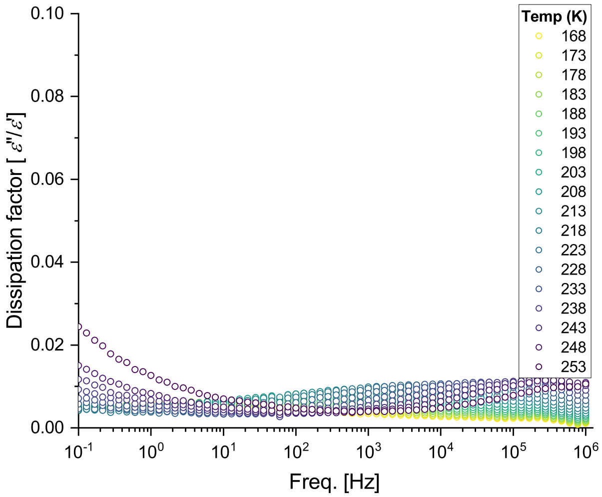

Figure S91. Broadband Dielectric Spectroscopy plots of *x* = 27.2 mol% **PEPEP-PNA/PEPEP-Me** MOFs.

Bode Plot

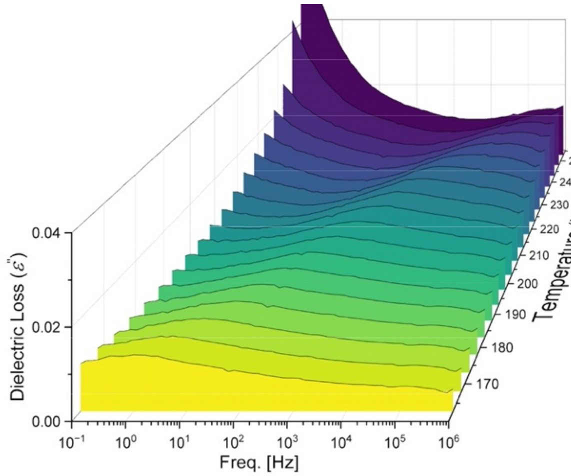

Bode plot with HN fitting

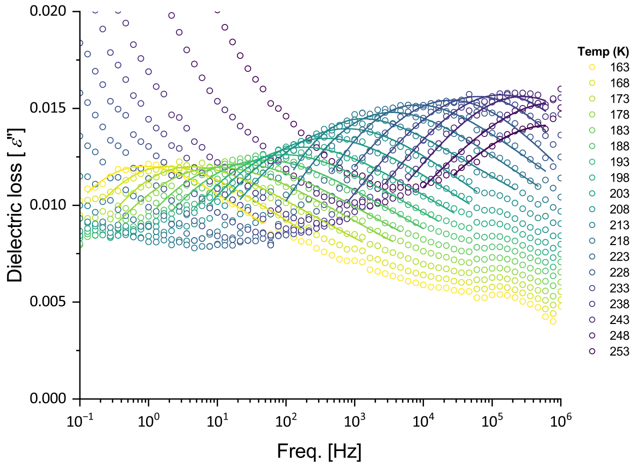

Cole-Cole plot

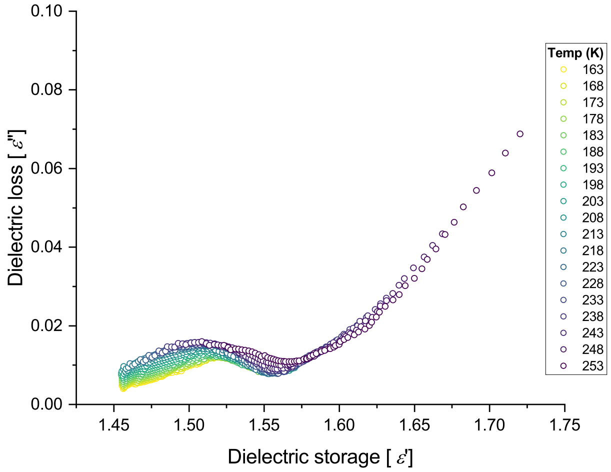

Phase Angle plot

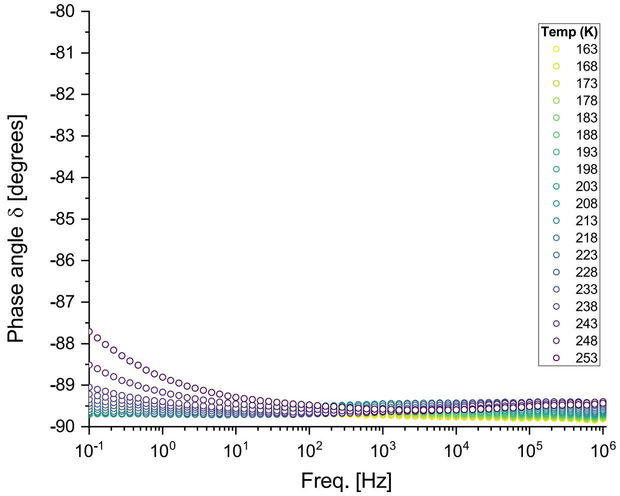

Dissipation factor plot

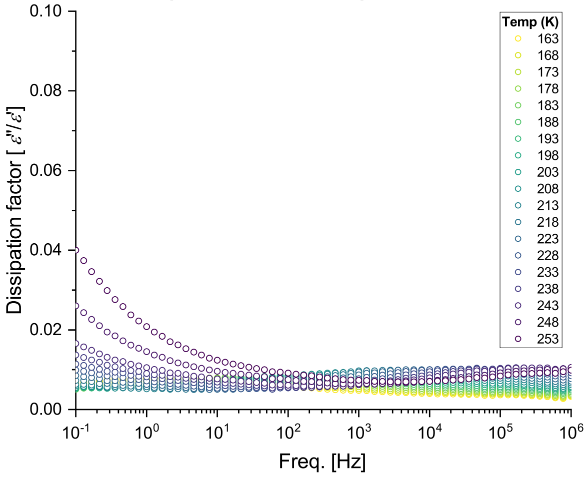

Figure S92. Broadband Dielectric Spectroscopy plots of x = 100 mol% **PEPEP-PNA/PEPEP-Me** MOFs.

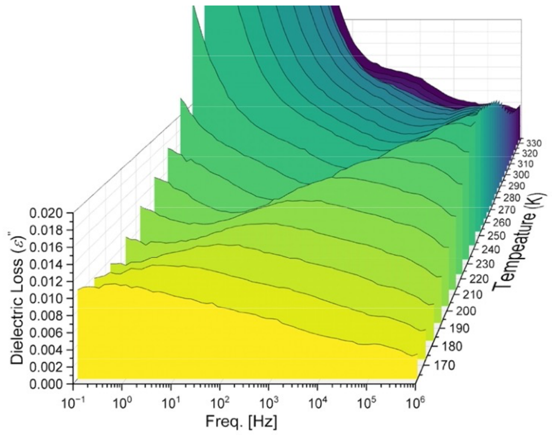
Bode Plot

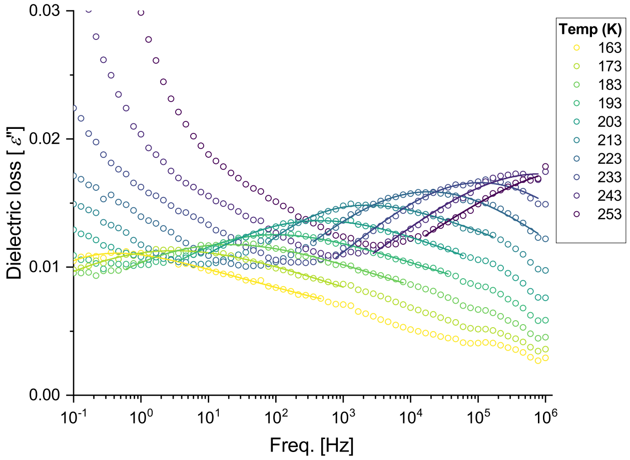
Bode plot with HN fitting

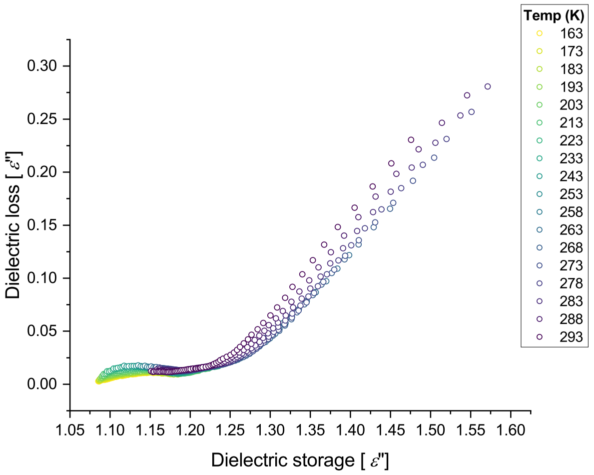
Cole-Cole plot

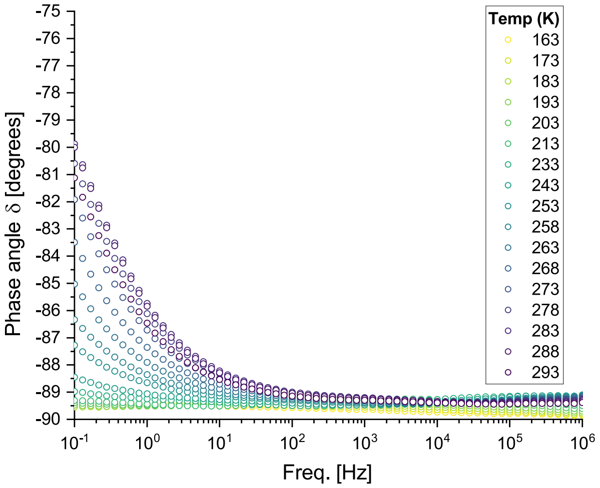
Phase Angle plot

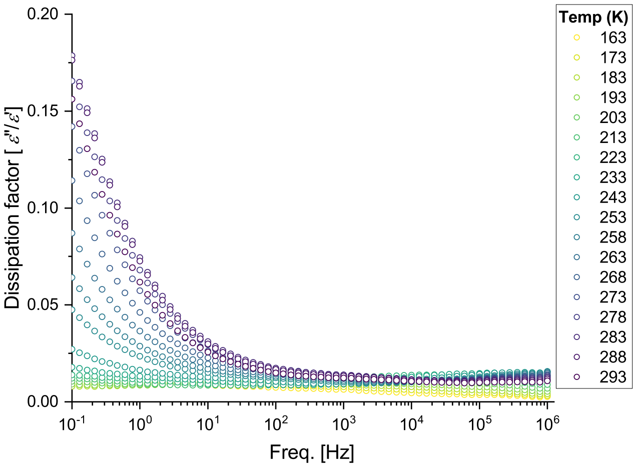
Dissipation factor plot

Figure S93. Eyring plots for each MTV composition.

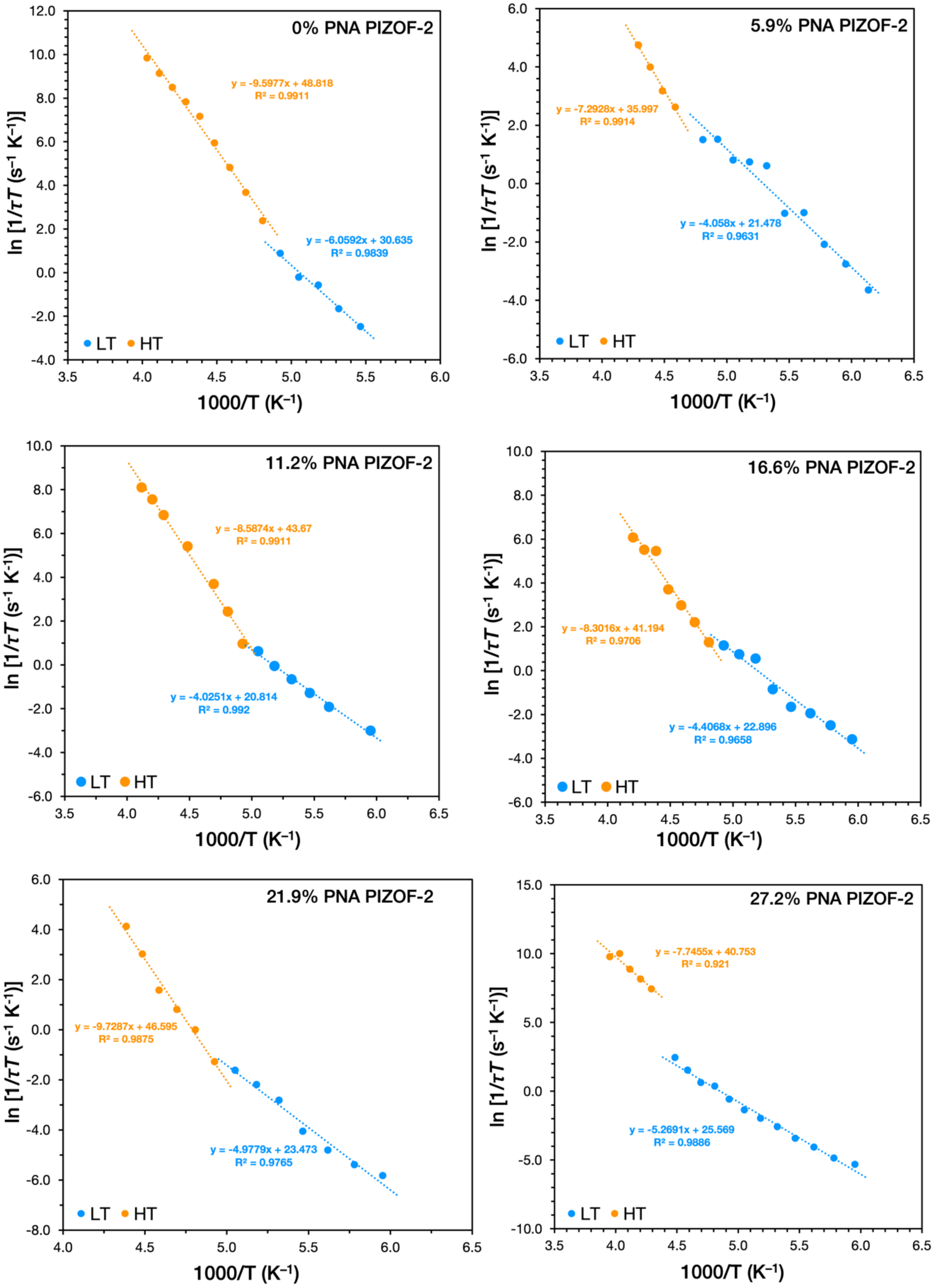

Figure S94. Eyring plot for x = 100% PNA.

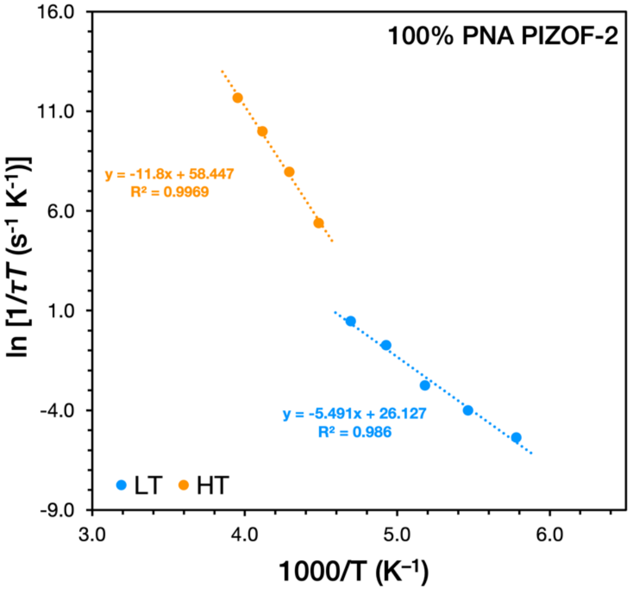

Figure S95. Activation enthalpy (left) and entropy (right) vs MTV composition plot.

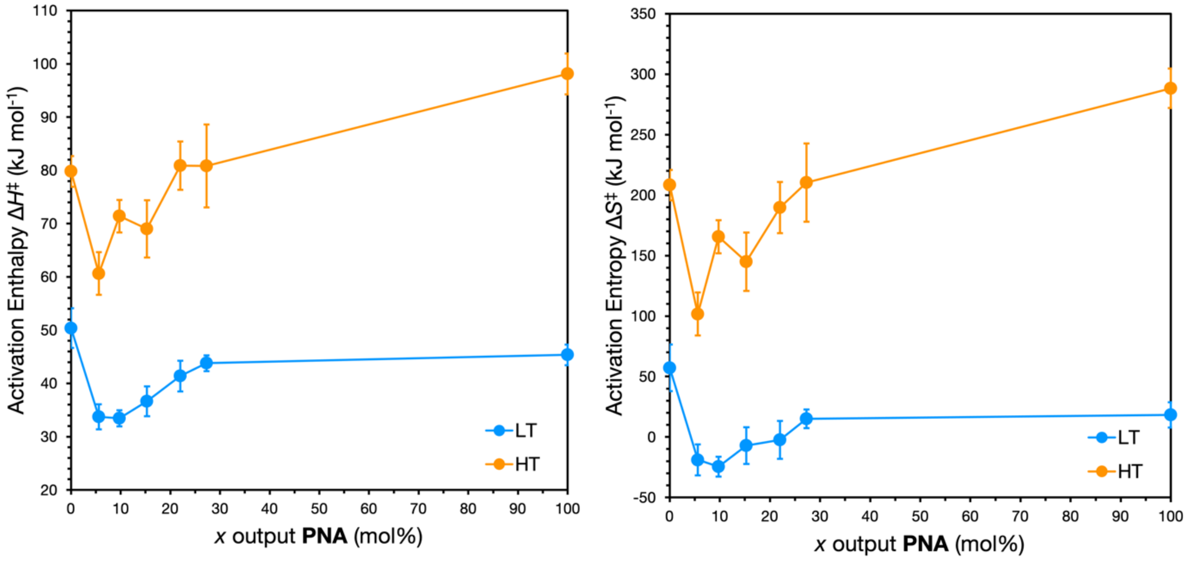

Figure S96. Entropy-Enthalpy Meyer-Neldel compensation plot.

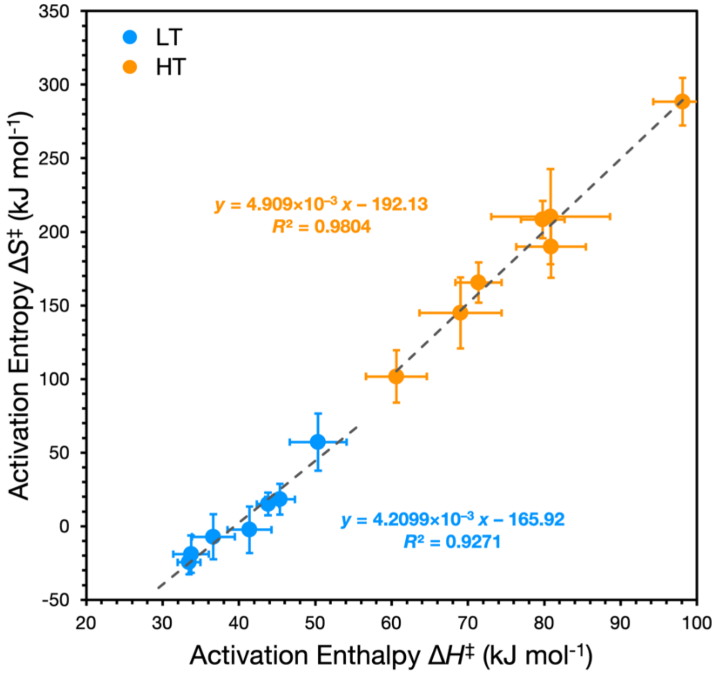

Table S8. Thermodynamic parameters of **PEPEP-PNA** MTV MOFs from Eyring analysis.

Low Temperature (LT) region		
x out (mol%)	Activation enthalpy (kJ mol^{-1})	Activation entropy (J mol^{-1} K^{-1})
0.0	50.38 ± 3.72	57.16 ± 19.32
5.9	33.74 ± 2.34	-18.96 ± 12.71
11.2	33.47 ± 1.50	-24.48 ± 8.18
16.6	36.64 ± 2.81	-7.18 ± 15.26
21.9	41.39 ± 2.87	-2.38 ± 15.75
27.2	43.81 ± 1.48	15.04 ± 7.68
100	45.37 ± 1.94	18.26 ± 10.45

High Temperature (HT) region		
x out (mol%)	Activation enthalpy (kJ mol^{-1})	Activation entropy (J mol^{-1} K^{-1})
0.0	80.0 ± 2.86	208.3 ± 12.5
5.9	60.63 ± 4.00	101.74 ± 17.7
11.2	71.40 ± 3.03	165.5 ± 13.7
16.6	69.02 ± 5.37	144.9 ± 24.1
21.9	80.88 ± 4.55	189.9 ± 21.16
27.2	80.82 ± 7.77	210.3 ± 32.3
100	98.11 ± 3.85	288.4 ± 16.2

Section S11. Rietveld refinement and crystal modeling

Rietveld refinement of PIZOF-2-PNA was perfomed in GSAS-II[S3] using powder data between 2 and 30 2-theta degrees. The profile function is a Tomson-Coax-Hasting modified pseudo-Voight function with five parameters (U, V, W, X, Y) and asymmetry, the background was fitted using a shifted order Chebyshev polynomial with eight parameters. The starting crystal was modeled in Materials Studio Modeling Suite starting with a cubic crystal with $Fd\bar{3}m$ symmetry of PIZOF-2 with added N and O in all four positions, and O atoms that represent guests in special positions at the pore. Hydrogen atoms were excluded from the refinement. The background and profile parameters were refined using LeBail routine. For Rietveld, first, scaling factor was refined along with lattice parameters, followed by scaling factor and zero shift. After, lattice parameters were refined adding crystal size, strain, absorption, and second order spherical harmonics model for preferred orientation, performing a refining cycle each time a parameter was added. Then, lattice parameters were refined along with isotropic thermal parameters for all framework atoms except nitro and guest oxygen atoms, which were set a 1.00 due to disorder. Atom position and occupancy of guest oxygen atoms were added to the refinements, performing refinement cycles until obtaining convergent results. Occupancy of some guest O atoms was larger than 1, this artifact is due to atoms O10, O19 and O20 representing electron density of guests in the pore, assumed to be water. A crystallographic information file (CIF) was generated along with a refinement plot. The CIF was submitted to the Cambridge Structural Database, with submission number 2455083.

Figure S97. Rietveld plot of PIZOF-2- 100 mol% PNA ($Fd\bar{3}m$).

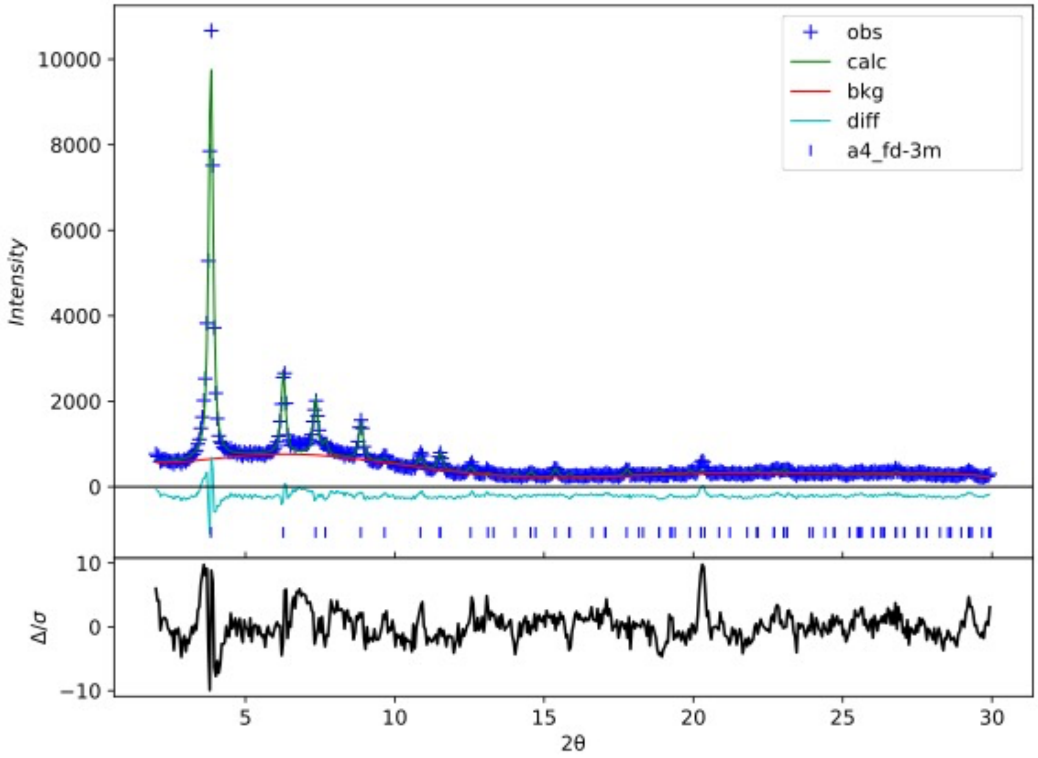

Table S9. Rietveld refinement data of PIZOF-2-PNA.

Name	**PIZOF-2-PNA**
Formula	$C_{24}N_2O_{15.802}Zr$
Crystal System	Cubic
Space group	$Fd\bar{3}m$
a (Å)	39.9250(150)
V (Å$^{3)}$	6.364(7)×10^4
Z	48
Range	2-30 degrees (2-theta)
Wavelength (Å)	1.54051
Temperature (K)	293.15
R_p	0.08116
wR_p	0.10086
R_B	0.09512
GOF	2.419

Figure S98. [100] view of a section (0 and ¼*a* along *x*) of 100 mol% PNA MOF unit cell with thermal parameters, obtained using Rietveld refinement ($Fd\bar{3}m$). Note the positional disorder of N and O around the central ring of the link (Wyckoff position 48*f*, local symmetry *mm2*). Red ellipsoids = oxygen, dark blue = zirconium, light blue = nitrogen, gray = carbon. Hydrogen atoms were not included in the refinement. Guest atoms not shown.

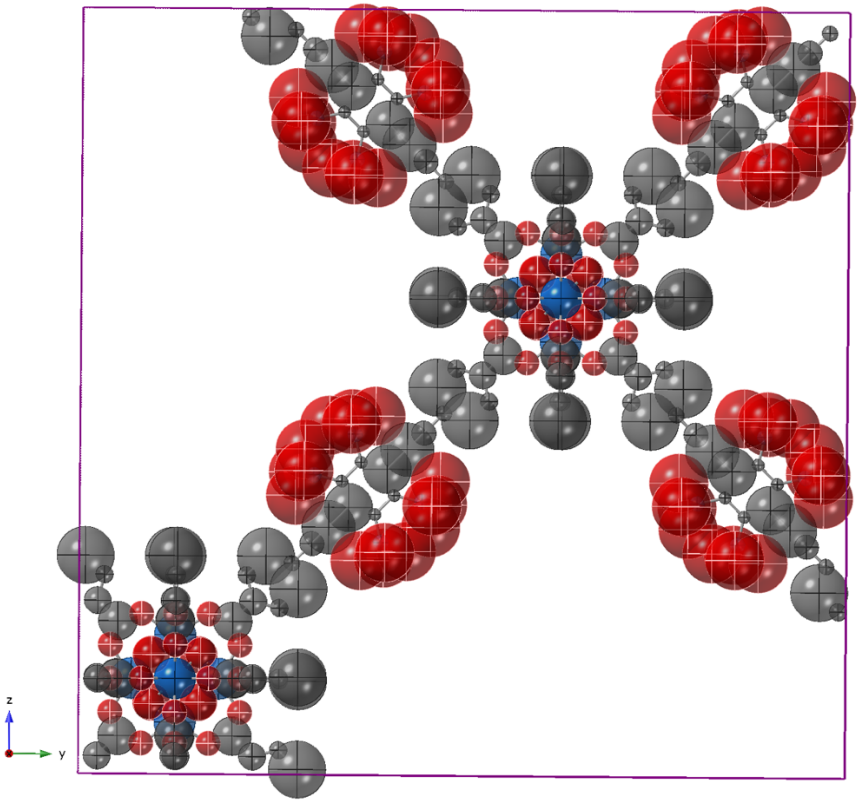

Figure S99. Crystal model of 100 mol% PNA MOF in CPK representation, compared to its underlying net (**fcu-c**). Nodes represent Zr-cluster, edges represent PEPEP links. Model built in Materials Studio Modeling Suite v. 8.0 using experimental lattice parameters obtained from Rietveld refinement and $R3$ space subgroup ($R3 \subset Fd\bar{3}m$).

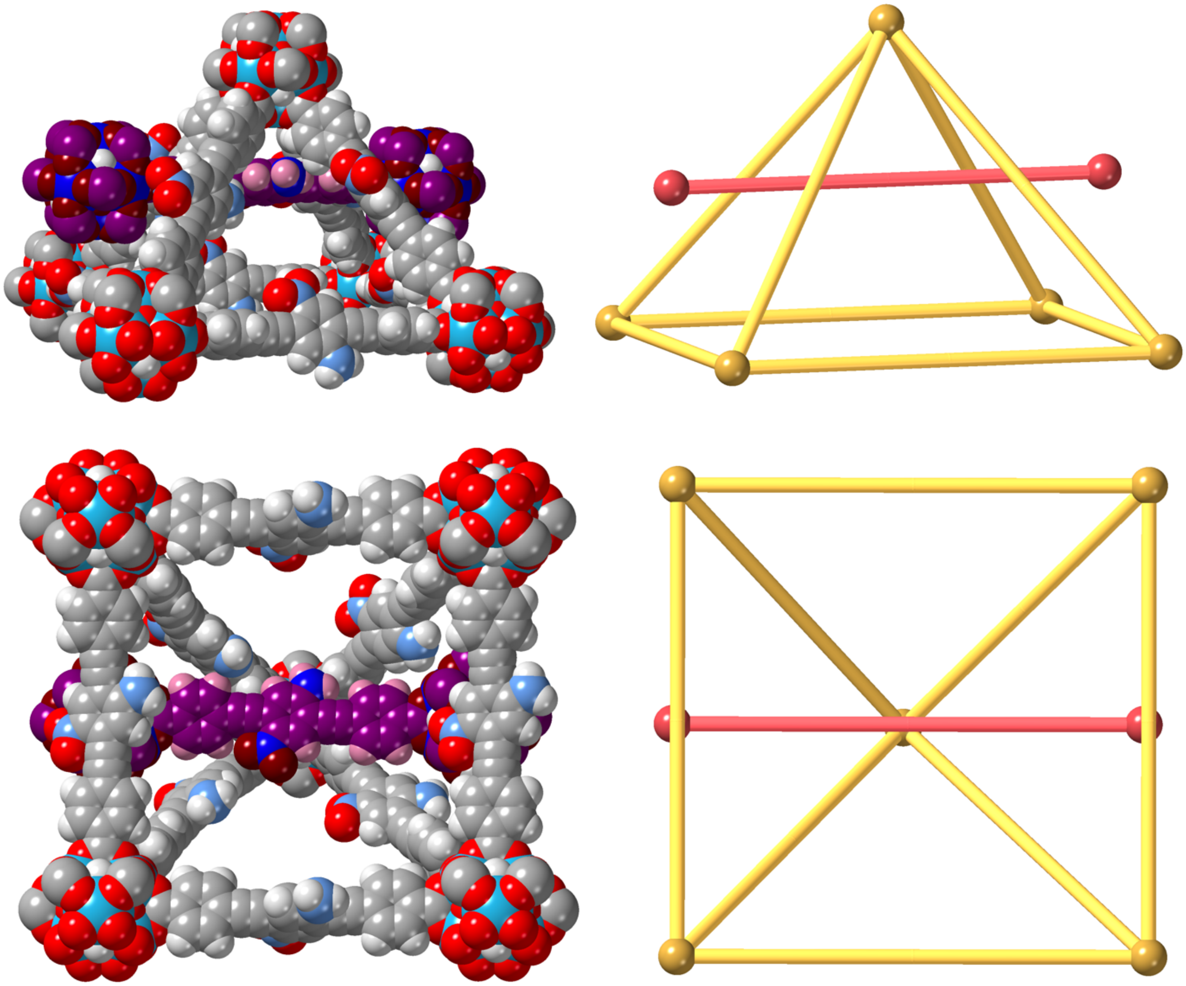

Figure S100. Crystal model of 0 mol% PNA MOF in CPK representation, compared to its underlying net (**fcu-c**). Nodes represent Zr-cluster, edges represent PEPEP links. Model built in Materials Studio Modeling Suite v. 8.0 using experimental lattice parameters obtained from Rietveld refinement and $F4_132$ subgroup ($F4_132 \subset Fd\text{-}3m$).

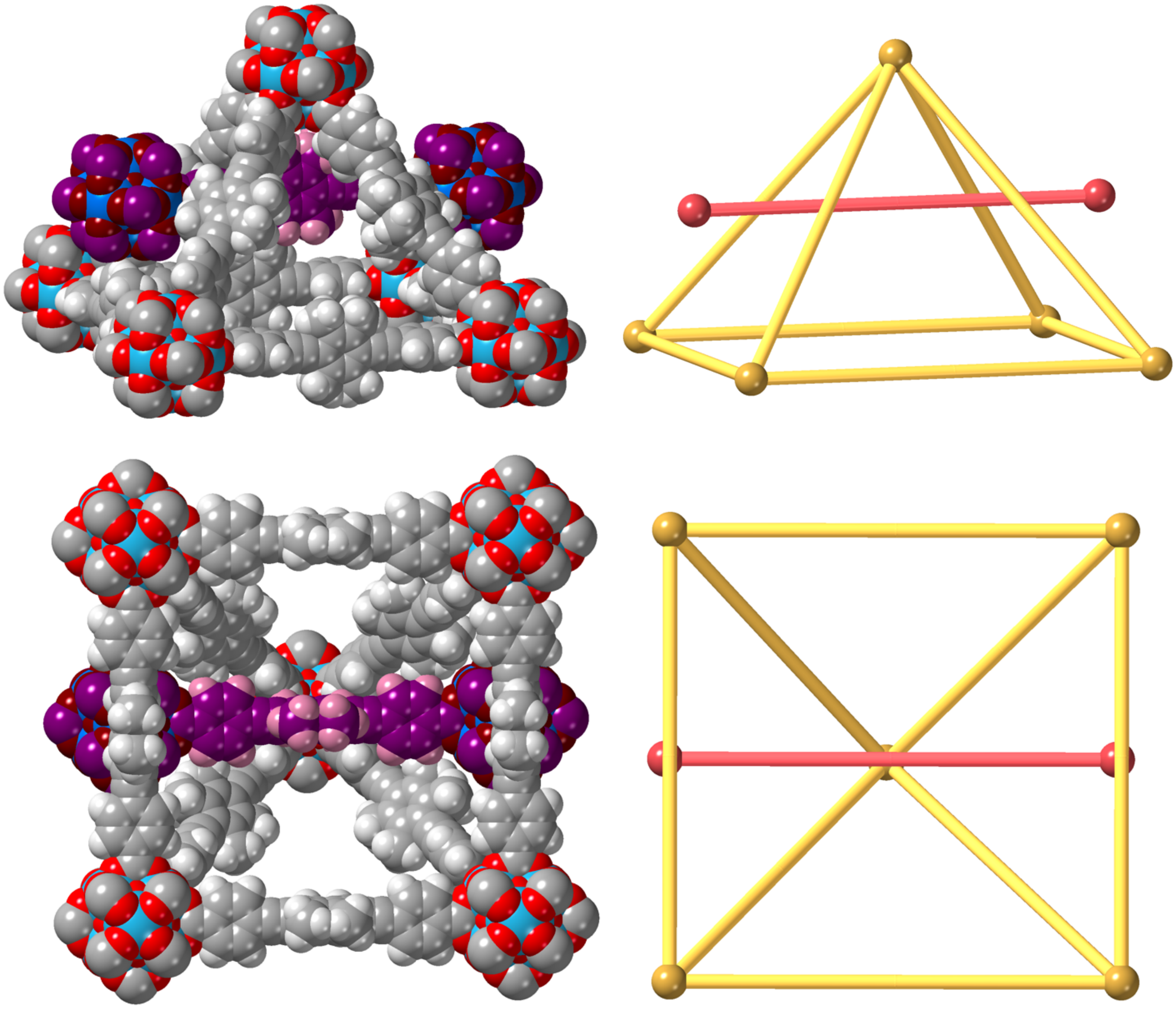

Section S12. NMR Spectra

Figure S101: ^{1}HNMR (400 MHz,$CDCl_3$, 20 °C) of compound **S1**

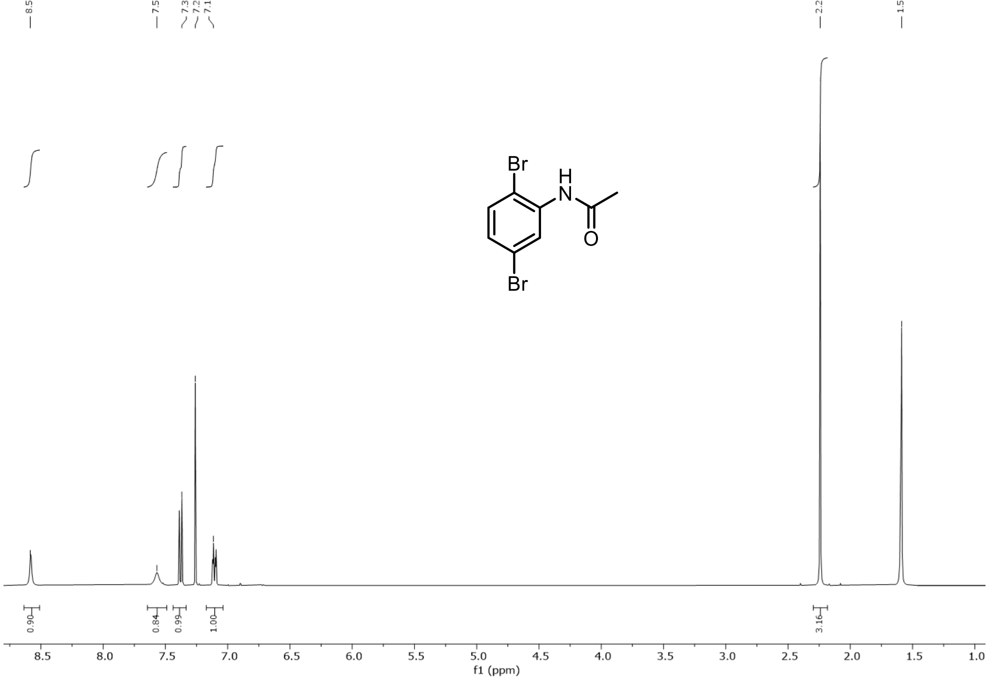

Figure S102: ^{13}CNMR (101 MHz, $CDCl_3$, 20 °C) of compound **S1**

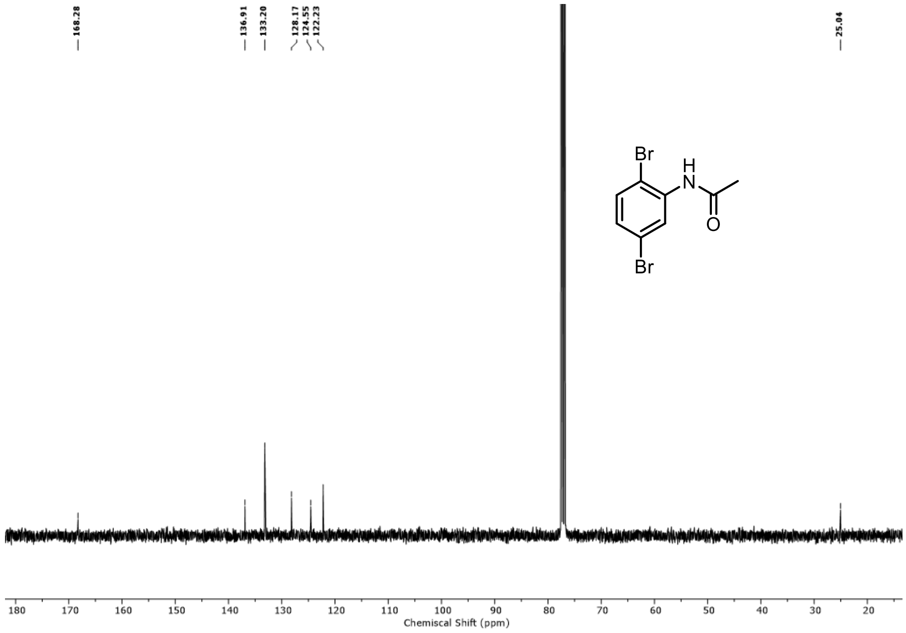

Figure S103: ^{1}HNMR (400 MHz, $CDCl_3$, 20 °C) of compound **S2**

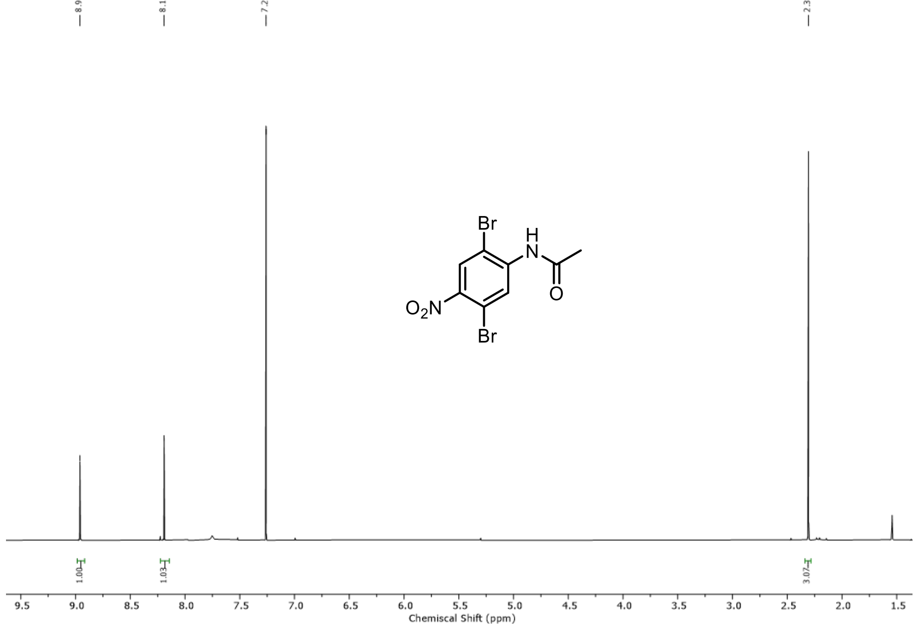

Figure S104: ^{13}CNMR (101 MHz, $CDCl_3$, 20 °C) of compound **S2**

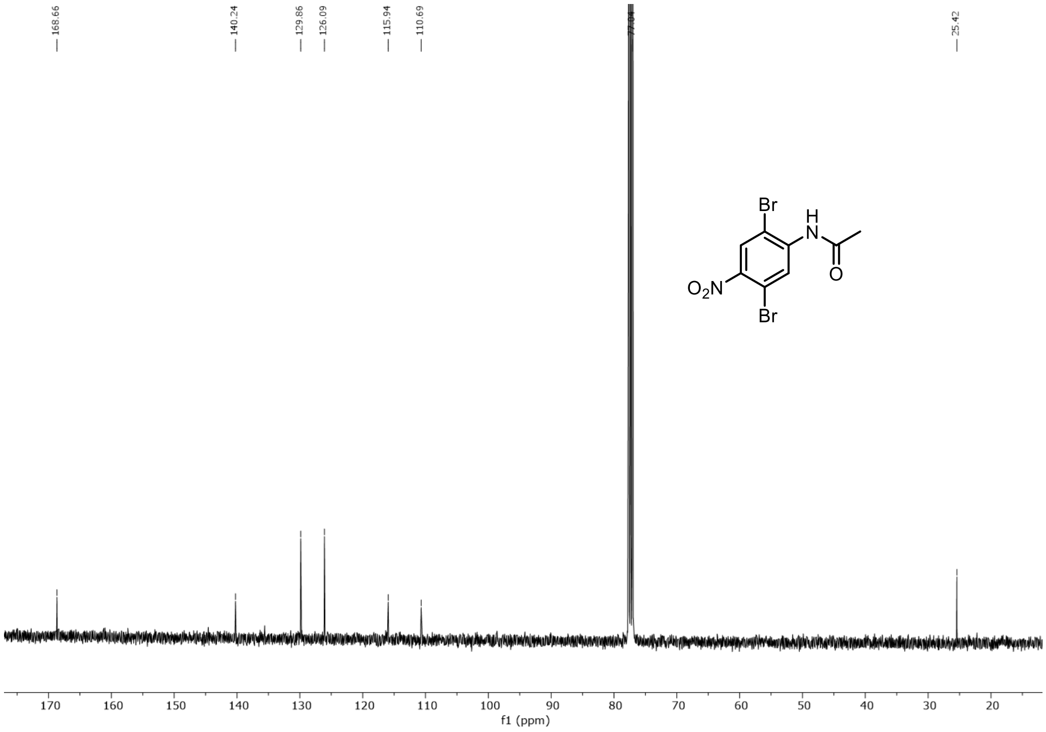

Figure S105: ^{1}HNMR (400 MHz, $CDCl_3$, 20 °C) of compound **S3**

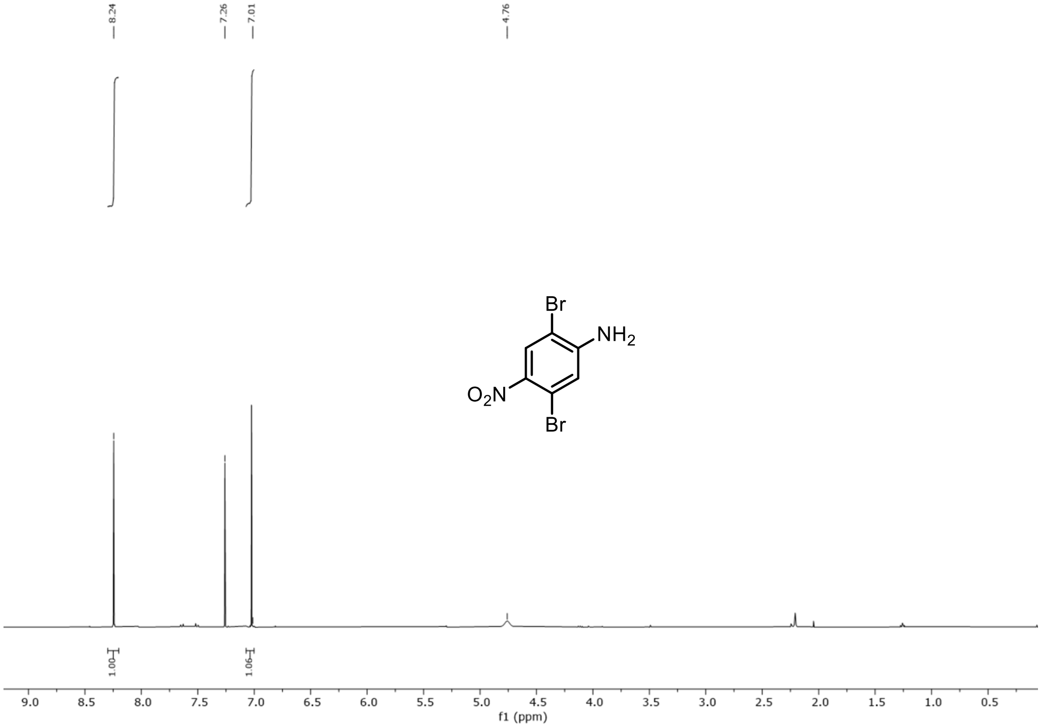

Figure S106: ^{13}CNMR (101 MHz, $CDCl_3$, 20 °C) of compound **S3**

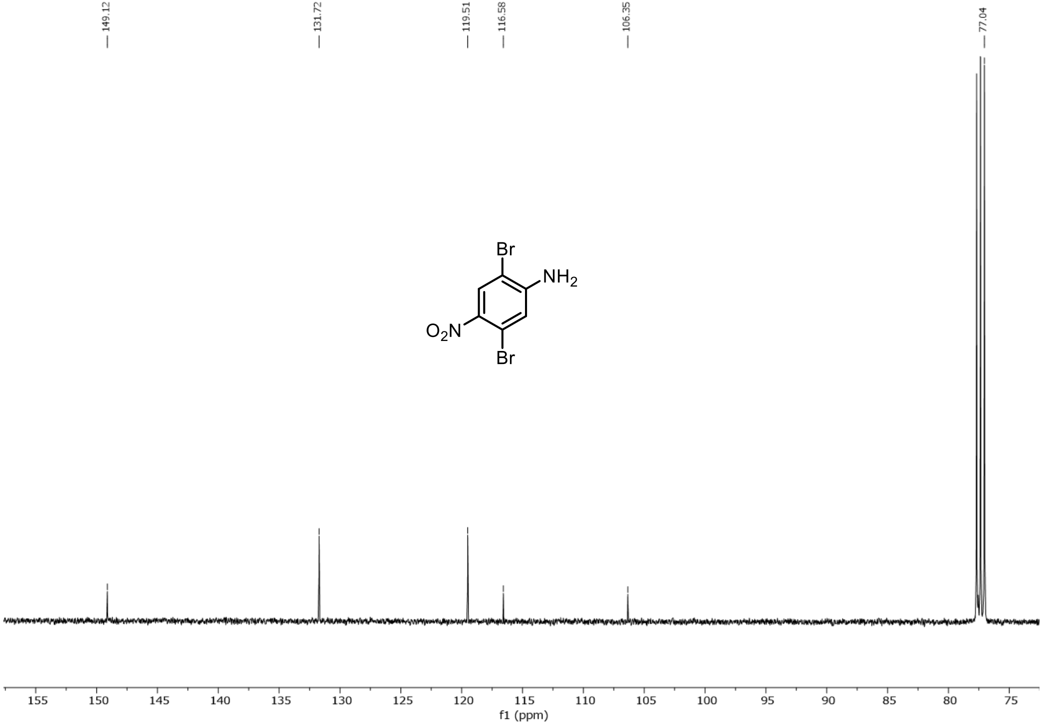

Figure S107: ^{1}HNMR (400 MHz, $CDCl_3$, 20 °C) of compound **S4**

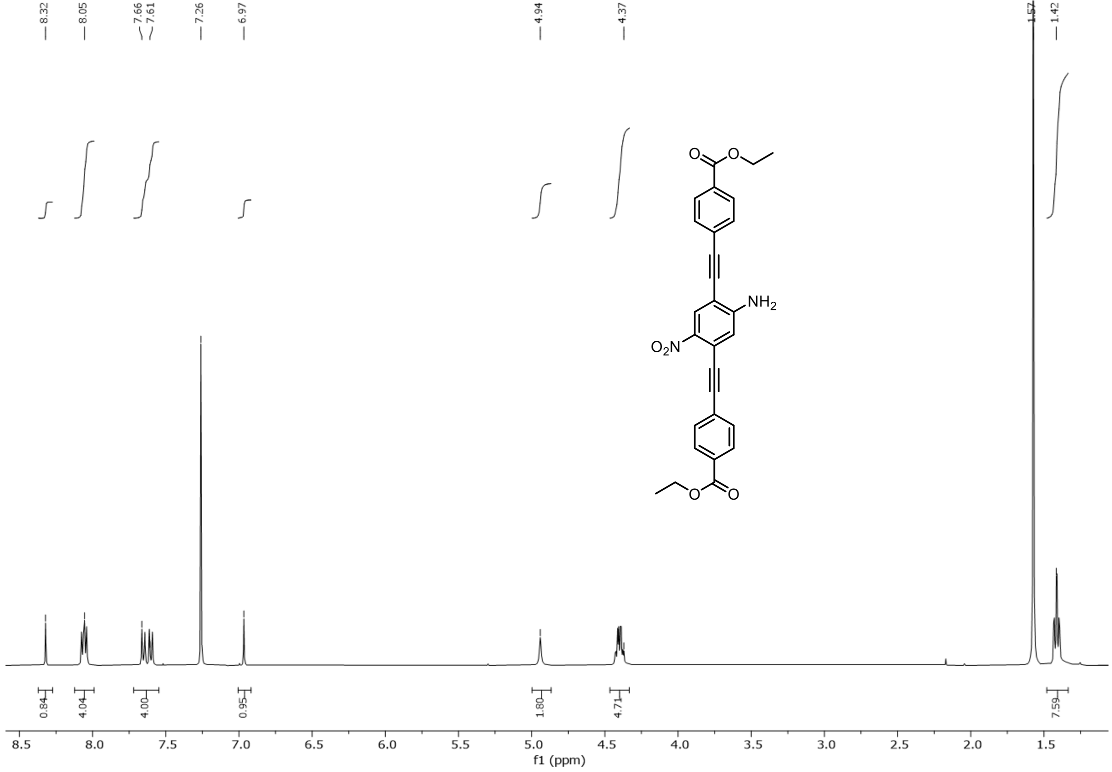

Figure S108: ^{13}CNMR (101 MHz, DMSO-d_6, 20 °C) of compound **S4**

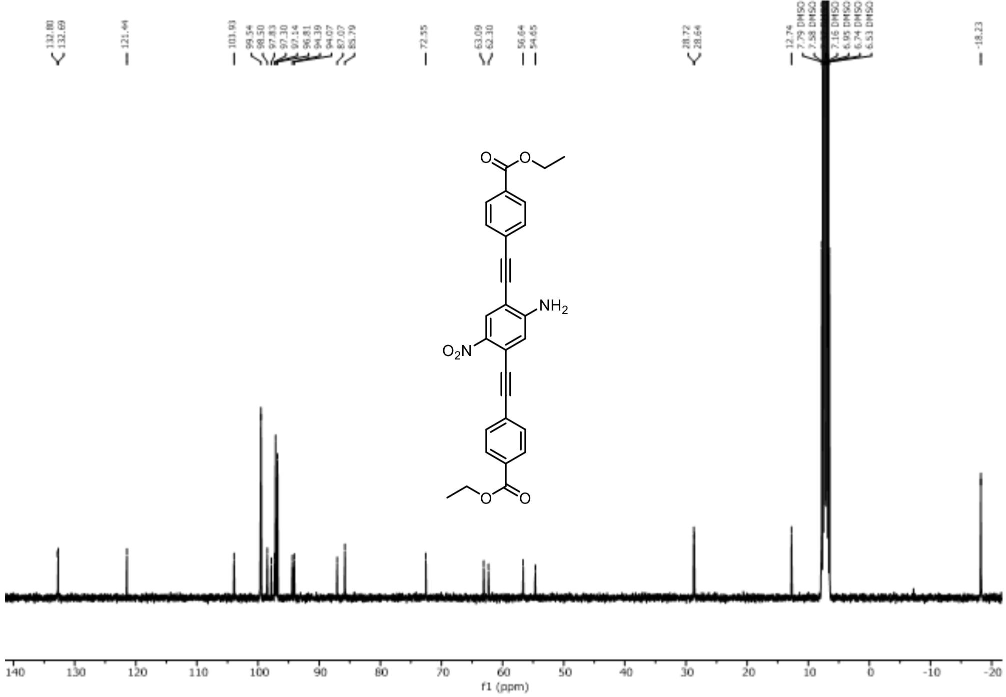

Figure S109: ^{1}HNMR (400 MHz, CDCl$_3$, 20 °C) of compound **S5**

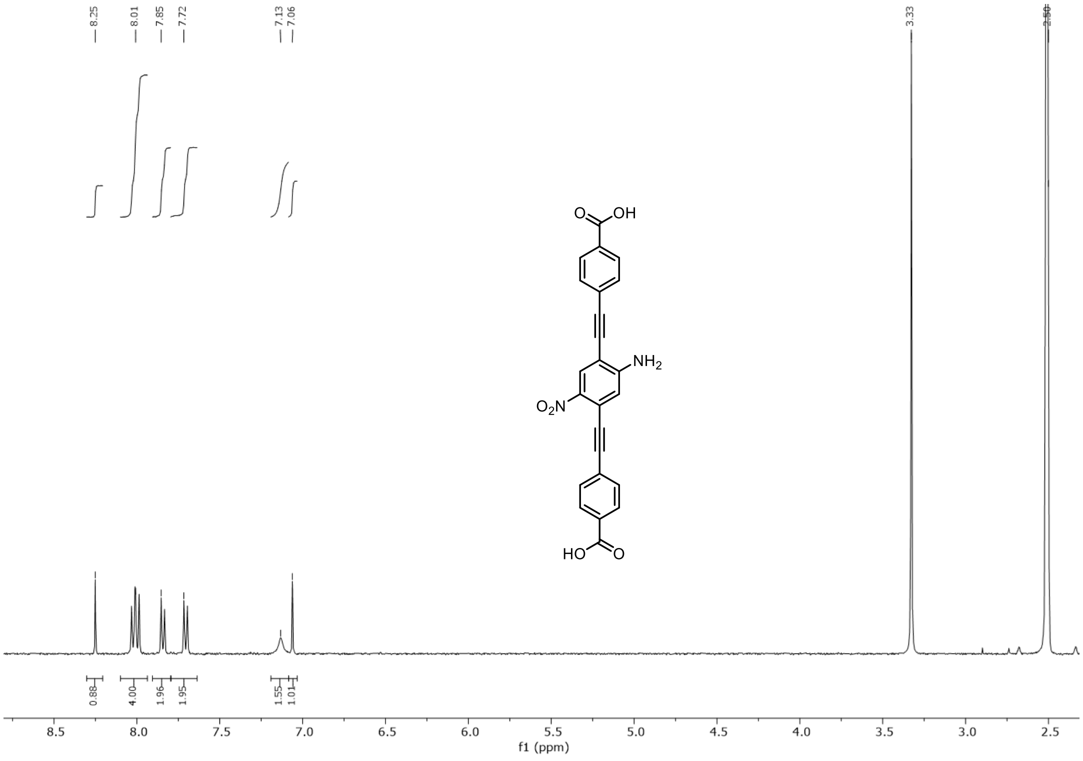

Figure S110: ^{13}CNMR (101 MHz, CDCl$_3$, 20 °C) of compound **S5**

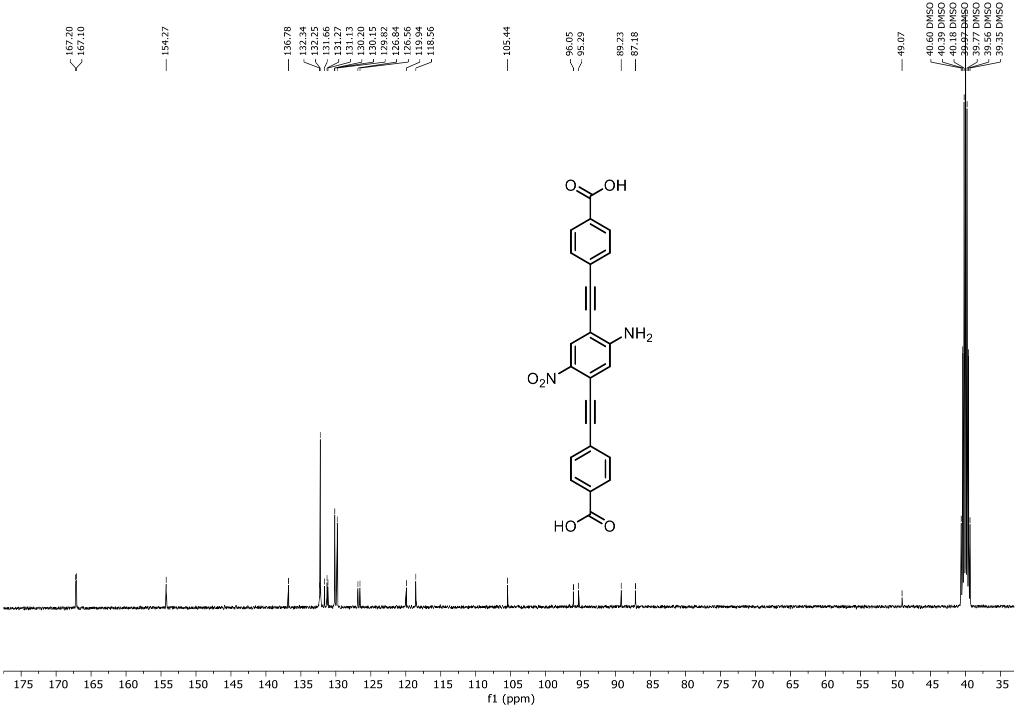

S13. Pawley refinement plots

Figure S111. Pawley plot of PIZOF-2-10 mol% PNA (input).

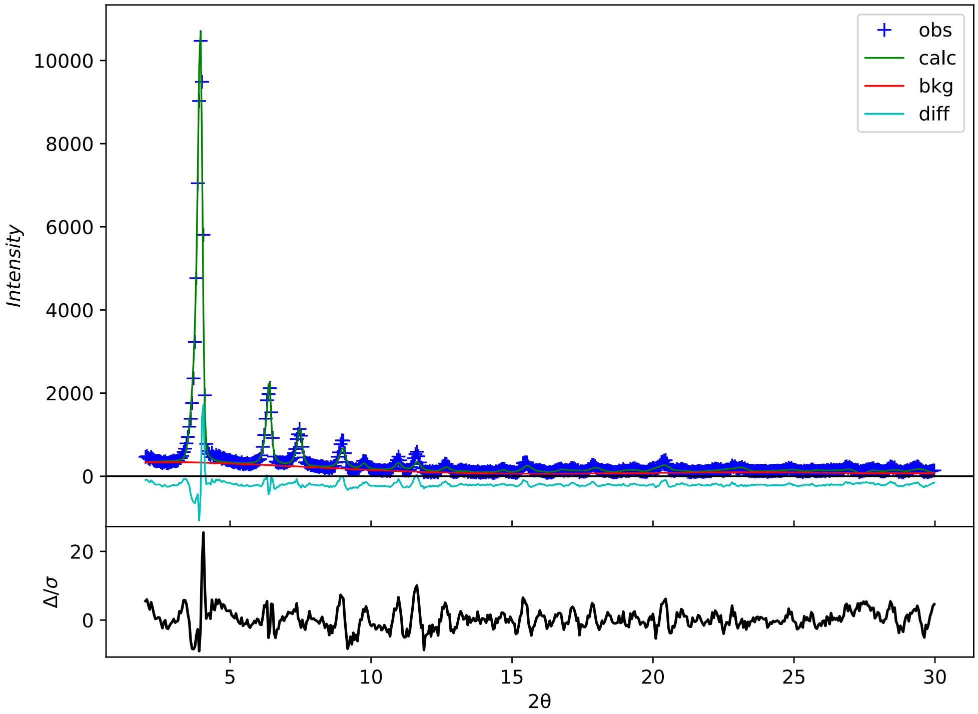

Figure S112. Pawley plot of PIZOF-2-20 mol% PNA (input).

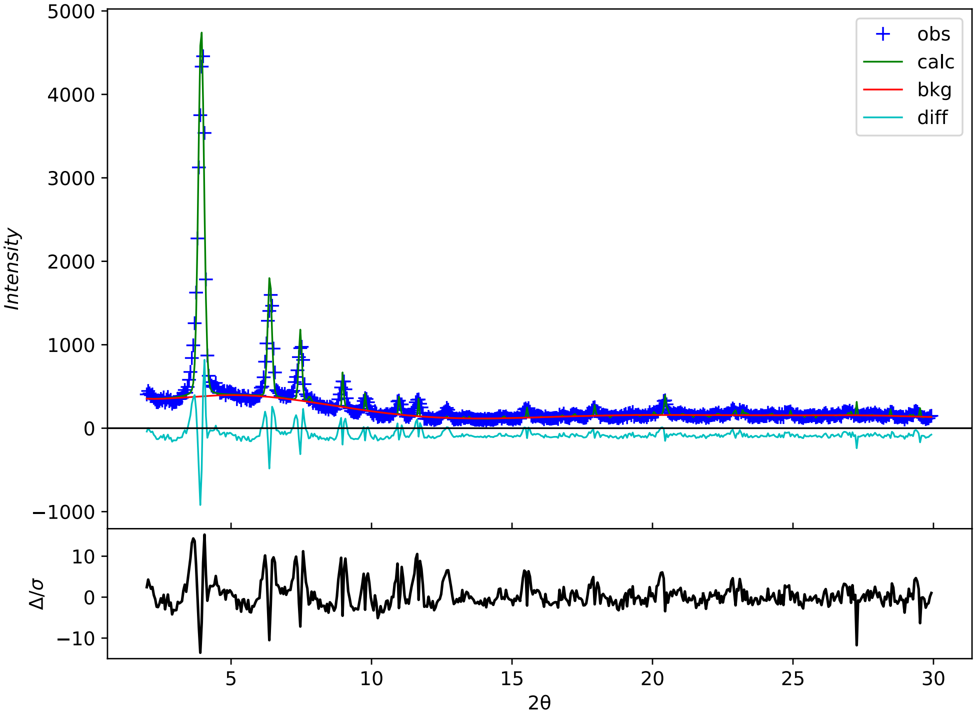

Figure S113. Pawley plot of PIZOF-2-30 mol% PNA (input).

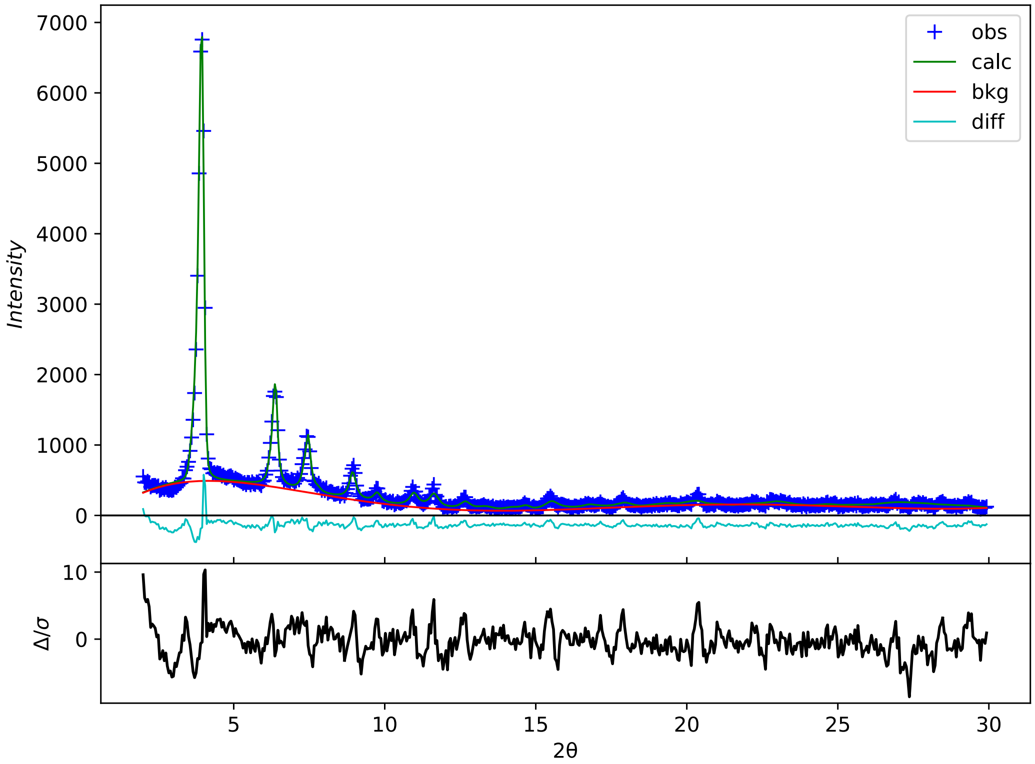

Figure S114. Pawley plot of PIZOF-2-40 mol% PNA (input).

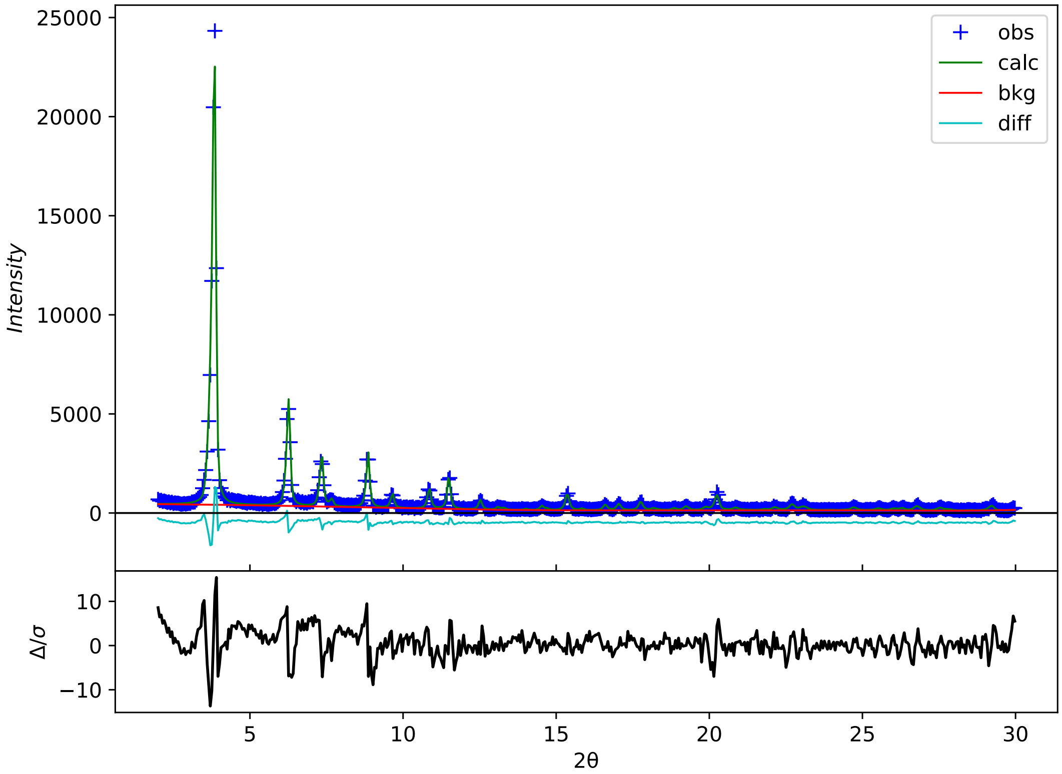

Figure S115. Pawley plot of PIZOF-2-50 mol% PNA (input).

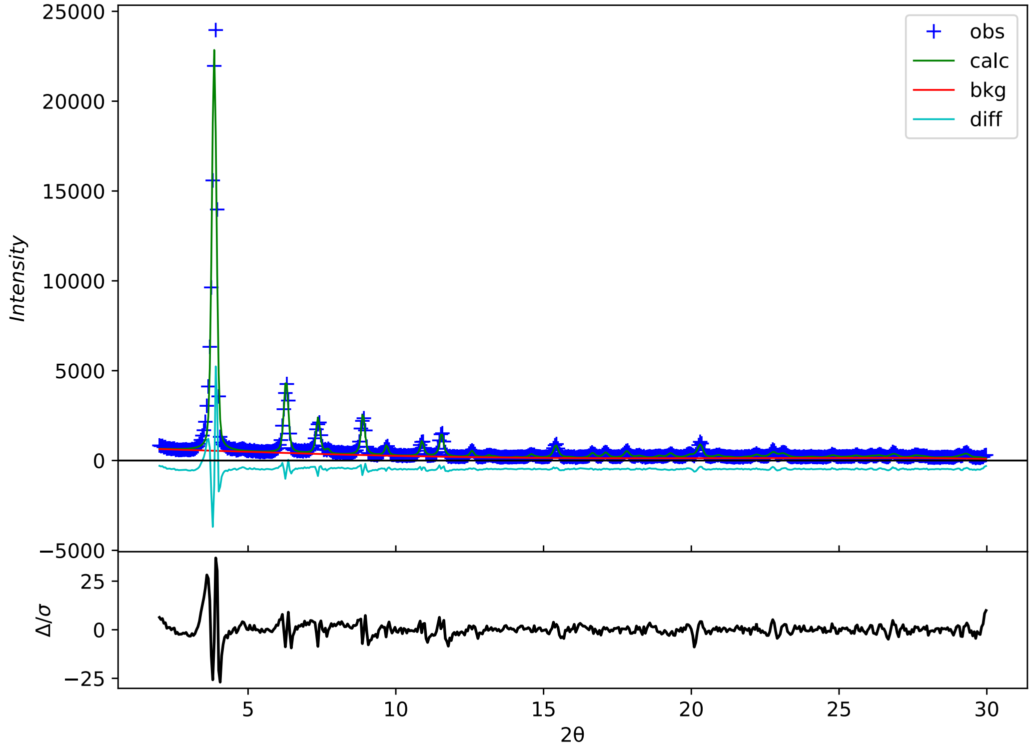

Figure S116. Pawley plot of PIZOF-2-100 mol% PNA.

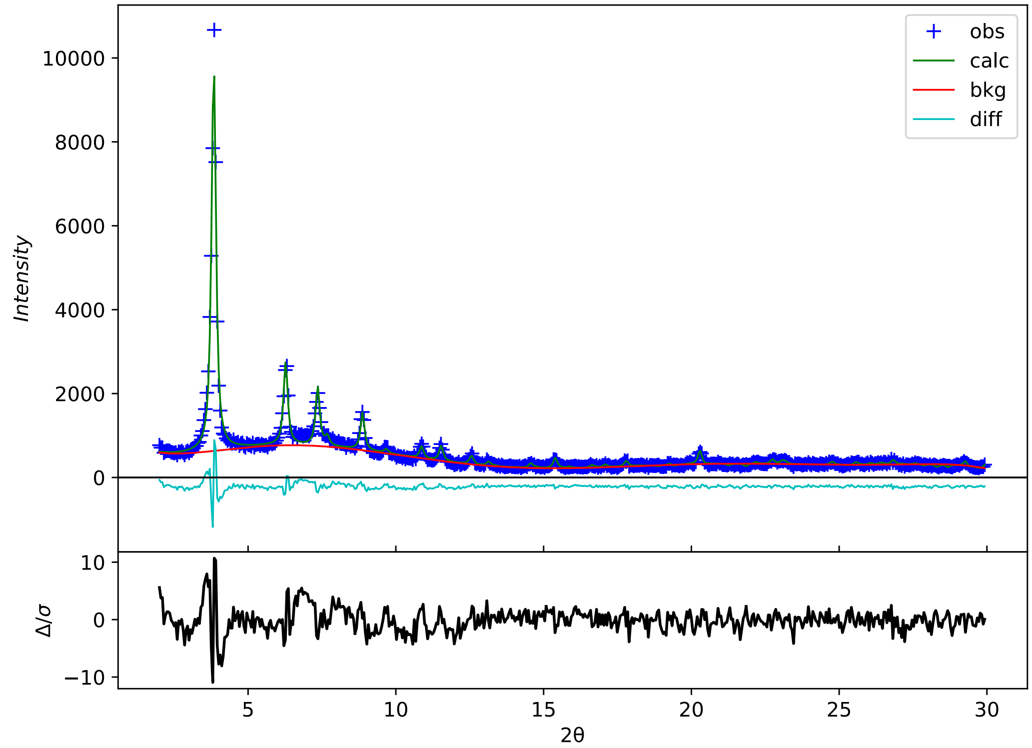

S14. References

[S1] Jerozal, R. T.; Pitt, T. A.; MacMillan, S. N.; Milner, P. J., High-Concentration Self-Assembly of Zirconium- and Hafnium-Based Metal–Organic Materials. *Journal of the American Chemical Society* **2023,** *145*, 13273-13283.

[S2] Marshall, R. J.; Kalinovskyy, Y.; Griffin, S. L.; Wilson, C.; Blight, B. A.; Forgan, R. S., Functional Versatility of a Series of Zr Metal–Organic Frameworks Probed by Solid-State Photoluminescence Spectroscopy. *Journal of the American Chemical Society* **2017,** *139*, 6253-6260.

[S3] Toby, B. H.; Von Dreele, R. B. GSAS-II: the genesis of a modern open-source all purpose crystallography software package”. *Journal of Applied Crystallography* **2013**, *46*, 544-549. doi:10.1107/S0021889813003531

[S4] Abramoff, M., Magalhaes, P. & Ram, S. *Biophotonics Int.* **2004**,*11*, 36–42.

[S5] Waskom, M. L., Seaborn: Statistical Data Visualization. *J. Open Source Softw.* **2021,** *6*, 3021.